SUPPORTING INFORMATION

Photomodulation of Transmembrane Transport and Potential by Stiff-Stilbene Based Bis-(thio)ureas

Sander J. Wezenberg,*[,a,b†] Li-Jun Chen,[c†] Jasper E. Bos,[a†] Ben L. Feringa,[b]
Ethan N. W. Howe,[c] Xin Wu,[c] Maxime A. Siegler,[d] and Philip A. Gale*[,c,e]

[a] *Leiden Institute of Chemistry, Leiden University, Einsteinweg 55, 2333 CC Leiden, The Netherlands*

[b] *Stratingh Institute for Chemistry, University of Groningen, Nijenborgh 4, 9747 AG, Groningen, The Netherlands*

[c] *School of Chemistry, The University of Sydney, Sydney NSW 2006, Australia*

[d] *Department of Chemistry, Johns Hopkins University, 3400 N. Charles St.,Baltimore, MD, 21218, United States*

[e] *The University of Sydney Nano Institute (SydneyNano), The University of Sydney, Sydney NSW 2006, Australia*

† These authors contributed equally to this paper

Email: s.j.wezenberg@lic.leidenuniv.nl, philip.gale@sydney.edu.au

Table of contents

Experimental Section

General methods and materials: THF and CH_2Cl_2 were dried using MBraun and Innovative Technology solvent purification systems. Dry DMSO and DMSO-d_6 were purchased from Acros Organics and were stored under N_2 over molecular sieves (4Å). The degassing of solvents was carried out by purging with N_2 for 30 min. Bis(amine) **S1**,[1] bis(phenylurea) **1a**,[1] and bis(phenylthiourea) **2a**[2] were prepared according to procedures reported in the literature. All other chemicals were commercial products and were used as received. Melting points (m.p.) were determined using a Büchi-M560 melting point apparatus. ^{1}H, ^{19}F and ^{13}C spectra were recorded on Varian Mercury-Plus 400 and Bruker AV 400 and Bruker 500 Ultra Shield instruments at 298 K unless indicated otherwise. Chemical shifts (δ) are denoted in parts per million (ppm) relative to residual protiated solvent (DMSO-d_6: for ^{1}H detection, δ = 2.50 ppm; for ^{13}C detection, δ = 39.52 ppm). The splitting pattern of peaks is designated as follows: s (singlet), d (doublet), dd (doublet of doublets), t (triplet), q (quartet), p (quintet), h (septet), m (multiplet), and br (broad). High-resolution mass spectrometry (ESI-MS) was performed on a LTQ Orbitrap XL spectrometer with ESI ionization. UV-Vis spectra were recorded on an Agilent Cary 8454 spectrometer in a 1 cm or 1 mm quartz cuvette. Fluorescence measurements were performed using an Agilent Cary Eclipse Fluorescence Spectrophotometer equipped with a stirrer plate and a temperature controller. Irradiation of NMR and UV-Vis samples was carried out at 20 °C using a Thorlab model M365FP1 high-power LED (15.5 mW) and a Thorlab model M385FP1 high-power LED (23.2 mW) positioned at a distance of 1 cm from the sample. POPC that contains ~1 mol% of free fatty acids was purchased from Corden Pharma GmbH and was stored at –20°C as a solution in chloroform (1 g POPC in 35 mL chloroform). Triton X-100 was used as detergent and was supplied by Sigma-Aldrich.

General procedure A for the synthesis of (*E*)-bis[(thio)ureas]: (*E*)-Bis(amine) (*E*)-**S1** (0.10 mmol) was dispersed in dry THF (2 mL) under N_2 atmosphere and the respective iso(thio)cyanate (0.20 mmol) was added whilst stirring the solution. The mixture was stirred for 16 h, upon which a precipitate formed. The precipitate was filtered off, washed with THF, and air-dried to afford the desired product.

General procedure B for the synthesis of (*Z*)-bis[(thio)ureas]: (*Z*)-Bis(amine) (*Z*)-**S1** (0.10 mmol) was dissolved in dry CH_2Cl_2 (2 mL) under N_2 atmosphere and the respective iso(thio)cyanate (0.20 mmol) was added whilst stirring the solution. The mixture was stirred for 16 h, upon which a precipitate formed. The precipitate was filtered off, washed with CH_2Cl_2, and air-dried to afford the desired product.

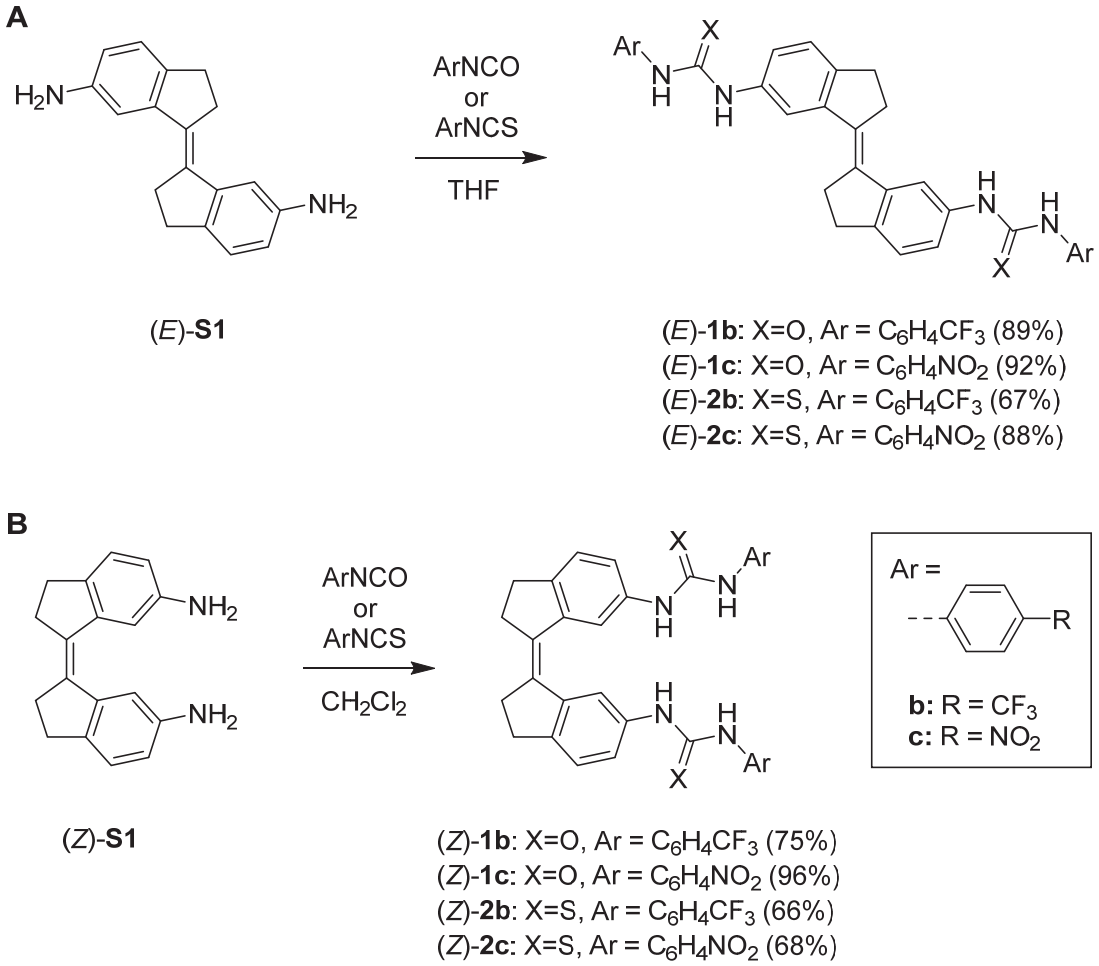

Scheme S1: *Synthesis of stiff-stilbene based bis[phenyl(thio)ureas].*

(*E*)-Bis(*p*-trifluoromethylphenylurea) [(*E*)-1b)]: General procedure A was followed and washing was performed with CH_2Cl_2 in addition to THF to afford (*E*)-**1b** (54 mg, 89%) as a brown solid; M.p. >352 °C (decomp); ^{1}H NMR (400 MHz, DMSO-d_6): δ = 9.06 (s, 2 H; NH), 8.83 (s, 2 H; NH), 7.92 (s, 2 arom. H), 7.70-7.61 (m, 8 arom. H), 7.29-7.21 (m, 4 arom. H), 3.16-3.01 (m, 8 H; CH_2) ppm; ^{13}C NMR (125 MHz, DMSO-d_6, APT): δ = 152.5, 143.6, 143.0, 140.7, 137.9, 135.6, 126.1 (2), 124.9, 117.9 (2), 114.6, 31.7, 29.9 ppm; ^{19}F NMR (470

MHz, DMSO-d_6): –60.0 ppm; HRMS (ESI) *m/z* (%): 637.2039 (100, $[M+H]^+$, calcd for $C_{34}H_{27}F_6N_4O_2^+$: 637.2033), 636.1961 (57, $[M]^+$, calcd for $C_{34}H_{26}F_6N_4O_2^+$: 636.1954).

(*E*)-Bis(*p*-nitrophenylurea) [(*E*)-1c)]: General procedure A was followed to afford (*E*)-**1c** (54 mg, 92%) as a yellow solid; M.p. >343 °C (decomp); ^{1}H NMR (400 MHz, DMSO-d_6): δ = 9.43 (s, 2 H; NH), 8.97 (s, 2 H; NH), 8.20 (d, *J* = 9.2 Hz, 4 arom. H), 7.94 (s, 2 arom. H), 7.71 (d, *J* = 9.3 Hz, 4 arom. H), 7.31-7.12 (m, 4 arom. H), 3.16-3.03 (m, 8 H; CH_2); too insoluble for a ^{13}C NMR measurement; HRMS (ESI) *m/z* (%): 591.1990 (100, $[M+H]^+$, calcd for $C_{32}H_{27}N_6O_6^+$: 591.1987), 590.1913 (91, $[M]^+$, calcd for $C_{32}H_{26}N_6O_6^+$: 590.1908).

(*E*)-Bis(*p*-trifluoromethylphenylthiourea) [(*E*)-2b)]: General procedure A was followed and washing was performed with CH_2Cl_2 in addition to THF to afford (*E*)-**2b** (43 mg, 67%) as a white solid; M.p. 231.5 – 232.1 °C; ^{1}H NMR (400 MHz, DMSO-d_6): 10.09 (s, 4 H; NH), 7.83 (s, 2 arom. H), 7.79-7.64 (m, 8 arom. H), 7.33-7.25 (m, 4 arom. H), 3.13-3.01 (m, 8 H; CH_2) ppm; ^{13}C NMR (125 MHz, DMSO-d_6, APT): δ = 179.6, 143.5 (2), 142.6, 137.6, 135.1, 125.6 (2), 124.7, 123.1, 122.7, 120.0, 31.7, 30.0 ppm, ^{19}F NMR (470 MHz, DMSO-d_6): –60.3 ppm; HRMS (ESI) *m/z*: 669.1574 ($[M+H]^+$, calcd for $C_{34}H_{27}F_6N_4S_2^+$: 669.1576).

(*E*)-Bis(*p*-nitrophenylthiourea) [(*E*)-2c)]: General procedure A was followed to afford (*E*)-**2c** (54 mg, 88%) as a yellow solid; M.p. 221.4 – 221.9 °C; ^{1}H NMR (400 MHz, DMSO-d_6): δ = 10.32 (s, 4 H; NH), 8.21 (d, *J* = 8.8 Hz, 4 arom. H), 7.88-7.82 (m, 6 arom. H), 7.34-7.27 (m, 4 arom. H), 3.14-3.02 (m, 8 H; CH_2) ppm; ^{13}C NMR (100 MHz, DMSO-d_6, APT): δ = 179.3, 146.4, 143.7, 142.6, 142.2, 137.4, 135.1, 124.8, 124.4, 123.0, 121.4, 119.9, 31.6, 30.1 ppm; HRMS (ESI) *m/z*: 623.1525 ($[M+H]^+$, calcd for $C_{32}H_{27}N_6O_4S_2^+$: 623.1530).

(*Z*)-Bis-*p*-trifluoromethylphenylurea [(*Z*)-1b)]: General procedure B was followed to afford (*Z*)-**1b** (47 mg, 75%) as a light-brown solid. M.p. >293 °C (decomp); ^{1}H NMR (400 MHz, DMSO-d_6): δ = 9.19 (s, 2 H; NH), 8.58 (s, 2 H; NH), 8.23 (s, 2 arom. H), 7.58 (d, *J* = 8.5 Hz, 4 arom. H), 7.40-7.31 (m, 6 arom. H), 7.25 (d, *J* = 8.2 Hz, 2 arom. H), 2.94-2.75 (m, 8 H; CH_2) ppm; ^{13}C NMR (125 MHz, DMSO-d_6, APT): δ = 152.4, 143.5, 141.8, 140.1, 137.1, 134.9, 125.9, 125.2, 117.9, 117.4, 113.9, 34.4, 29.4 ppm; ^{19}F NMR (470 MHz, DMSO-d_6): –60.4 ppm; HRMS (ESI) *m/z*: 637.2032 ($[M+H]^+$, calcd for $C_{34}H_{27}F_6N_4O_2^+$: 637.2033).

(*Z*)-Bis-*p*-nitrophenylurea [(*Z*)-1c)]: General procedure B was followed, with the modification that 1.5× the amount of reactants and solvent was used, to afford (*Z*)-**1c** (85 mg, 96%) as a brown solid; M.p. >188 °C (decomp); ^{1}H NMR (400 MHz, DMSO-d_6): δ = 9.44 (s, 2 H; NH), 8.68 (s, 2 H; NH), 8.32 (s, 2 arom. H), 7.90 (d, J = 9.2 Hz, 4 arom. H), 7.55 (d, J = 9.2 Hz, 4 arom. H), 7.33 (d, J = 8.1 Hz, 2 arom. H), 7.26 (d, J = 8.2 Hz, 2 arom H.), 2.95-2.76 (m, 8 H; CH_2) ppm; ^{13}C NMR (100 MHz, DMSO-d_6, APT): δ = 152.0, 146.4, 142.1, 140.6, 140.1, 136.8, 135.0, 125.2, 124.9, 118.0, 117.1, 114.0, 34.4, 29.4 ppm; HRMS (ESI) *m/z* (%): 591.1979 (100, $[M+H]^+$, calcd for $C_{32}H_{27}N_6O_6^+$: 591.1987), 590.1907 (32, $[M]^+$, calcd for $C_{32}H_{26}N_6O_6^+$: 590.1908).

(*Z*)-Bis-*p*-trifluoromethylphenylthiourea [(*Z*)-2b)]: General procedure B was followed, with the modification that 2 equivalents of triethylamine (0.20 mmol) were added, to afford (*Z*)-**2b** (41 mg, 66%) as a white solid; M.p. >195 °C (decomp); ^{1}H NMR (400 MHz, DMSO-d_6): δ = 10.11 (s, 2 H; NH), 9.91 (s, 2 H; NH), 8.19 (s, 2 arom. H), 7.76 (d, J = 8.4 Hz, 4 arom. H), 7.47 (d, J = 8.5 Hz, 4 arom. H), 7.30-7.21 (m, 4 arom. H), 2.96-2.77 (m, 8 H; CH_2) ppm; ^{13}C NMR (125 MHz, DMSO-d_6, APT): δ = 179.4, 144.8, 143.4, 139.9, 137.0, 134.9, 125.4, 124.9, 123.7, 122.2, 119.1, 34.8, 29.6 ppm; ^{19}F NMR (470 MHz, DMSO-d_6): –60.5 ppm; HRMS (ESI) *m/z*: 669.1585 ($[M+H]^+$, calcd for $C_{34}H_{27}F_6N_4S_2^+$: 669.1576).

(*Z*)-Bis-*p*-nitrophenylthiourea [(*Z*)-2c)]: General procedure B was followed, with the modification that 2 equivalents of triethylamine (0.20 mmol) were added, to afford (*Z*)-**2c** (40 mg, 68%) as a yellow solid; M.p. >229 °C (decomp); ^{1}H NMR (400 MHz, DMSO-d_6): δ = 10.38 (s, 2 H; NH), 10.08 (s, 2 H; NH), 8.22 (s, 2 arom. H), 7.98 (d, J = 9.1 Hz, 4 arom. H), 7.82 (d, J = 9.1 Hz, 4 arom. H), 7.31 (d, J = 8.0 Hz, 2 arom. H), 7.21 (d, J = 8.1 Hz, 2 arom. H), 2.98-2.80 (m, 8 H; CH_2) ppm; ^{13}C NMR (125 MHz, DMSO-d_6, APT): δ = 179.2, 146.3, 145.1, 141.8, 139.9, 136.8, 134.9, 125.0, 124.2, 123.8, 120.9, 119.4, 34.8, 29.6 ppm; HRMS (ESI) *m/z*: 623.1538 ($[M+H]^+$, calcd for $C_{32}H_{27}N_6O_4S_2^+$: 623.1530).

^{1}H, ^{13}C, and ^{19}F NMR spectra of new compounds

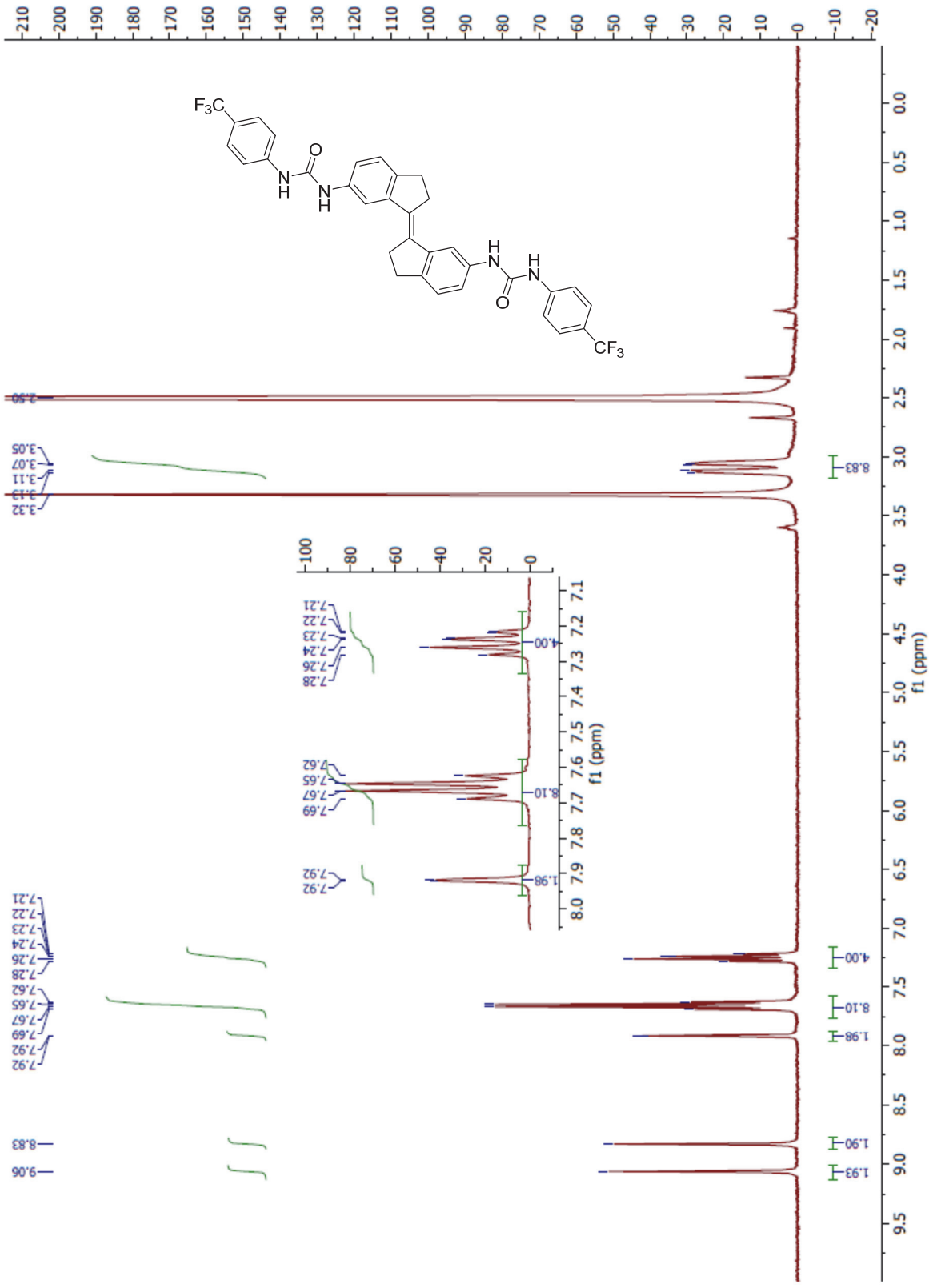

Figure S1. 400 MHz ^{1}H NMR spectrum of (*E*)-**1b** measured at 298 K in DMSO-*d*$_6$.

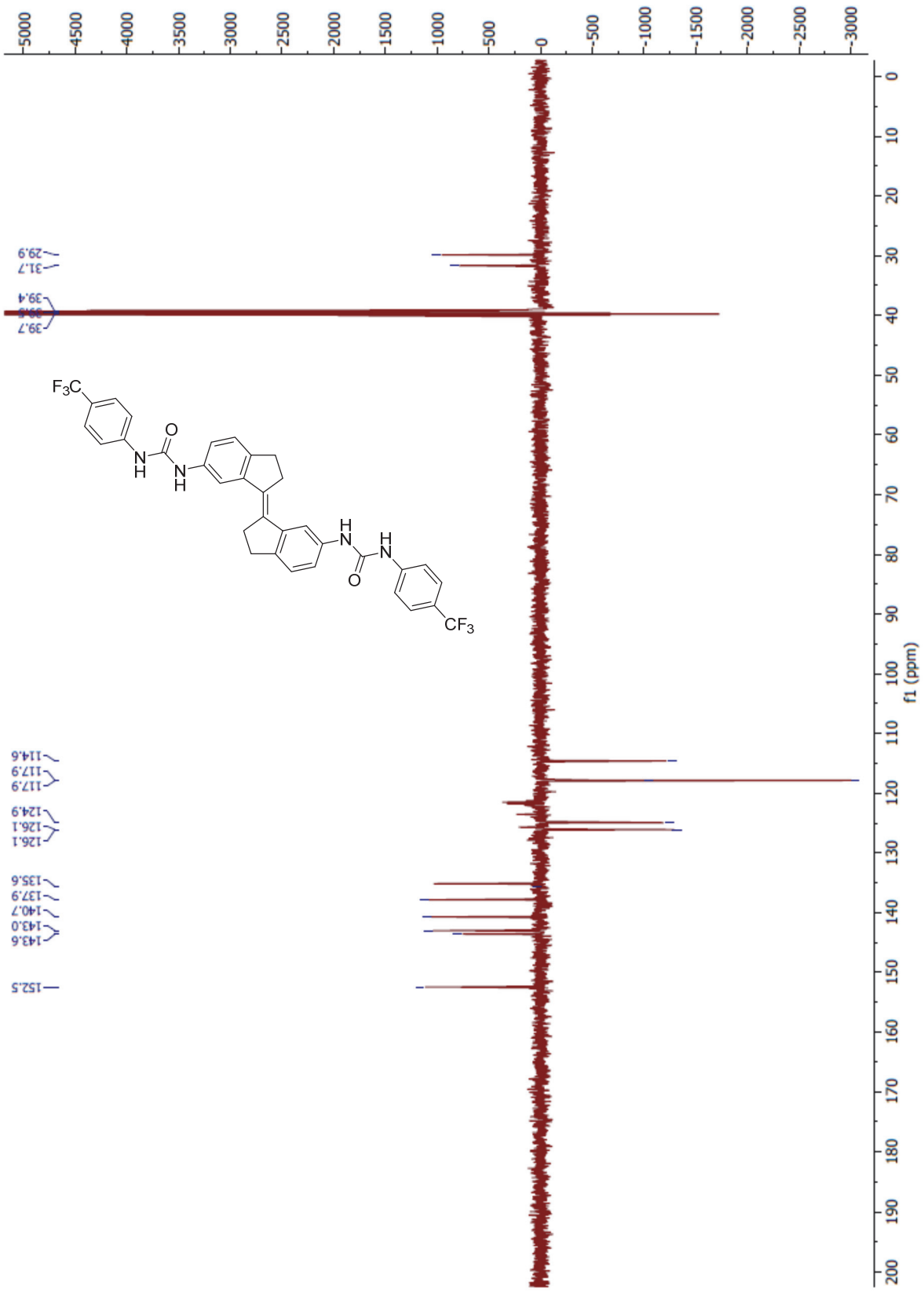

Figure S2. 125 MHz ^{13}C NMR (APT) spectrum of (*E*)-**1b** measured at 298 K in DMSO-d_6.

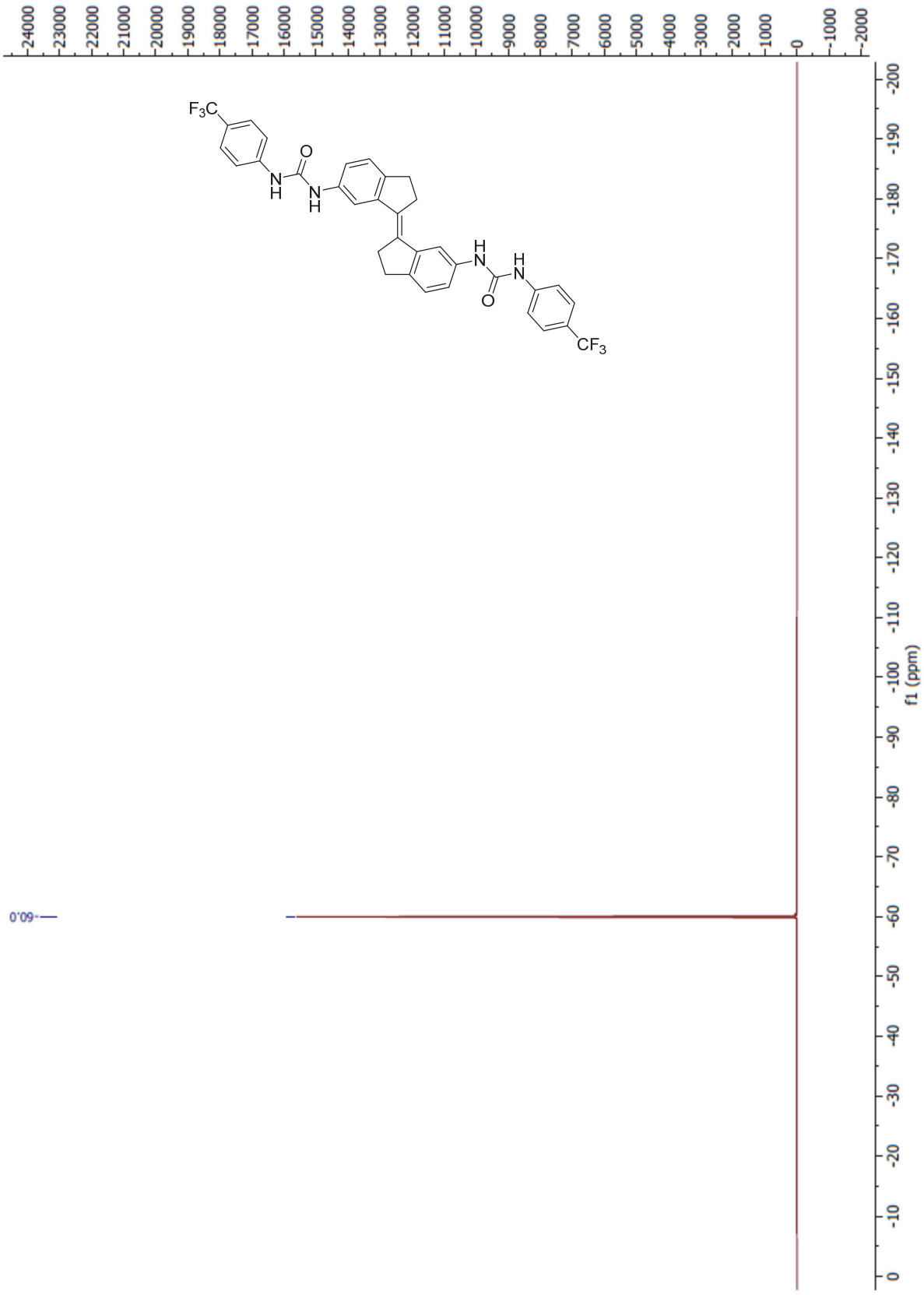

Figure S3. 470 MHz ^{19}F NMR spectrum of (*E*)-**1b** measured at 298 K in DMSO-d_6.

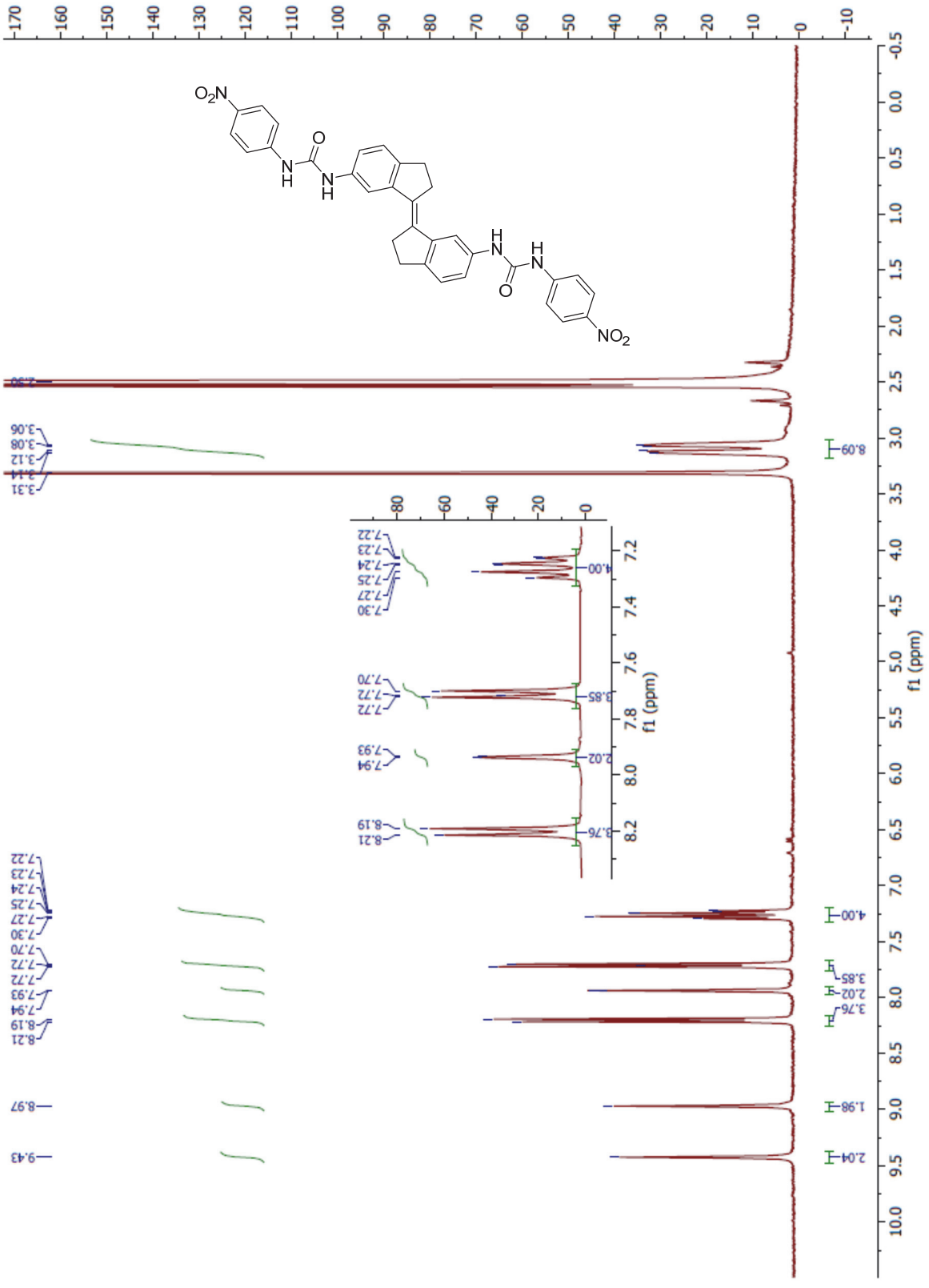

Figure S4. 400 MHz ^{1}H NMR spectrum of (*E*)-**1c** measured at 298 K in DMSO-d_6.

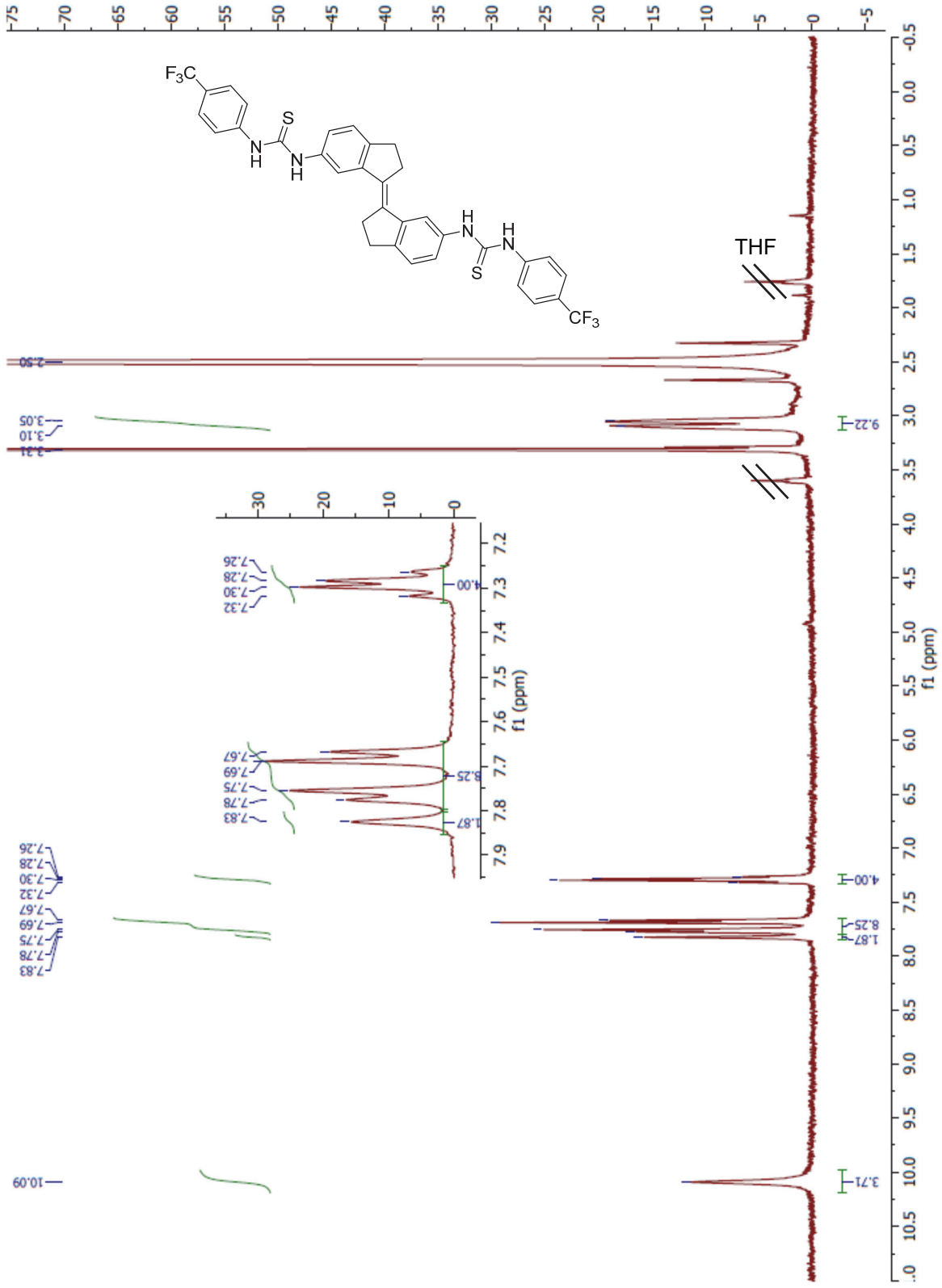

Figure S5. 400 MHz ^{1}H NMR spectrum of (*E*)-**2b** measured at 298 K in DMSO-d_6.

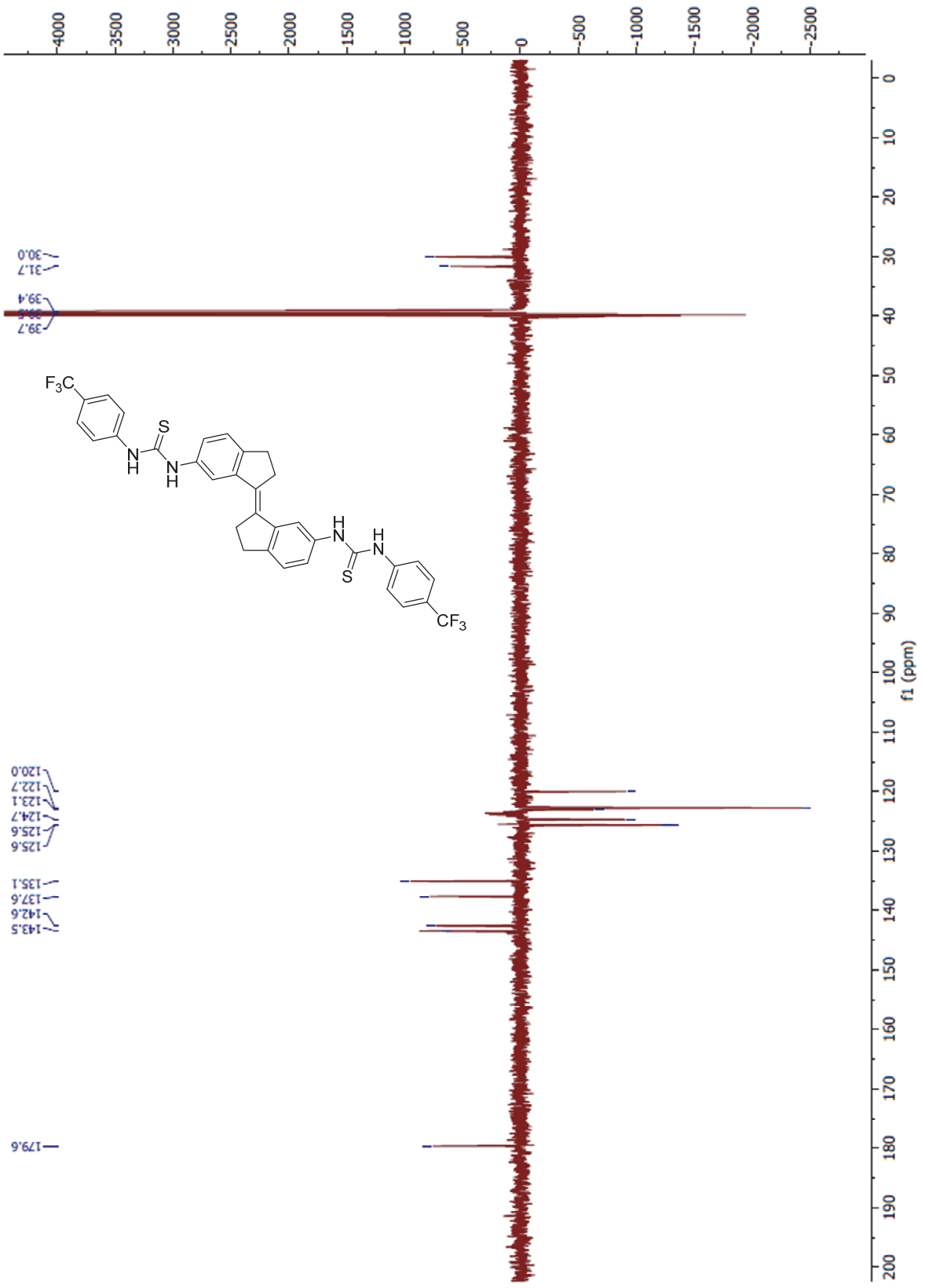

Figure S6. 125 MHz ^{13}C NMR (APT) spectrum of (*E*)-**2b** measured at 298 K in DMSO-d_6.

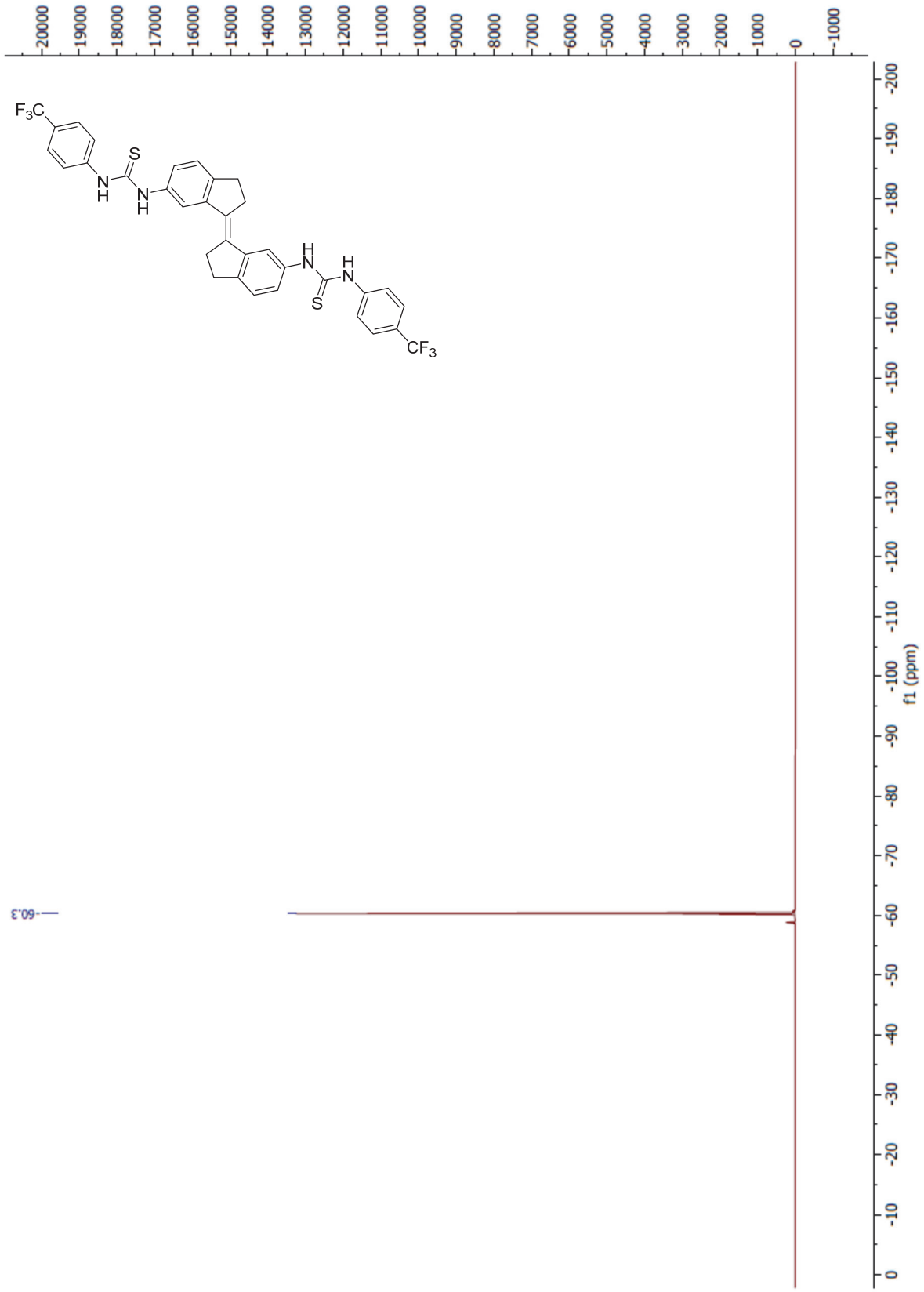

Figure S7. 470 MHz ^{19}F NMR spectrum of (*E*)-**2b** measured at 298 K in DMSO-d_6.

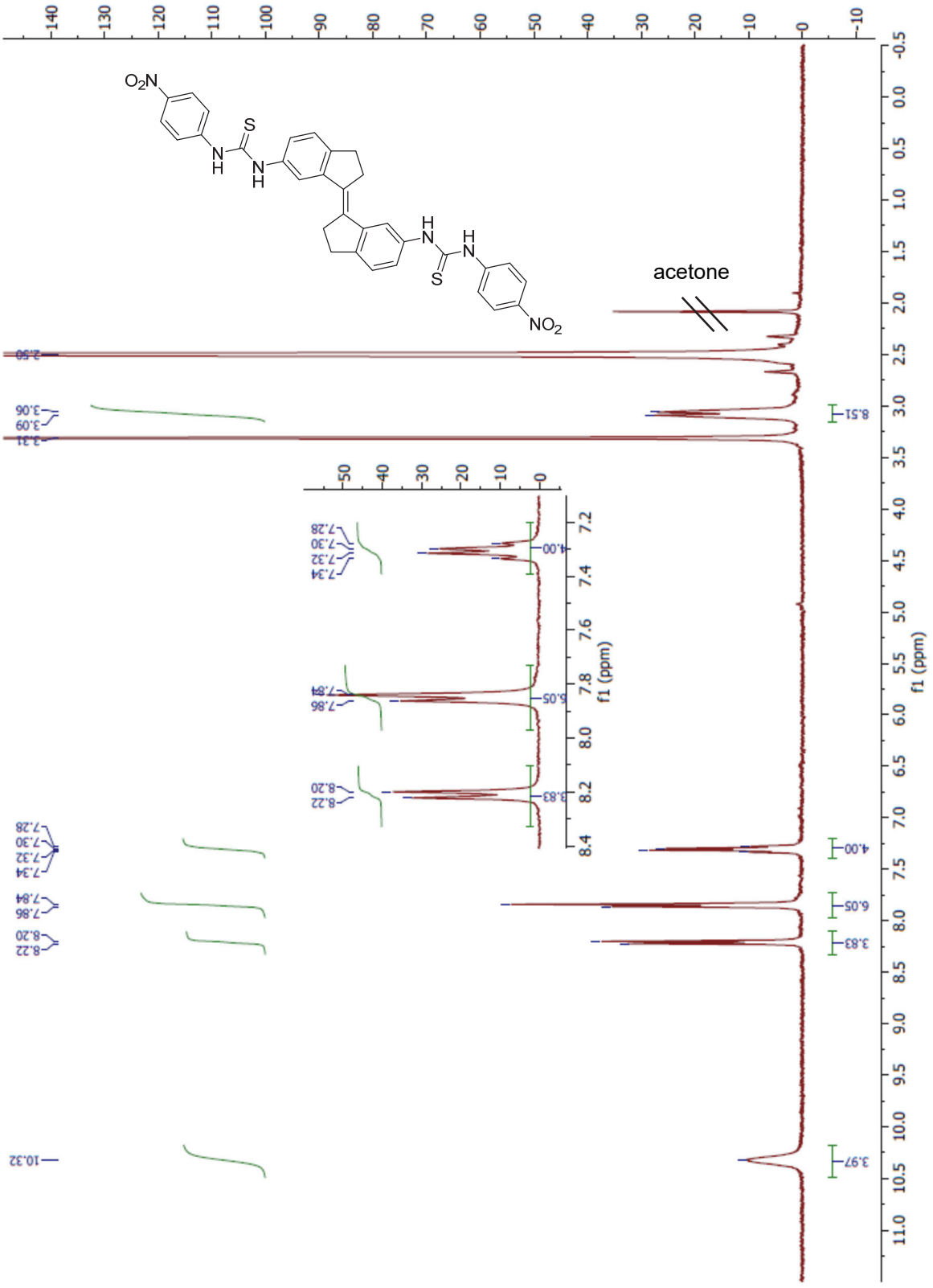

Figure S8. 400 MHz ^{1}H NMR spectrum of (*E*)-**2c** measured at 298 K in DMSO-*d*$_6$.

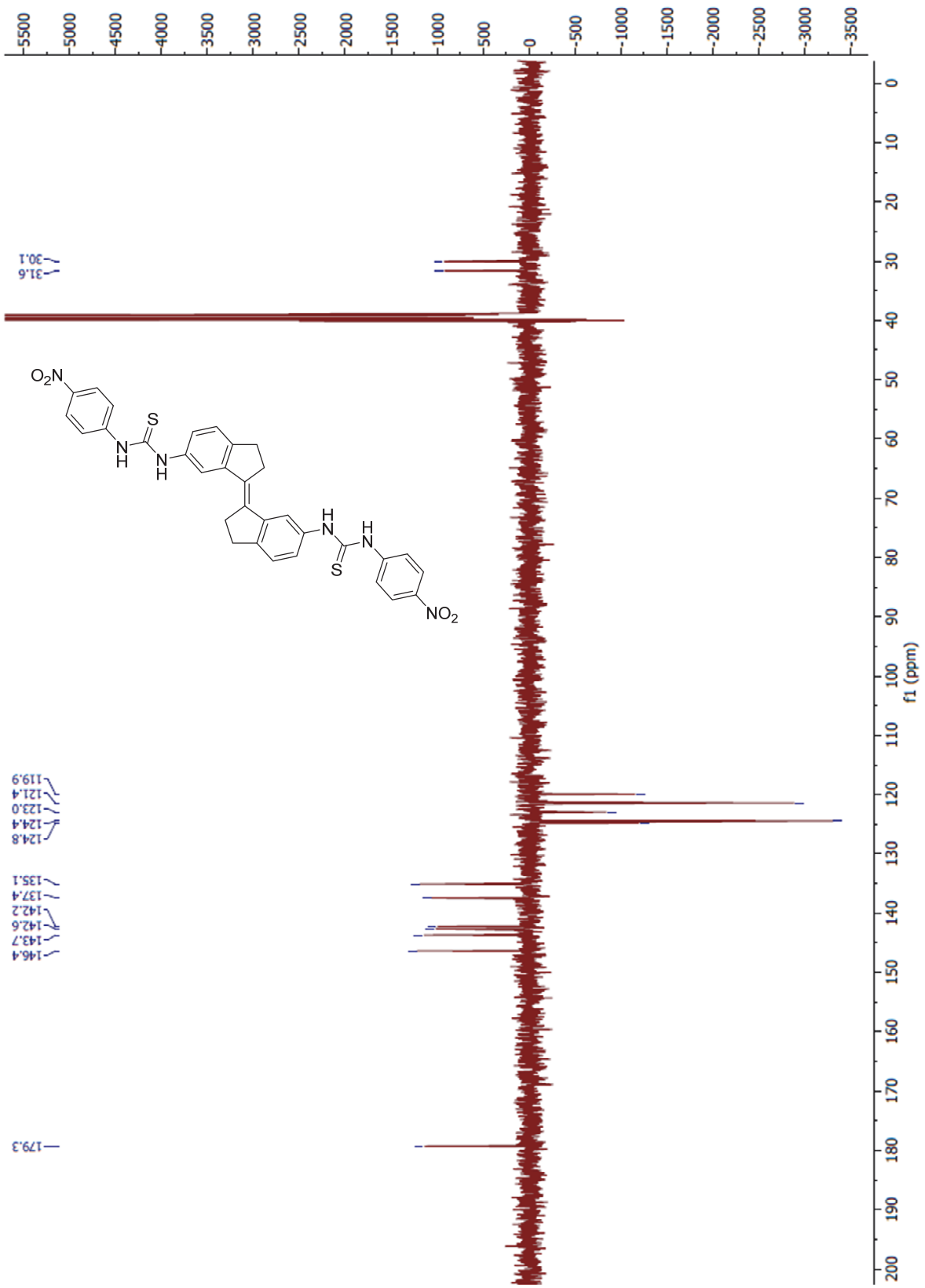

Figure S9. 100 MHz ^{13}C NMR (APT) spectrum of (*E*)-**2c** measured at 298 K in DMSO-*d*$_6$.

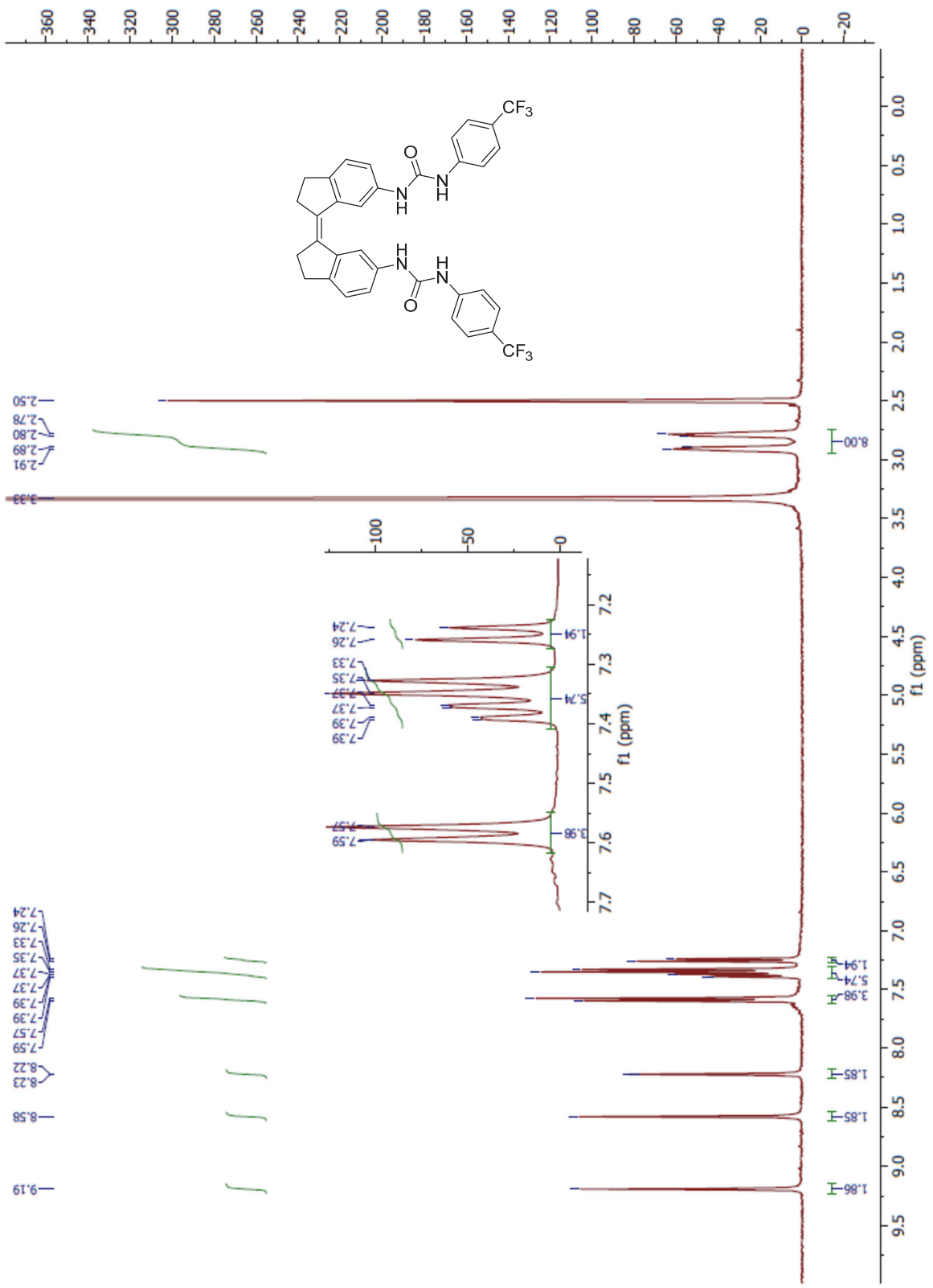

Figure S10. 400 MHz ^{1}H NMR spectrum of (*Z*)-**1b** measured at 298 K in DMSO-d_6.

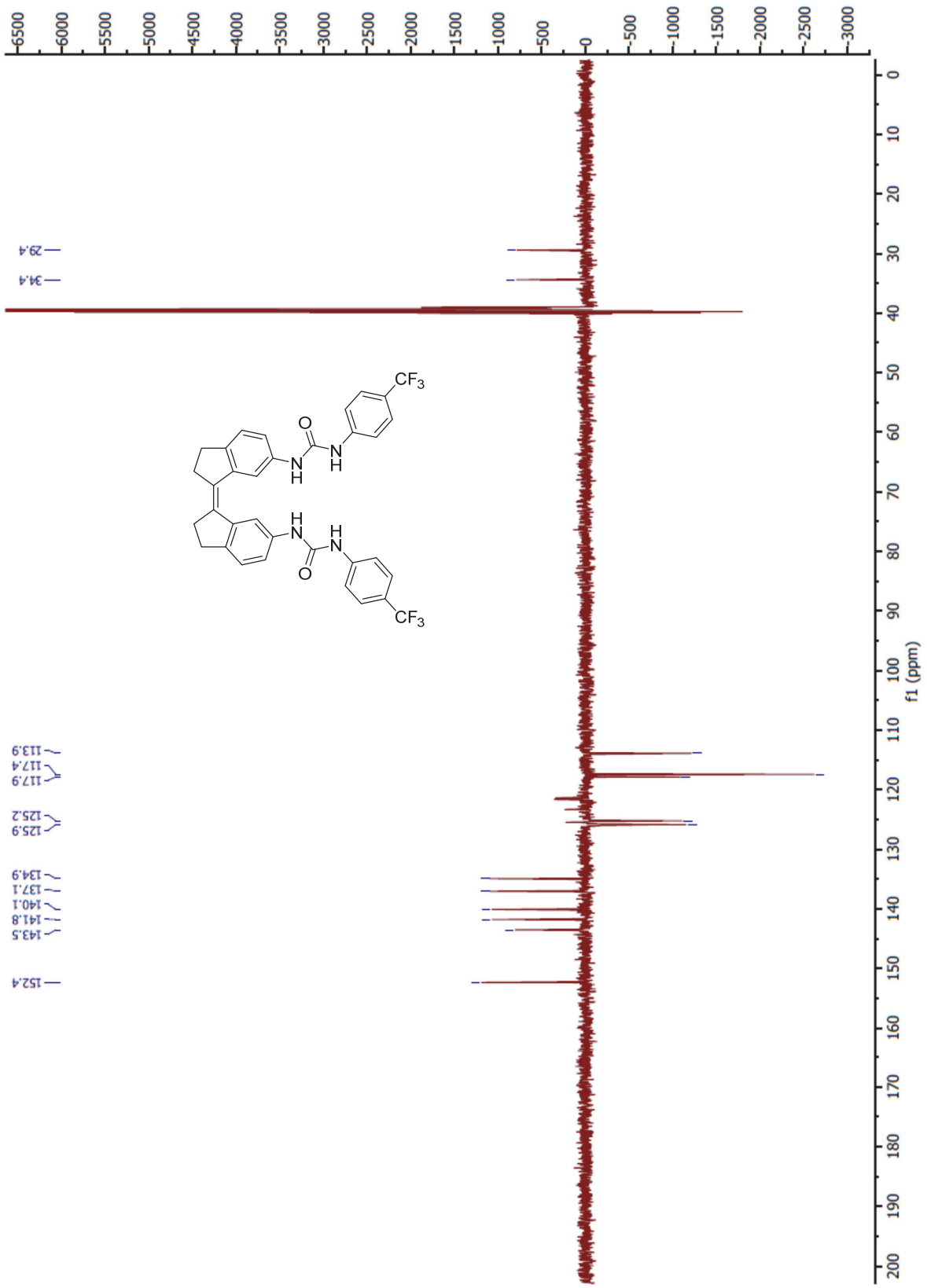

Figure S11. 125 MHz ^{13}C NMR (APT) spectrum of (*Z*)-**1b** measured at 298 K in DMSO-*d*$_6$.

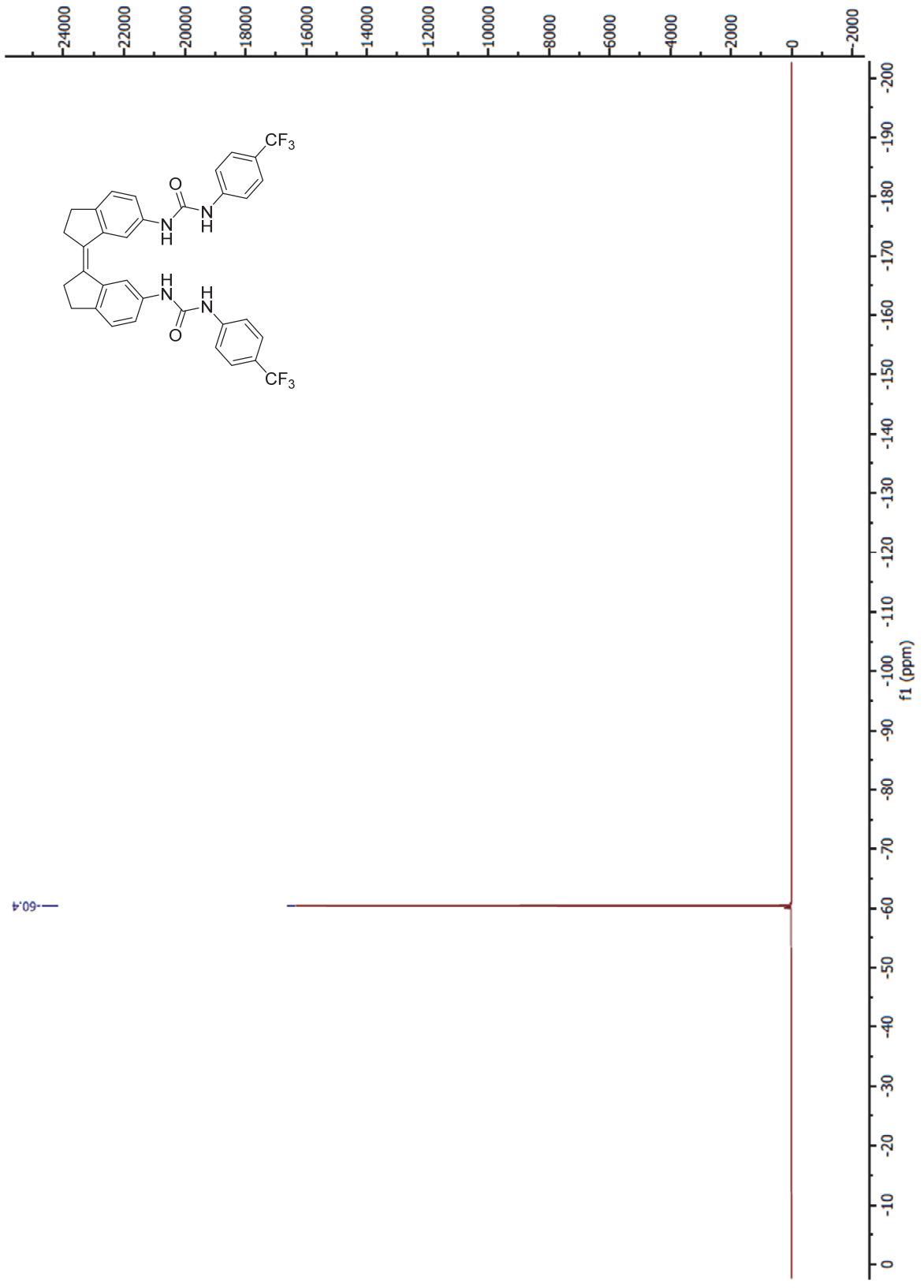

Figure S12. 470 MHz ^{19}F NMR spectrum of (*Z*)-**1b** measured at 298 K in DMSO-d_6.

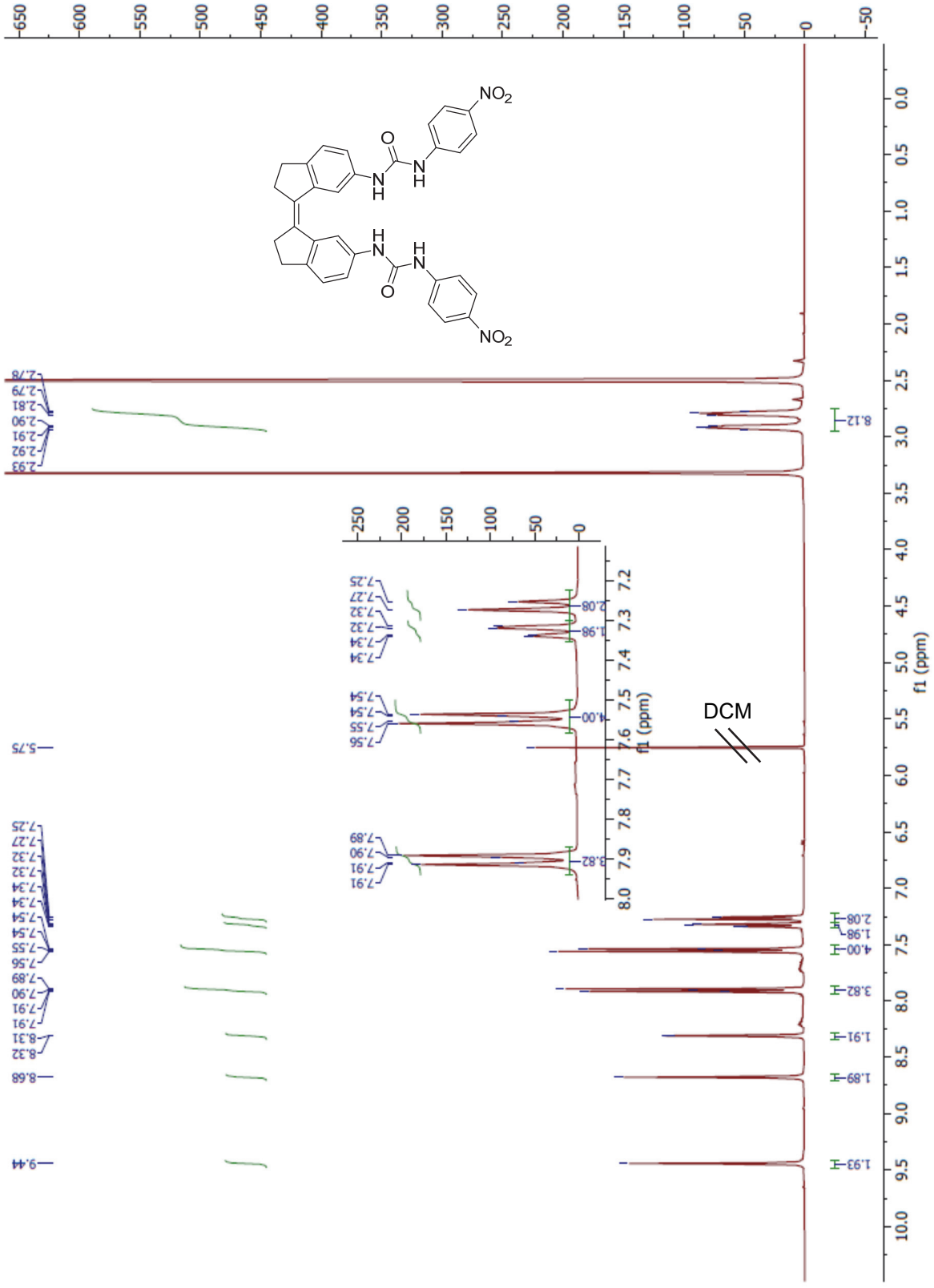

Figure S13. 400 MHz ^{1}H NMR spectrum of (*Z*)-**1c** measured at 298 K in DMSO-d_6.

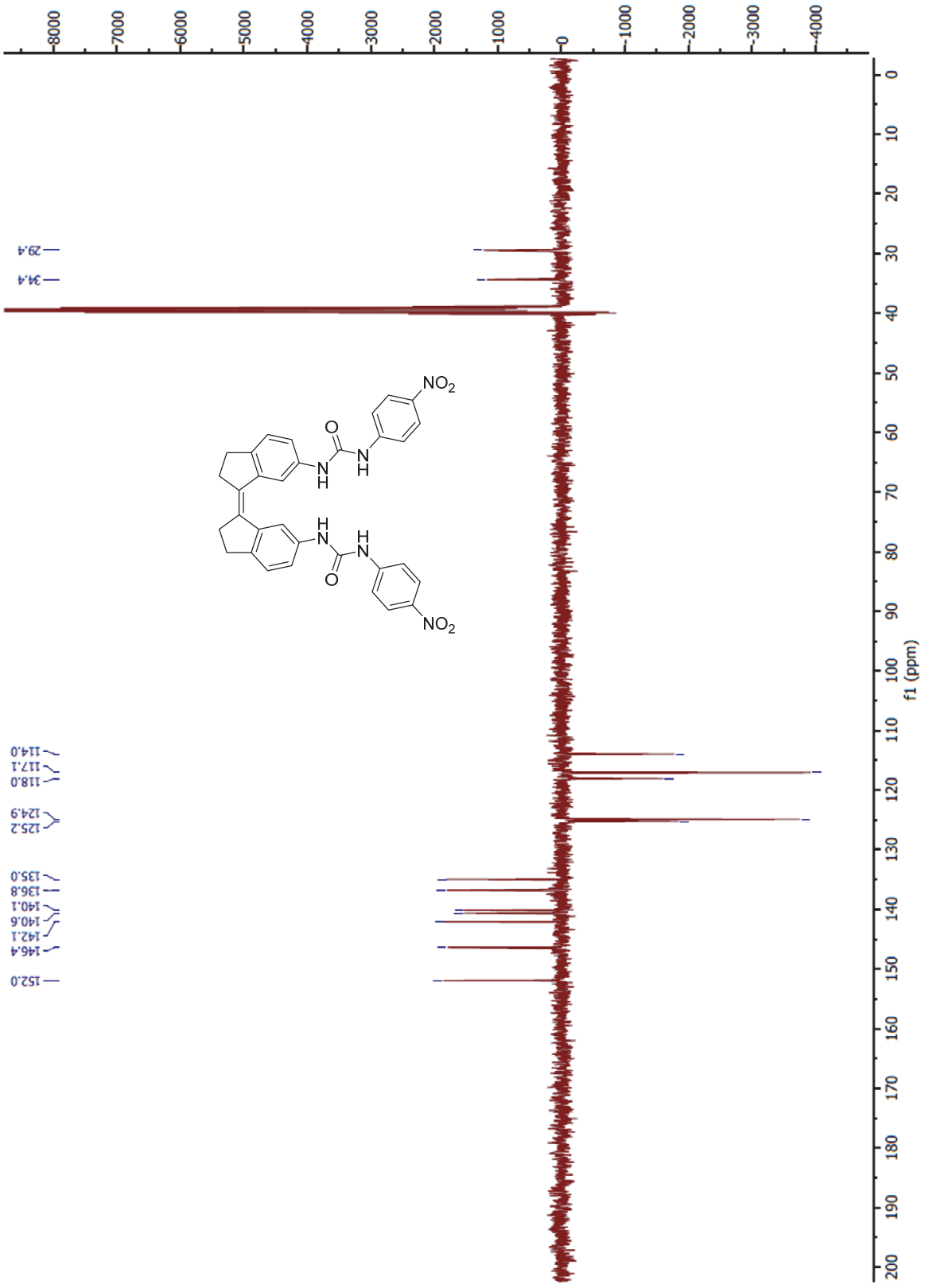

Figure S14. 100 MHz ^{13}C NMR (APT) spectrum of (*Z*)-**1c** measured at 298 K in DMSO-*d*$_6$.

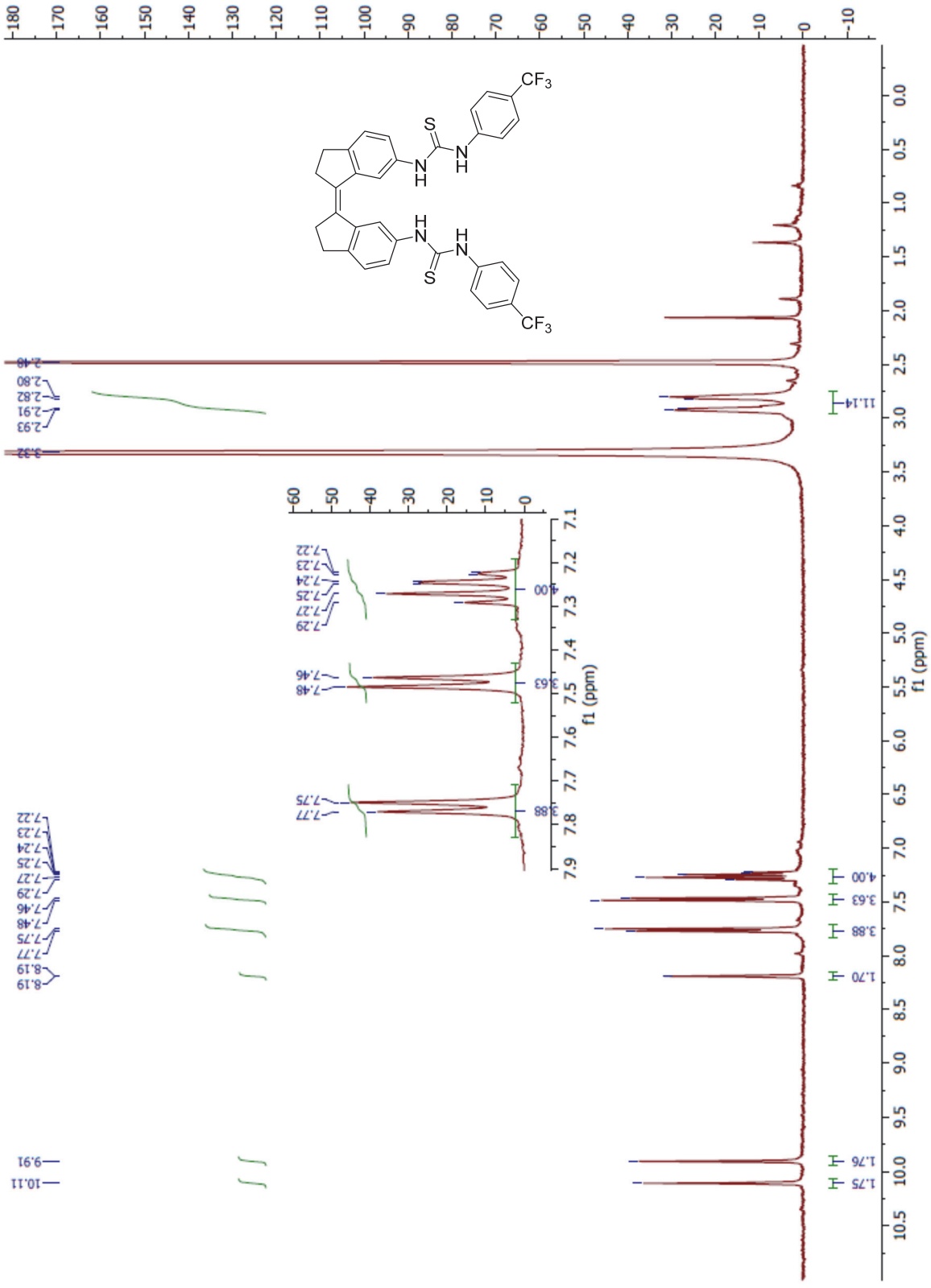

Figure S15. 400 MHz ^{1}H NMR spectrum of (*Z*)-**2b** measured at 298 K in DMSO-d_6.

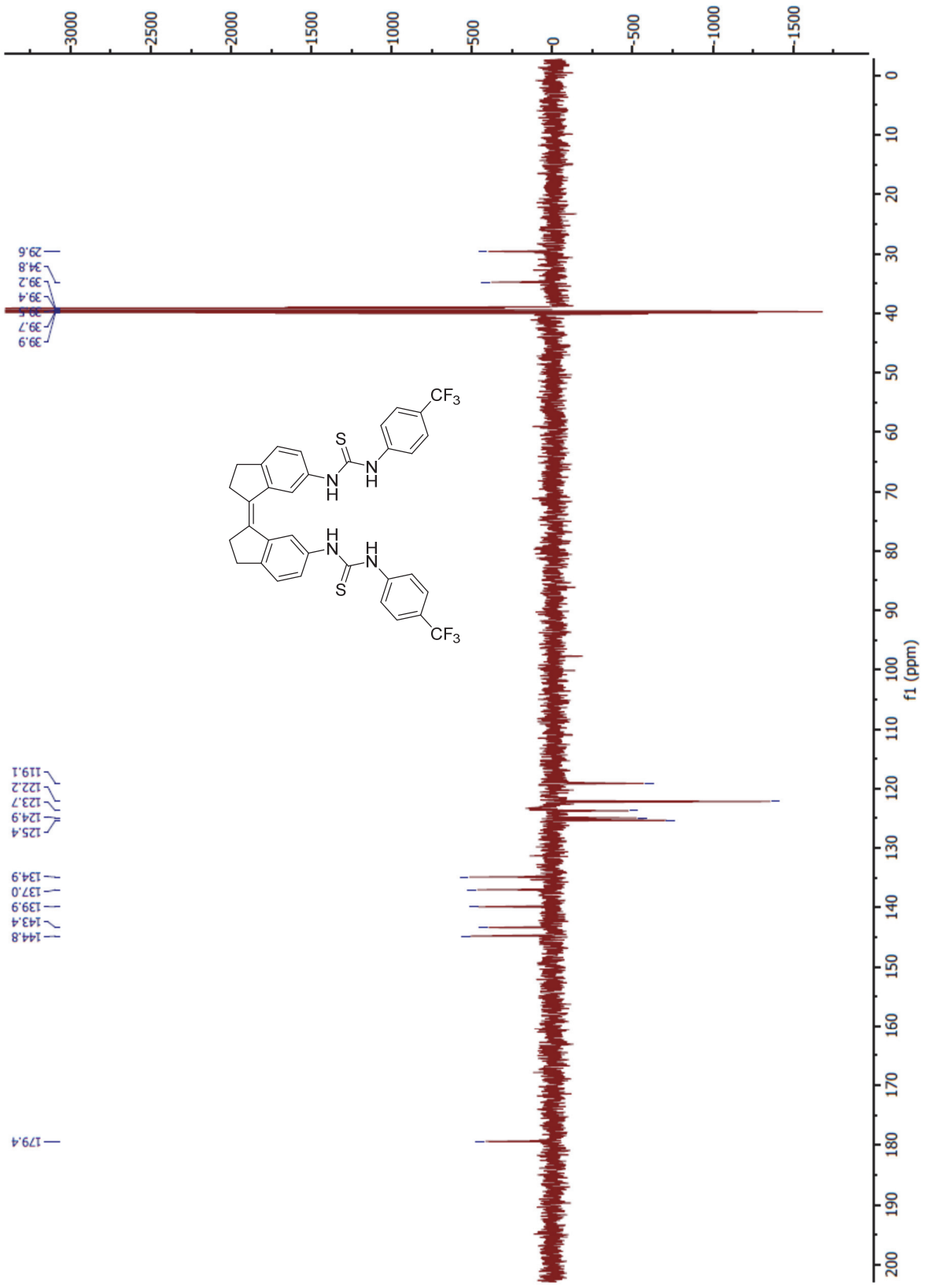

Figure S16. 125 MHz ^{13}C NMR (APT) spectrum of (*Z*)-**2b** measured at 298 K in DMSO-*d*$_6$.

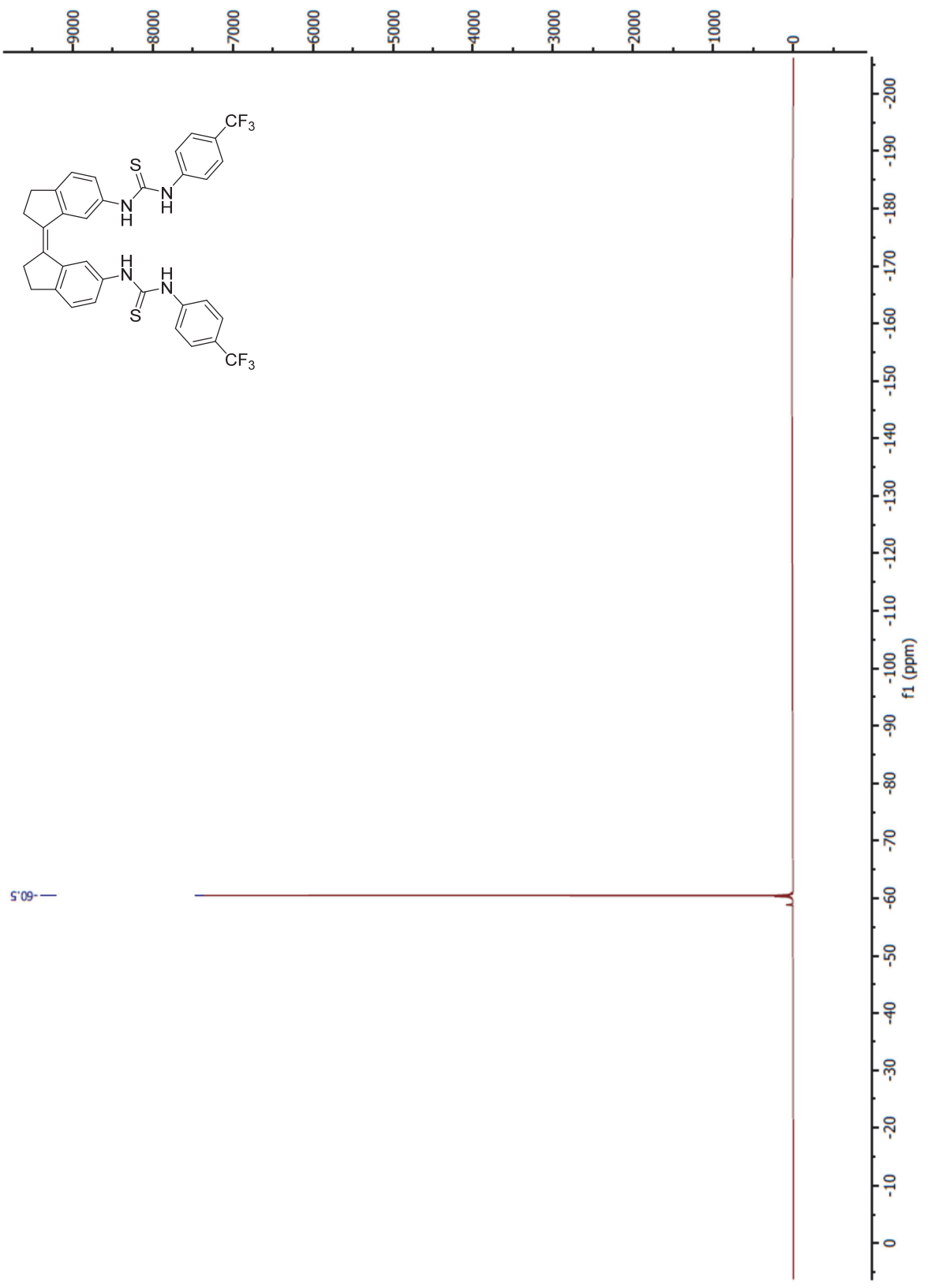

Figure S17. 470 MHz ^{19}F NMR spectrum of (*Z*)-**2b** measured at 298 K in DMSO-d_6.

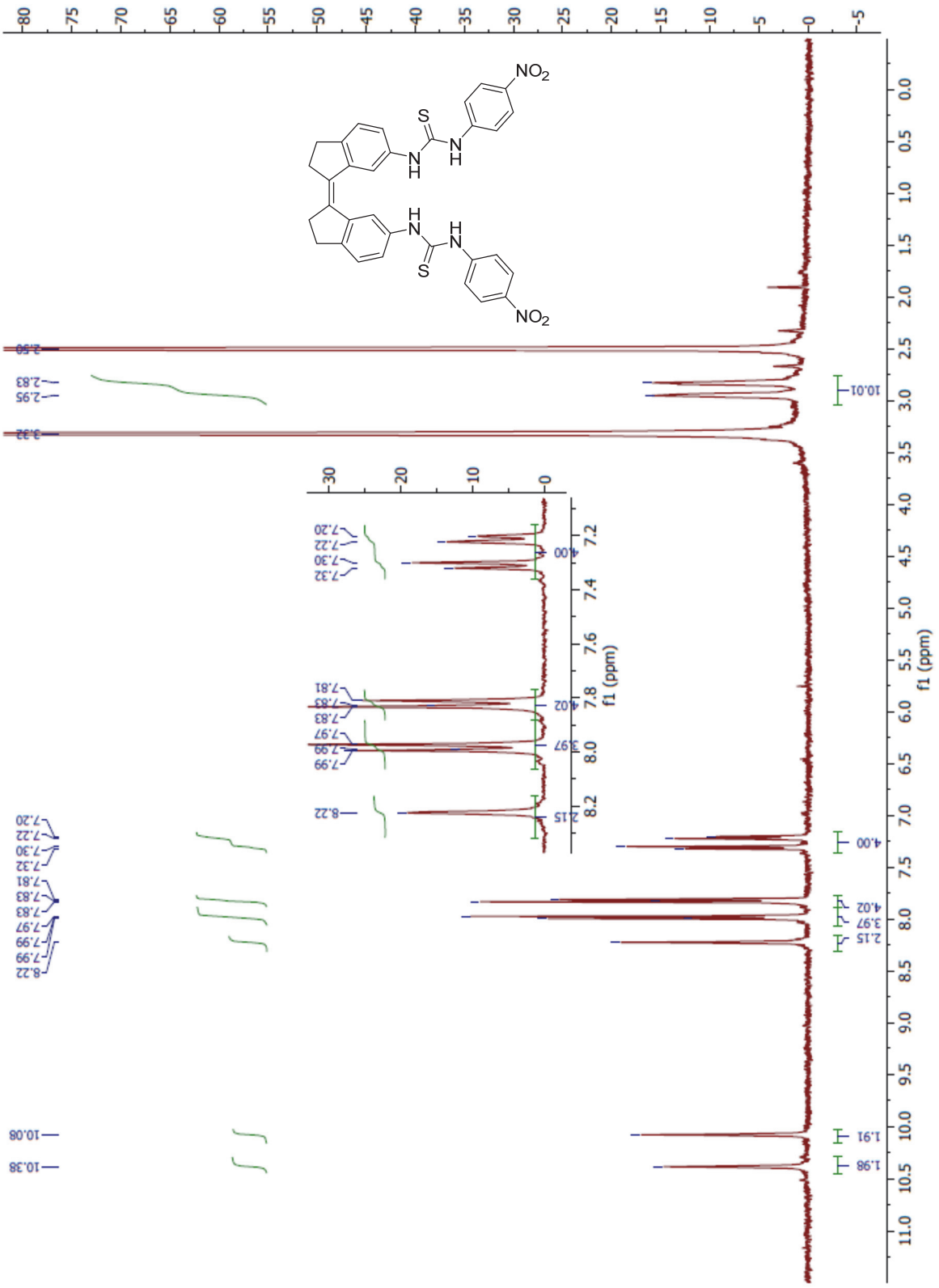

Figure S18. 400 MHz ^{1}H NMR spectrum of (*Z*)-**2c** measured at 298 K in DMSO-*d*$_6$.

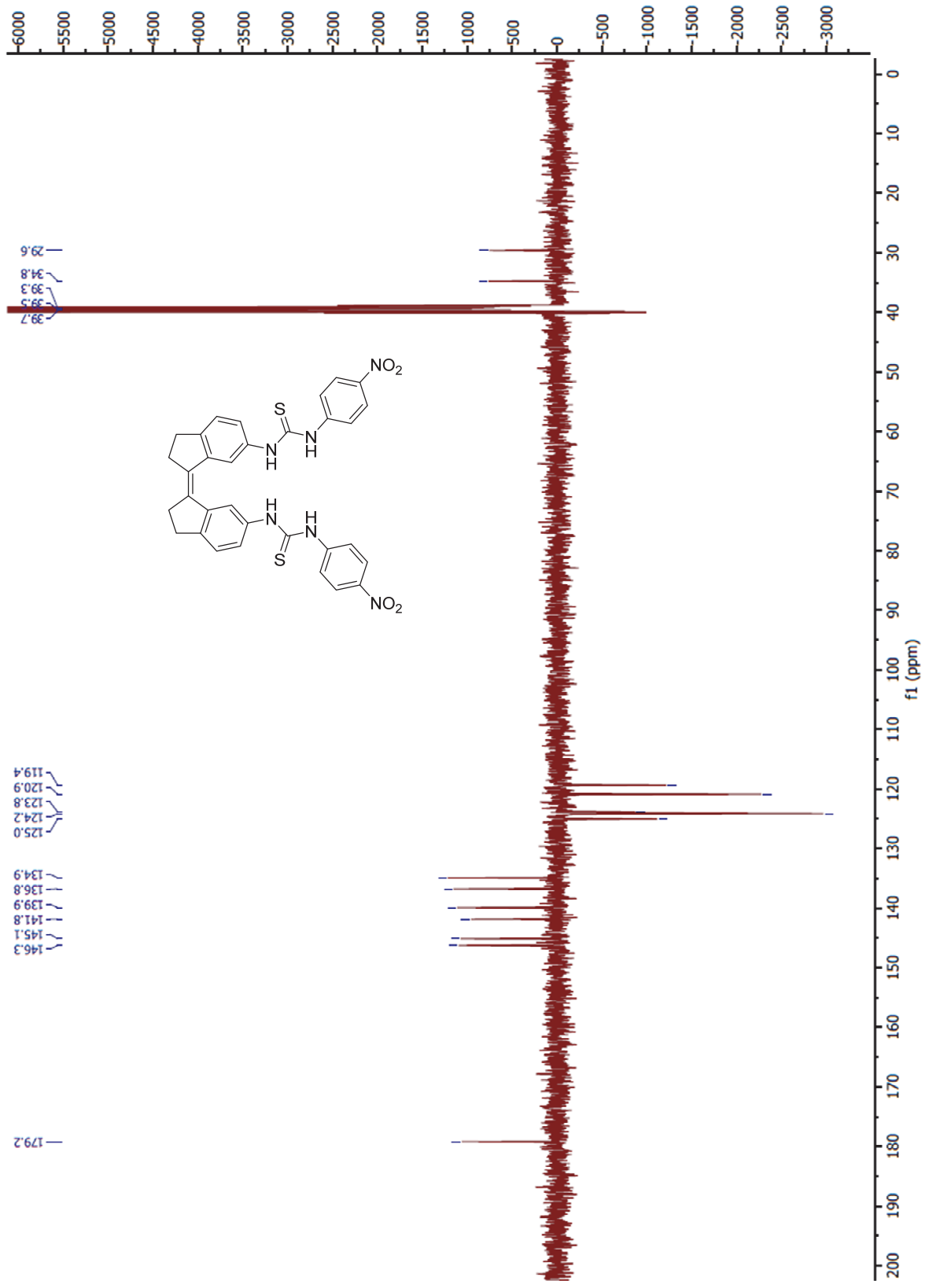

Figure S19. 100 MHz ^{13}C NMR (APT) spectrum of (*Z*)-**2c** measured at 298 K in DMSO-*d*6.

UV-Vis photoisomerization studies

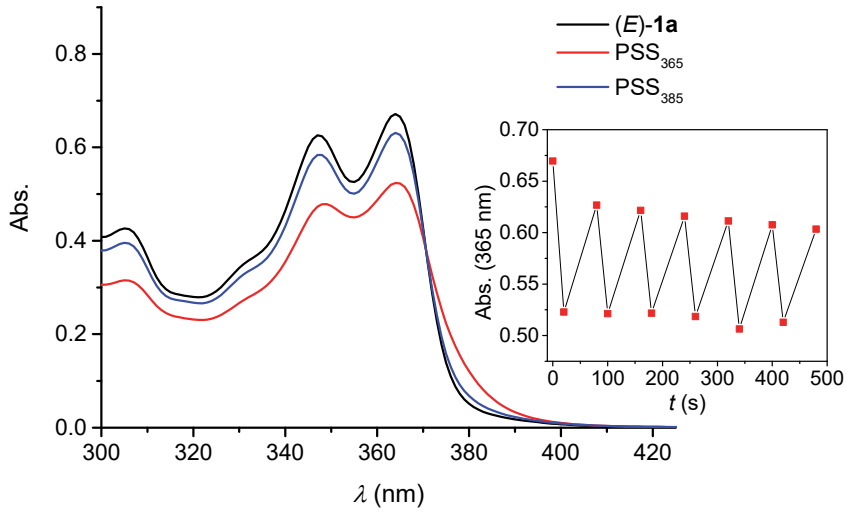

Figure S20. UV-Vis spectra of (*E*)-**1a** in degassed DMSO (2.5×10^{-4} M, 1 mm quartz cuvette) before and after irradiation with 365 nm and 385 nm light. The inset shows the change in absorption (λ = 365 nm) of the same sample upon multiple irradiation cycles.

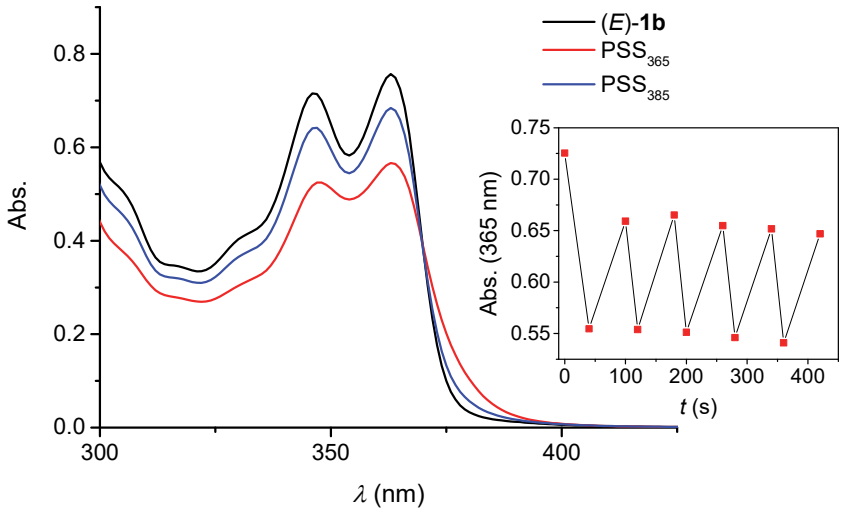

Figure S21. UV-Vis spectra of (*E*)-**1b** in degassed DMSO (2.5×10^{-4} M, 1 mm quartz cuvette) before and after irradiation with 365 nm and 385 nm light. The inset shows the change in absorption (λ = 365 nm) of the same sample upon multiple irradiation cycles.

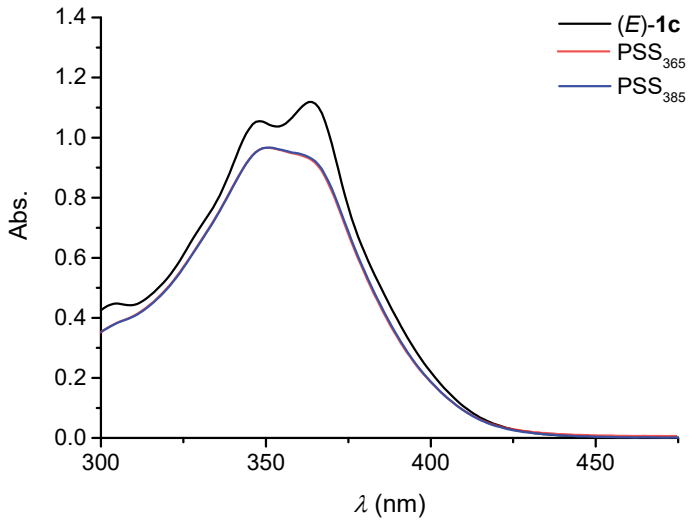

Figure S22. UV-Vis spectra of (*E*)-**1c** in degassed DMSO (2.5×10^{-4} M, 1 mm quartz cuvette) before and after irradiation with 365 nm and 385 nm light. Please note that as the PSS_{365} and PSS_{385} ratios are virtually the same, no 365/385 nm irradiation cycles were performed.

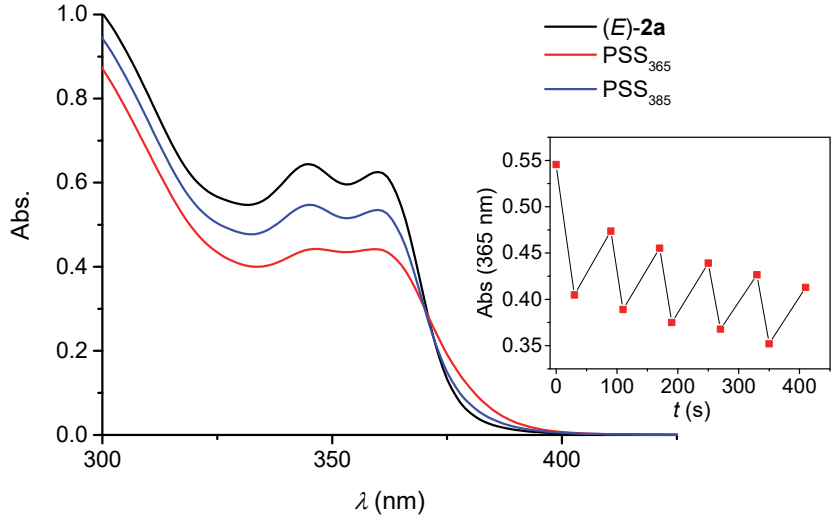

Figure S23. UV-Vis spectra of (*E*)-**2a** in degassed DMSO (2.5×10^{-4} M, 1 mm quartz cuvette) before and after irradiation with 365 nm and 385 nm light. The inset shows the change in absorption (λ = 365 nm) of the same sample upon multiple irradiation cycles.

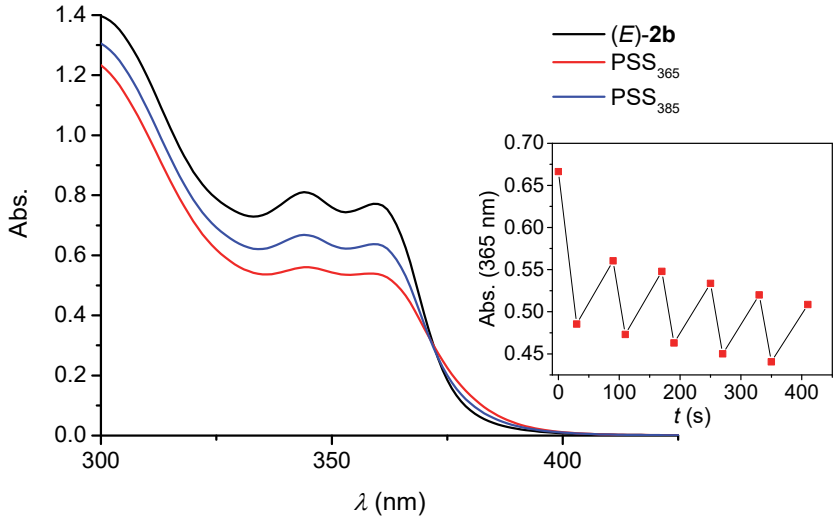

Figure S24. UV-Vis spectra of (*E*)-**2b** in degassed DMSO (2.5×10^{-4} M, 1 mm quartz cuvette) before and after irradiation with 365 nm and 385 nm light. The inset shows the change in absorption (λ = 365 nm) of the same sample upon multiple irradiation cycles.

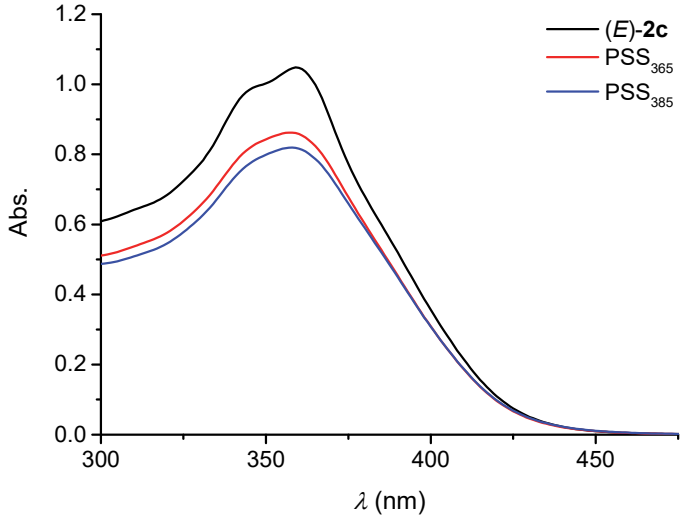

Figure S25. UV-Vis spectra of (*E*)-**2c** in degassed DMSO (2.5×10^{-4} M, 1 mm quartz cuvette) before and after irradiation with 365 nm and 385 nm light. The further decay in absorption upon 385 nm irradiation is likely due to some degradation, cf. PSS ratios in Figure S29.

The UV-Vis photoisomerization study with bis-thiourea **2a** in POPC vesicles (mean diameter 200 nm) was performed as follows. A solution of POPC and (*E*)-**2a** (1 mol% with respect to POPC) was concentrated under reduced pressure and further dried under vacuum for 12 h. The lipid film was hydrated by vortexing with a KCl solution (300 mM buffered to pH 7.2 with 5 mM HEPES) and subjected to 9 freeze-thaw cycles, after which it stood at rt for 30 min. Subsequently, the lipid suspension was extruded 25 times through a 200 nm polycarbonate membrane to obtain unilamellar vesicles with an average diameter of 200 nm. Immediately prior to the measurement, the liposome solution was diluted and degassed.

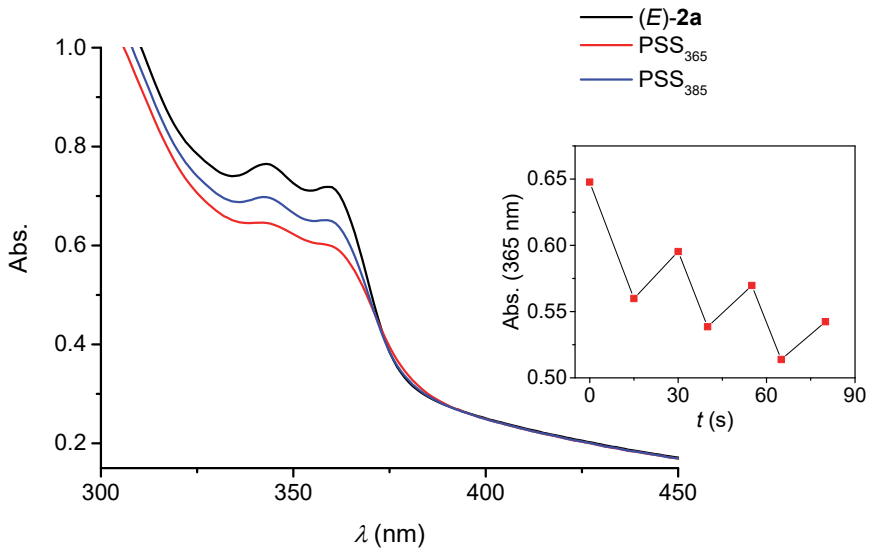

Figure S26. UV-Vis spectra of liposomes containing (*E*)-**2a** in degassed KCl buffer (9.1×10^{-5} M, 1 mol% with respect to lipids, 1 mm quartz cuvette) before and after irradiation with 365 nm and 385 nm light. The inset shows the change in absorption (λ = 365 nm) of the same sample upon multiple irradiation cycles. Note that part of the light is scattered by liposomes.

^{1}H NMR photoisomerization studies

The ^{1}H NMR photoisomerization study of compound **1a** was reported elsewhere.[1] This study was not performed for compound **1c** as the (*E*)-isomer was poorly soluble and precipitated.

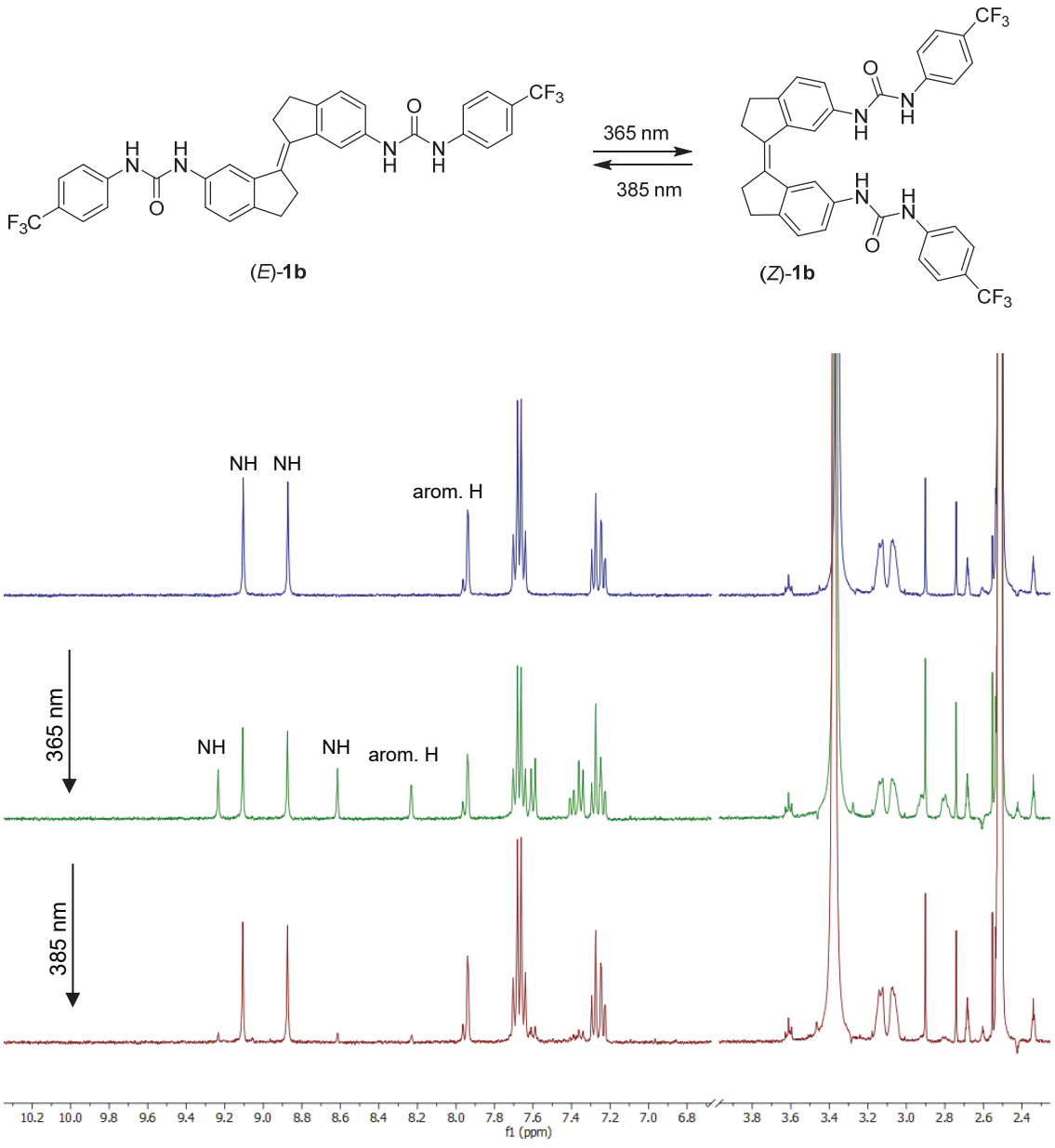

Figure S27. Aromatic and aliphatic regions in the ^{1}H NMR spectrum (400 MHz, 293 K) of (*E*)-**1b** (2 mM in degassed DMSO-d_6) before (top) and after irradiation at 365 nm for 20 min. (middle) and 385 nm for 20 min. (bottom). The PSS ratios were calculated by averaging the integrals of the indicated NH and arom. H signals, revealing a PSS_{365} ratio of 65:35 (*E*/*Z*) and a PSS_{385} ratio of 93:7 (*E*/*Z*). The signals at δ = 7.95, 2.89, and 2.73 ppm belong to a DMF trace impurity in the used solvent,[3] which is harmless in this experiment.

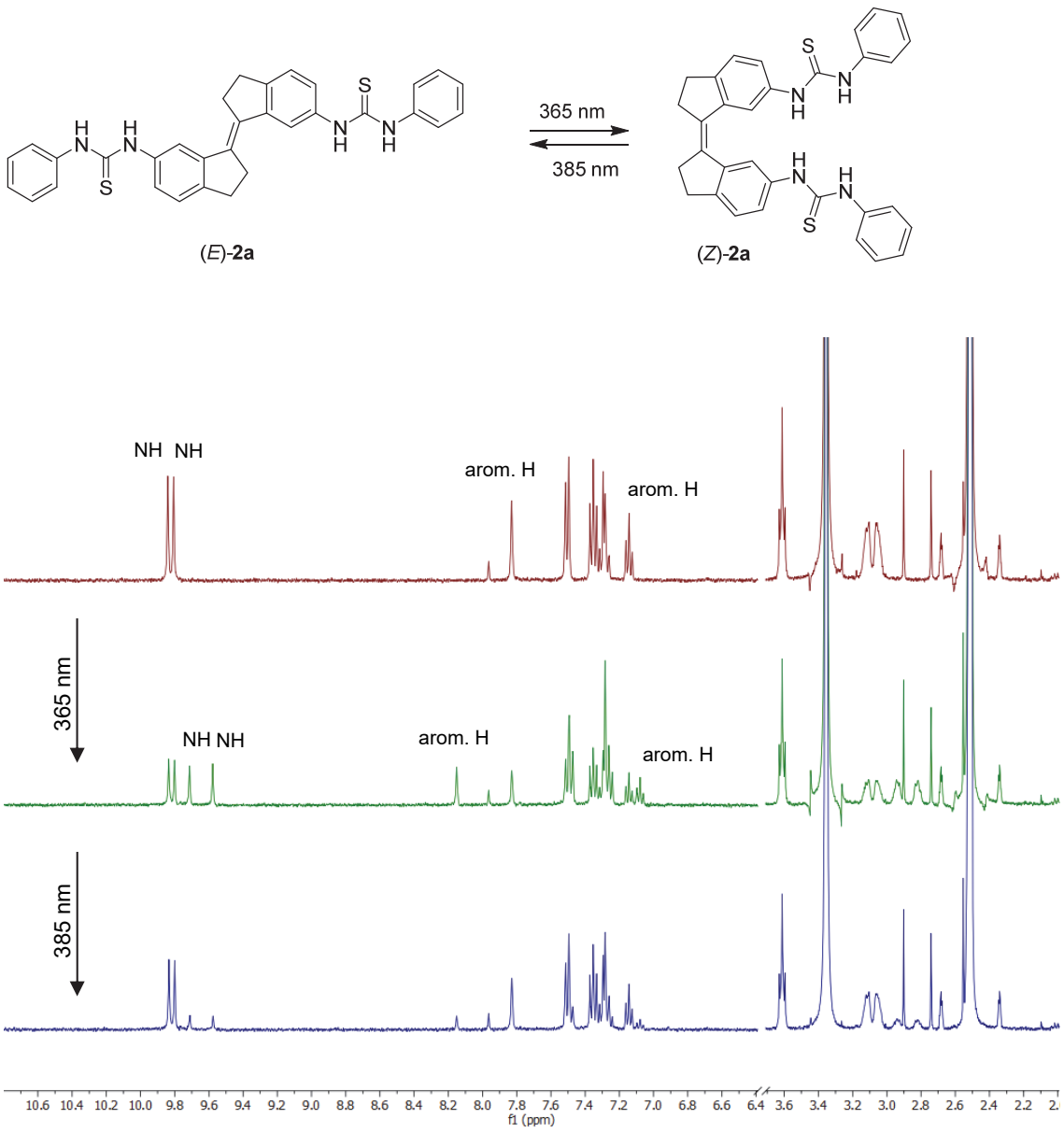

Figure S28. Aromatic and aliphatic regions in the ^{1}H NMR spectrum (400 MHz, 293 K) of (*E*)-**2a** (2 mM in degassed DMSO-d_6) before (top) and after irradiation at 365 nm for 20 min. (middle) and 385 nm for 20 min. (bottom). The PSS ratios were calculated by averaging the integrals of the indicated NH and arom. H signals, revealing a PSS_{365} ratio of 53:47 (*E*/*Z*) and a PSS_{385} ratio of 83:17 (*E*/*Z*). The signals at δ = 7.95, 2.89, and 2.73 ppm belong to a DMF trace impurity in the used degassed solvent,[3] which is harmless in this experiment.

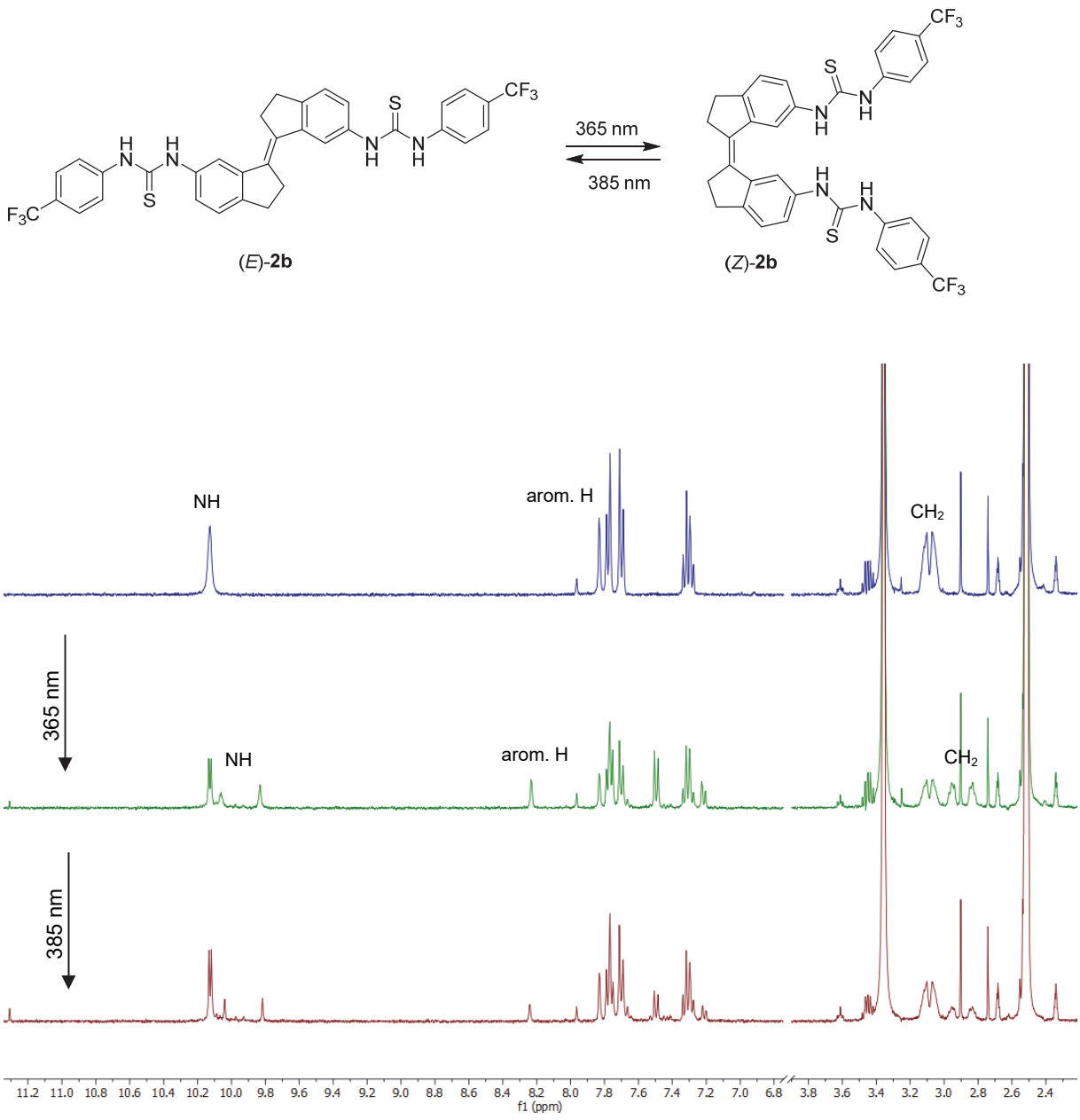

Figure S29. Aromatic and aliphatic regions in the ^{1}H NMR spectrum (400 MHz, 293 K) of (*E*)-**2b** (2 mM in degassed DMSO-d_6) before (top) and after irradiation at 365 nm for 20 min. (middle) and 385 nm for 20 min. (bottom). The PSS ratios were calculated by averaging the integrals of the indicated NH, arom. H, and CH_2 signals, revealing a PSS_{365} ratio of 53:47 (*E*/*Z*) and a PSS_{385} ratio of 74:26 (*E*/*Z*). The signals at δ = 7.95, 2.89, and 2.73 ppm belong to a DMF trace impurity in the used degassed solvent,[3] which is harmless in this experiment.

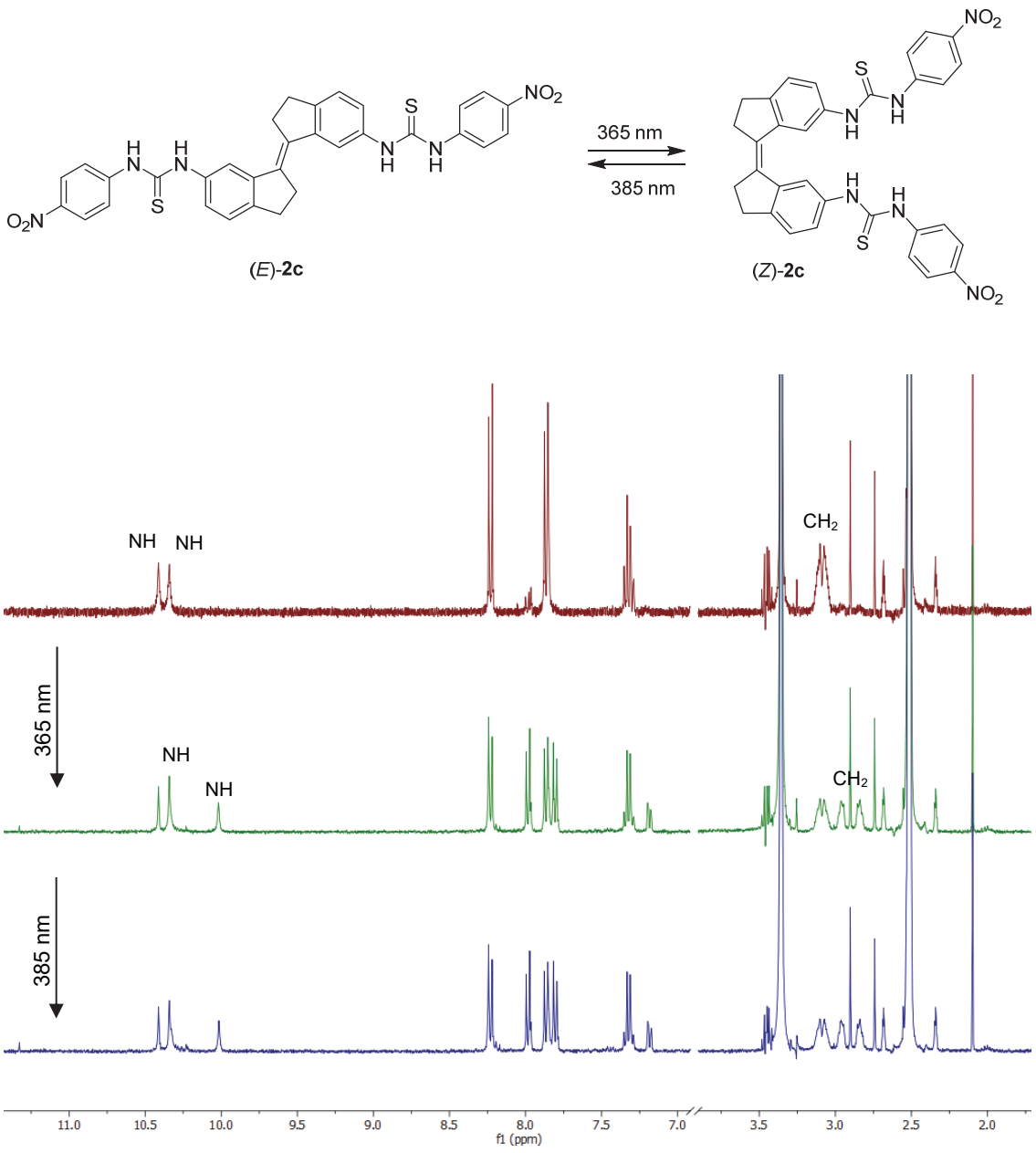

Figure S30. Aromatic and aliphatic regions in the ^{1}H NMR spectrum (400 MHz, 293 K) of (*E*)-**2c** (2 mM in degassed DMSO-d_6) before (top) and after irradiation at 365 nm for 20 min. (middle) and 385 nm for 10 min. (bottom). The PSS ratios were calculated by averaging the integrals of the indicated NH and CH_2 signals, revealing a PSS_{365} ratio of 48:52 (*E*/*Z*) and a PSS_{385} ratio of 48:52 (*E*/*Z*). The signals at δ = 7.95, 2.89, and 2.73 ppm belong to a DMF trace impurity in the used degassed solvent,[3] which is harmless in this experiment.

^{1}H NMR titrations and data fitting

Titrations and data fitting were carried out in the same manner as previously reported for compound **1a**.[1] That is, a 5 mM solution (in DMSO-d_6/0.5%H_2O) of the receptor was prepared (solution A) and $[Bu_4N]^+[Cl]^-$ was dissolved in this receptor solution to reach a concentration of about 50 mM (solution B). Solution B was then added stepwise to 0.5 mL of solution A and after each addition a ^{1}H NMR spectrum (500 MHz) was recorded. Compound (*E*)-**1c** was too insoluble for a ^{1}H NMR titration experiment.

As in the case of the (*E*)-isomers the (thio)urea groups will separately bind a chloride ion, the titration data obtained for these isomers was fitted to a 1:2 (receptor/chloride) binding model (Scheme S2). In the case of the (*Z*)-isomers, on the one hand, Job plot analysis pointed to 1:2 complex formation, while on the other, DFT calculations hinted at the simultaneous binding of the (thio)urea substituents to chloride in a 1:1 fashion as is also observed in the single crystal X-ray structure. Job's method may be unreliable when the system is not fully saturated and additionally, residual plots were compared of the data fits to either a 1:1 or 1:2 binding model.[4] This residual analysis, however, was also not conclusive and therefore, we based ourselves on DFT and solid-state analysis to assume that 1:1 binding is most likely.

In the data analysis using the 1:2 binding model, no clear distinction could be made between the ^{1}H NMR chemical shifts of the 1:1 and 1:2 complexes throughout the titration and hence, the two (thio)urea binding sites were treated as equal ($K_{1m} = K_{2m}$, cooperativity factor $\alpha = 1$). Furthermore, similar as described for the fitting to the 1:2 binding model for compound **1a**,[1] the data was first fitted to a 1:1 model first to affors K_{11}, after which the stability constant of the 1:2 complex [$K_{12} = (K_{11}/2)^2$] was included. Please note that therefore in the data fitting for the (*Z*)-isomer to either a 1:1 or 1:2 binding model, the value for K_{11} is identical, whereas the microscopic constant (K_{1m}) differs. All data fits were performed with HypNMR.[5]

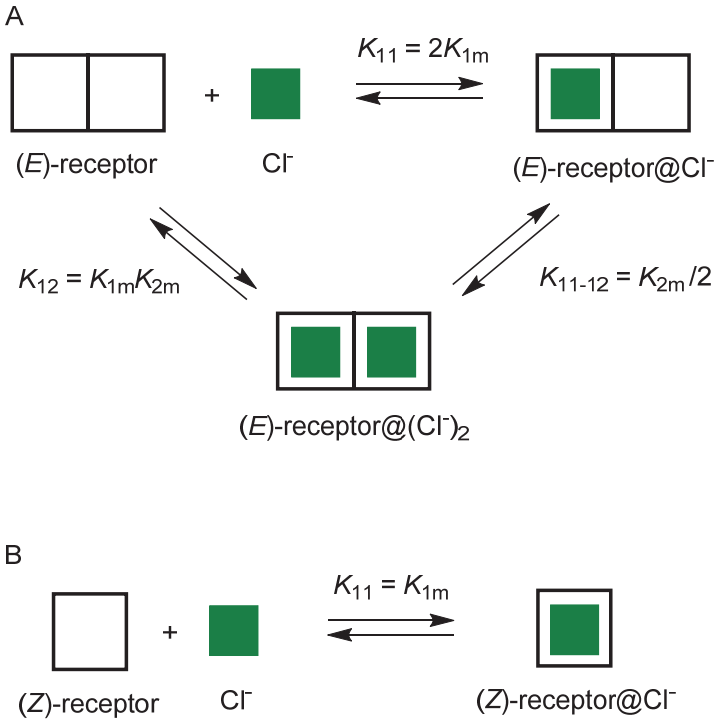

Scheme S2. Schematic representation of the equilibria and species involved in the stepwise formation of a 1:2 (receptor/chloride) complex for the (*E*)-isomer (A) and 1:1 complexation anticipated for the (*Z*)-isomer (B). The relation of the stability constants of the 1:1 complex (K_{11}), the 1:2 complex (K_{12}), and the stepwise constant ($K_{11\text{-}12}$) to the microscopic binding constants (K_{1m}, K_{2m}) is additionally shown.

Addition of $[Bu_4N]^+[Cl]^-$ to (*E*)-1b:

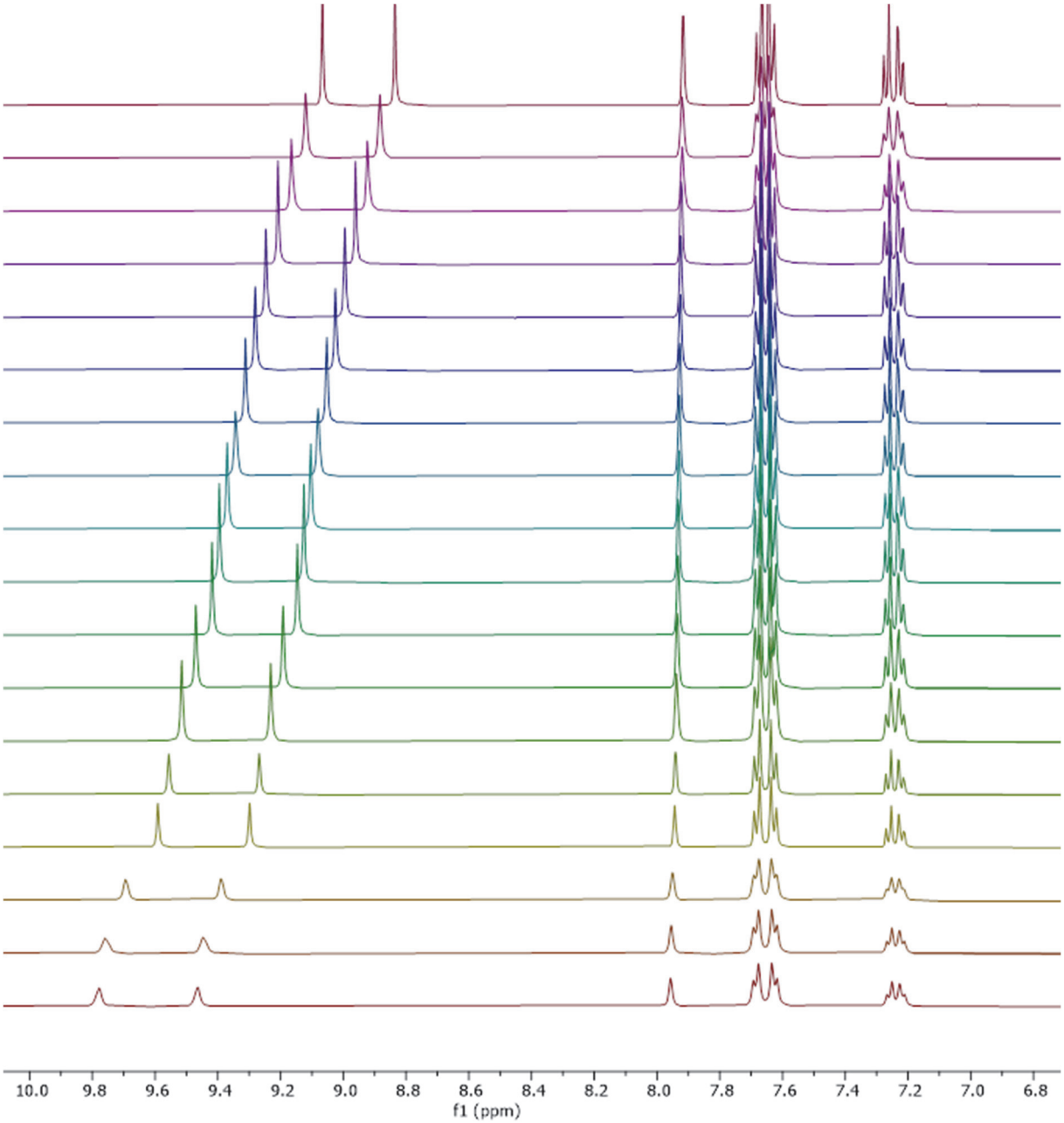

Figure S31. ^{1}H NMR spectral changes (500 MHz, 293 K) in the aromatic region of (*E*)-**1b** in DMSO-d_6/0.5%H_2O (5.1×10^{-3} M) upon the stepwise addition of $[Bu_4N]^+[Cl]^-$ (from top to bottom: 0.00, 0.21, 0.41, 0.60, 0.78, 0.96, 1.13, 1.30, 1.46, 1.61, 1.76, 2.11, 2.44, 2.74, 3.02, 3.97, 4.70, 5.17 equivalents).

Addition of $[Bu_4N]^+[Cl]^-$ to (*E*)-2a:

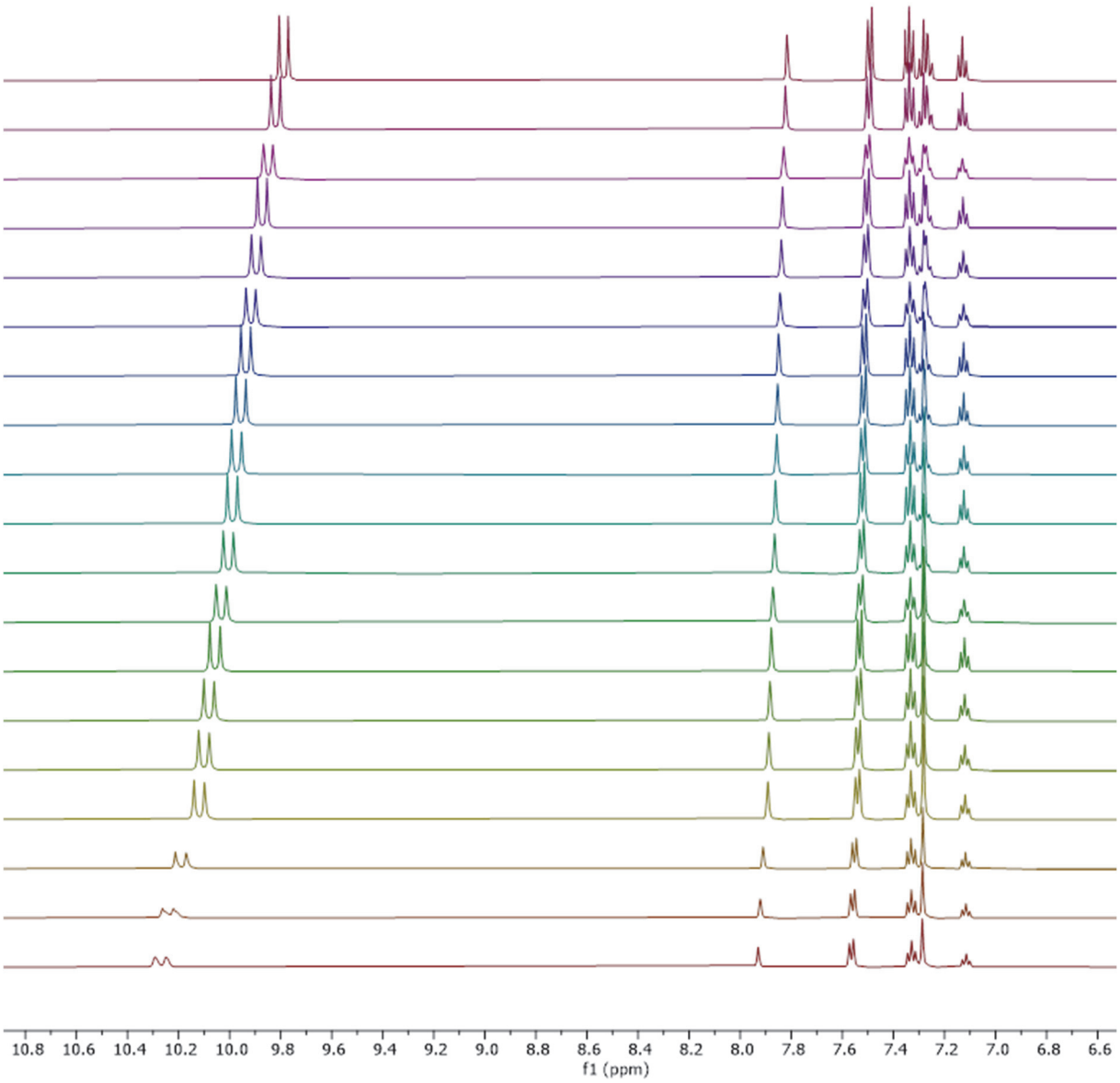

Figure S32. ^{1}H NMR spectral changes (500 MHz, 293 K) in the aromatic region of (*E*)-**2a** in DMSO-d_6/0.5%H_2O (5.1×10^{-3} M) upon the stepwise addition of $[Bu_4N]^+[Cl]^-$ (from top to bottom: 0.00, 0.19, 0.37, 0.55, 0.71, 0.88, 1.03, 1.18, 1.33, 1.47, 1.61, 1.87, 2.11, 2.34, 2.55, 2.76, 3.62, 4.26, 4.72 equivalents).

Addition of $[Bu_4N]^+[Cl]^-$ to (*E*)-2b:

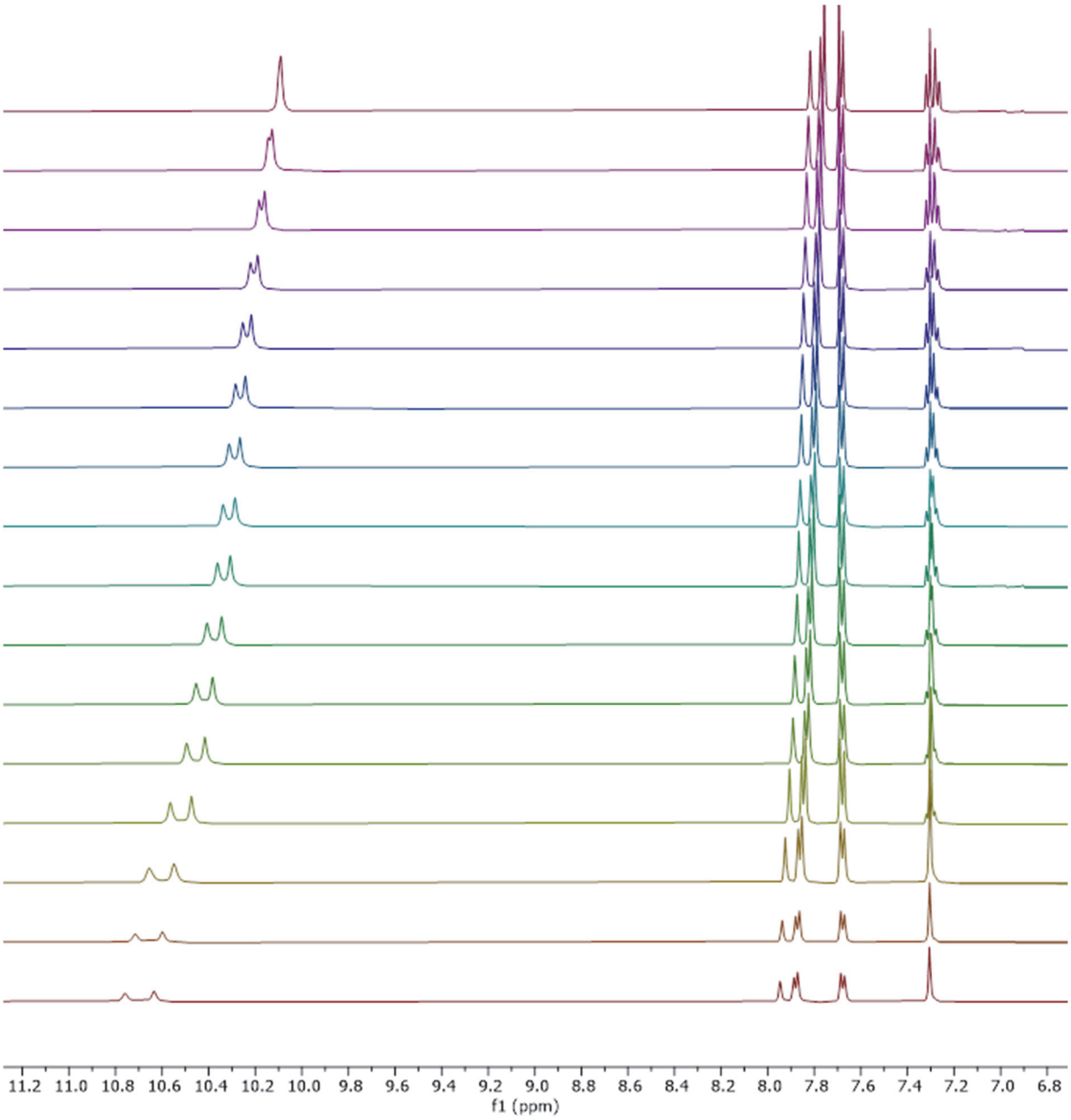

Figure S33. ^{1}H NMR spectral changes (500 MHz, 293 K) in the aromatic region of (*E*)-**2b** in DMSO-d_6/0.5%H_2O (5.2×10^{-3} M) upon the stepwise addition of $[Bu_4N]^+[Cl]^-$ (from top to bottom: 0.00, 0.20, 0.39, 0.58, 0.75, 0.92, 1.09, 1.25, 1.40, 1.69, 2.03, 2.34, 2.90, 3.81, 4.52, 4.98 equivalents).

Addition of $[Bu_4N]^+[Cl]^-$ to (*E*)-2c:

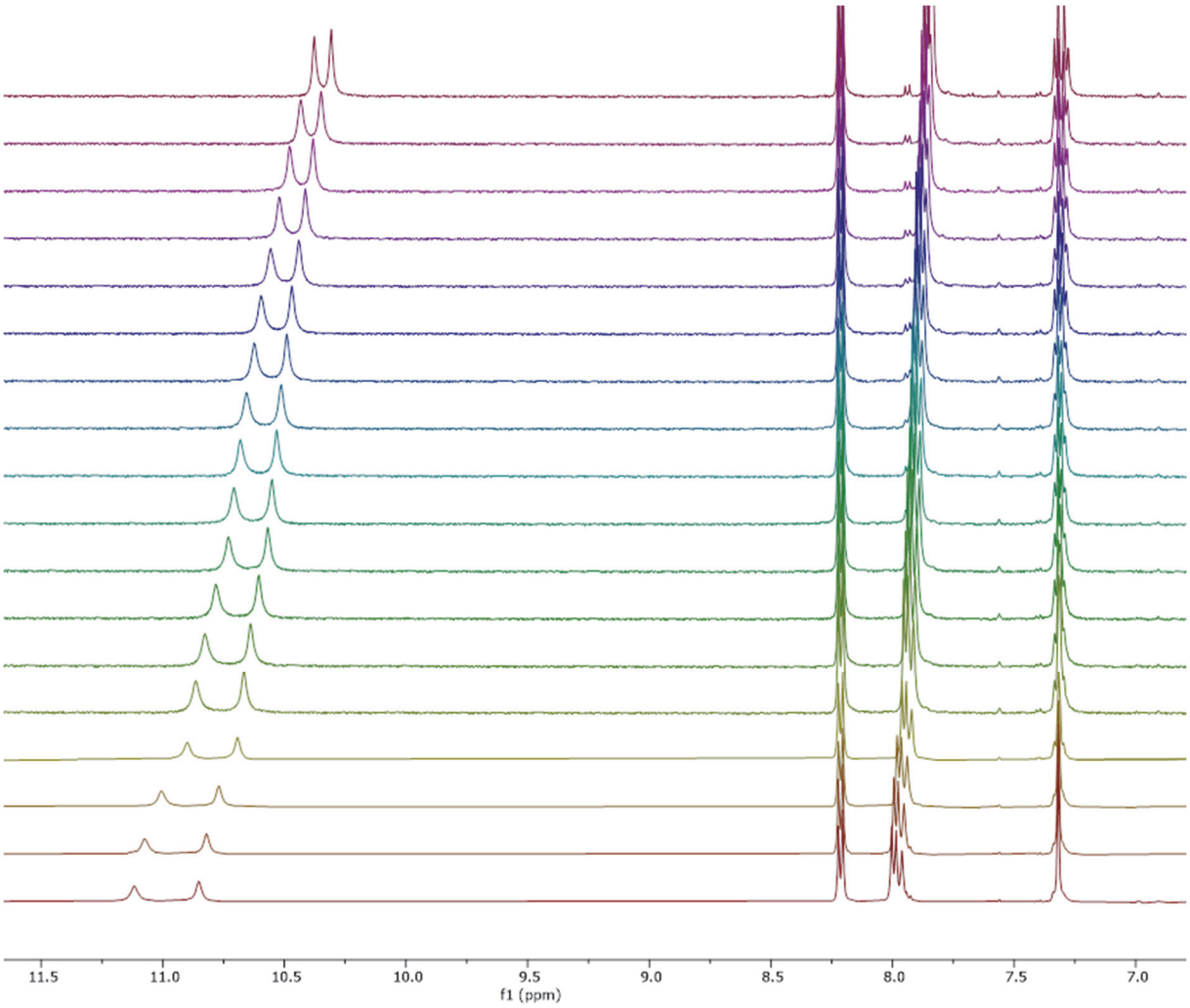

Figure S34. ^{1}H NMR spectral changes (500 MHz, 293 K) in the aromatic region of (*E*)-**2c** in DMSO-d_6/0.5%H_2O (5.4×10^{-3} M) upon the stepwise addition of $[Bu_4N]^+[Cl]^-$ (from top to bottom: 0.00, 0.18, 0.36, 0.53, 0.70, 0.86, 1.01, 1.16, 1.30, 1.44, 1.57, 1.88, 2.17, 2.44, 2.69, 3.53, 4.19, 4.66 equivalents).

Addition of $[Bu_4N]^+[Cl]^-$ to (*Z*)-1b:

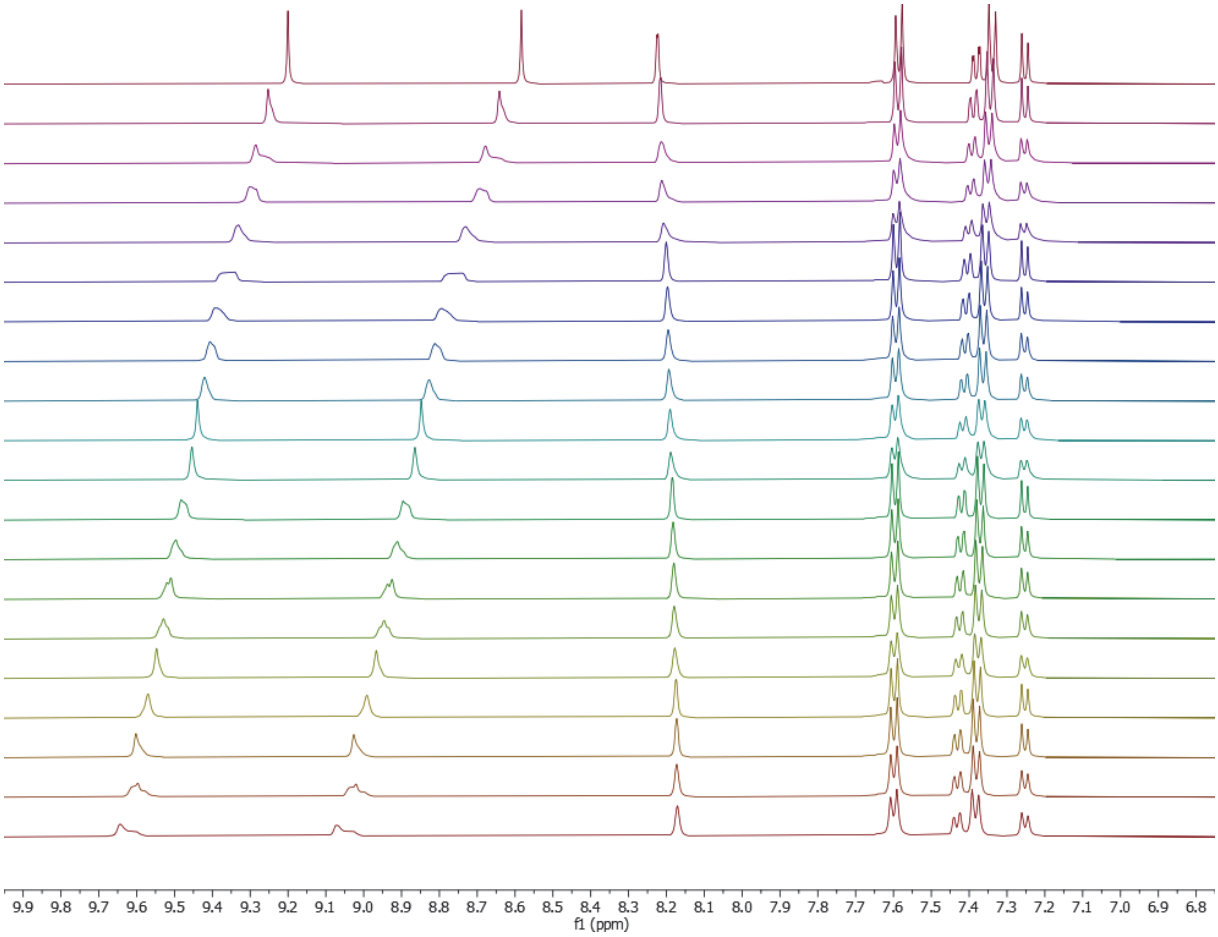

Figure S35. ^{1}H NMR spectral changes (500 MHz, 293 K) in the aromatic region of (*Z*)-**1b** in DMSO-d_6/0.5%H_2O (5.0×10^{-3} M) upon the stepwise addition of $[Bu_4N]^+[Cl]^-$ (from top to bottom: 0.00, 0.20, 0.39, 0.58, 0.76, 0.93, 1.10, 1.26, 1.41, 1.56, 1.70, 1.98, 2.24, 2.48, 2.71, 2.92, 3.41, 3.83, 4.54, 5.04 equivalents).

Addition of $[Bu_4N]^+[Cl]^-$ to (*Z*)-1c:

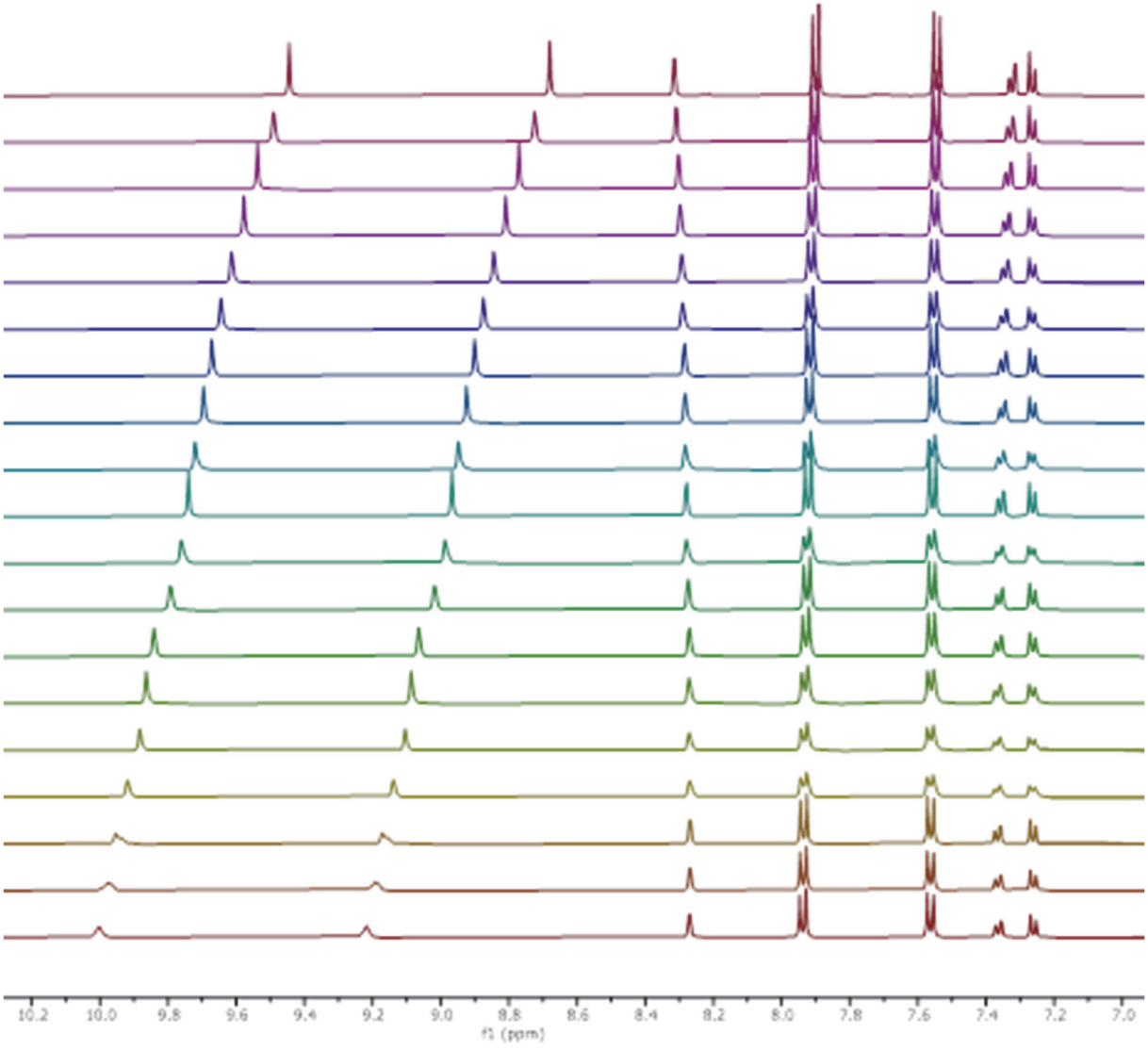

Figure S36. ^{1}H NMR spectral changes (500 MHz, 293 K) in the aromatic region of (*Z*)-**1c** in DMSO-d_6/0.5%H_2O (5.1×10^{-3} M) upon the stepwise addition of $[Bu_4N]^+[Cl]^-$ (from top to bottom: 0.00, 0.19, 0.38, 0.57, 0.74, 0.92, 1.08, 1.24, 1.40, 1.56, 1.70, 1.99, 2.52, 2.76, 3.00, 3.52, 4.01, 4.82, 5.46 equivalents).

Addition of $[Bu_4N]^+[Cl]^-$ to (*Z*)-2a:

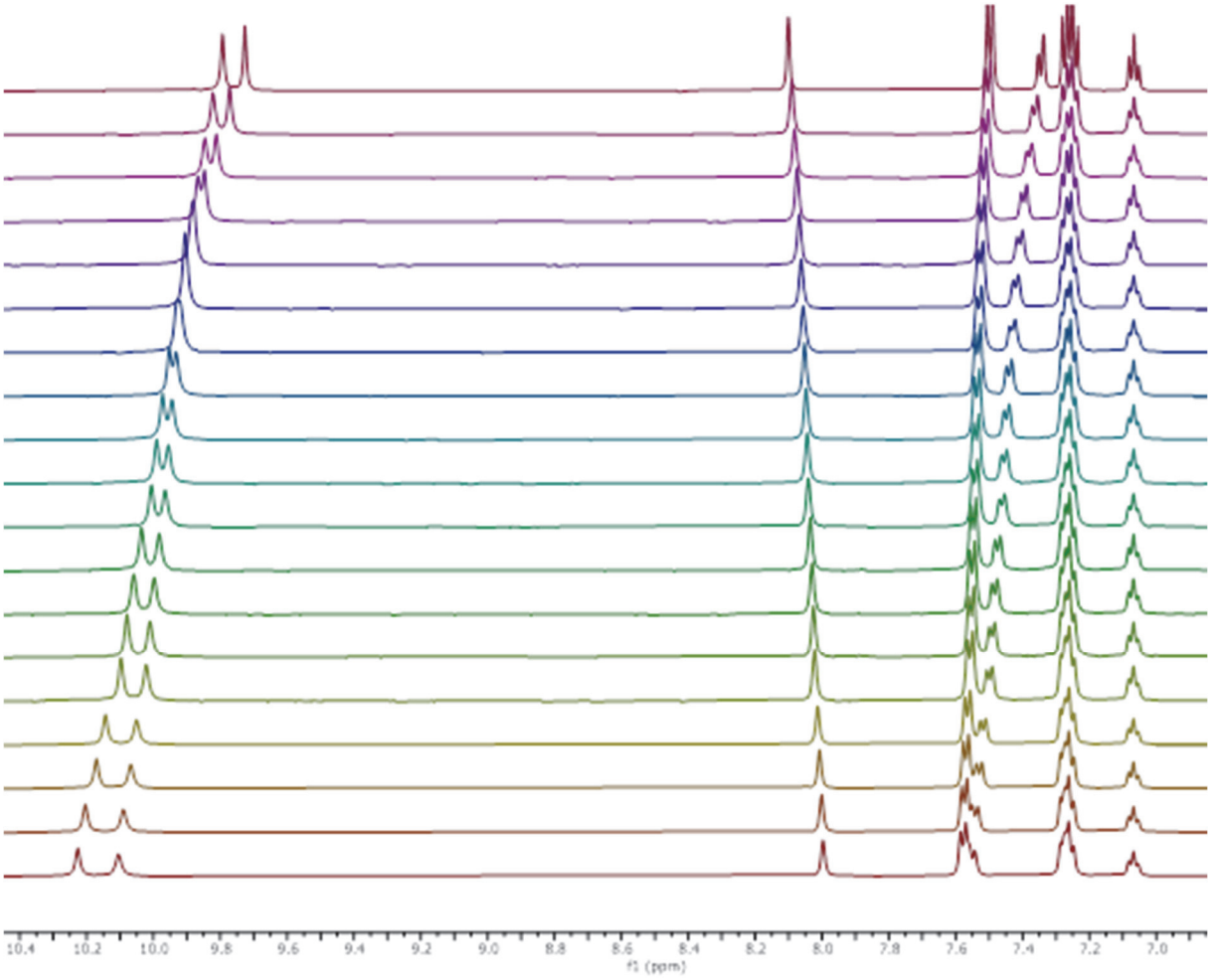

Figure S37. ^{1}H NMR spectral changes (500 MHz, 293 K) in the aromatic region of (*Z*)-**2a** in DMSO-d_6/0.5%H_2O (5.0×10^{-3} M) upon the stepwise addition of $[Bu_4N]^+[Cl]^-$ (from top to bottom: 0.00, 0.20, 0.39, 0.58, 0.75, 0.92, 1.09, 1.25, 1.40, 1.55, 1.69, 1.97, 2.22, 2.46, 2.69, 3.39, 3.81, 4.52, 5.00 equivalents).

Addition of $[Bu_4N]^+[Cl]^-$ to (*Z*)-2b:

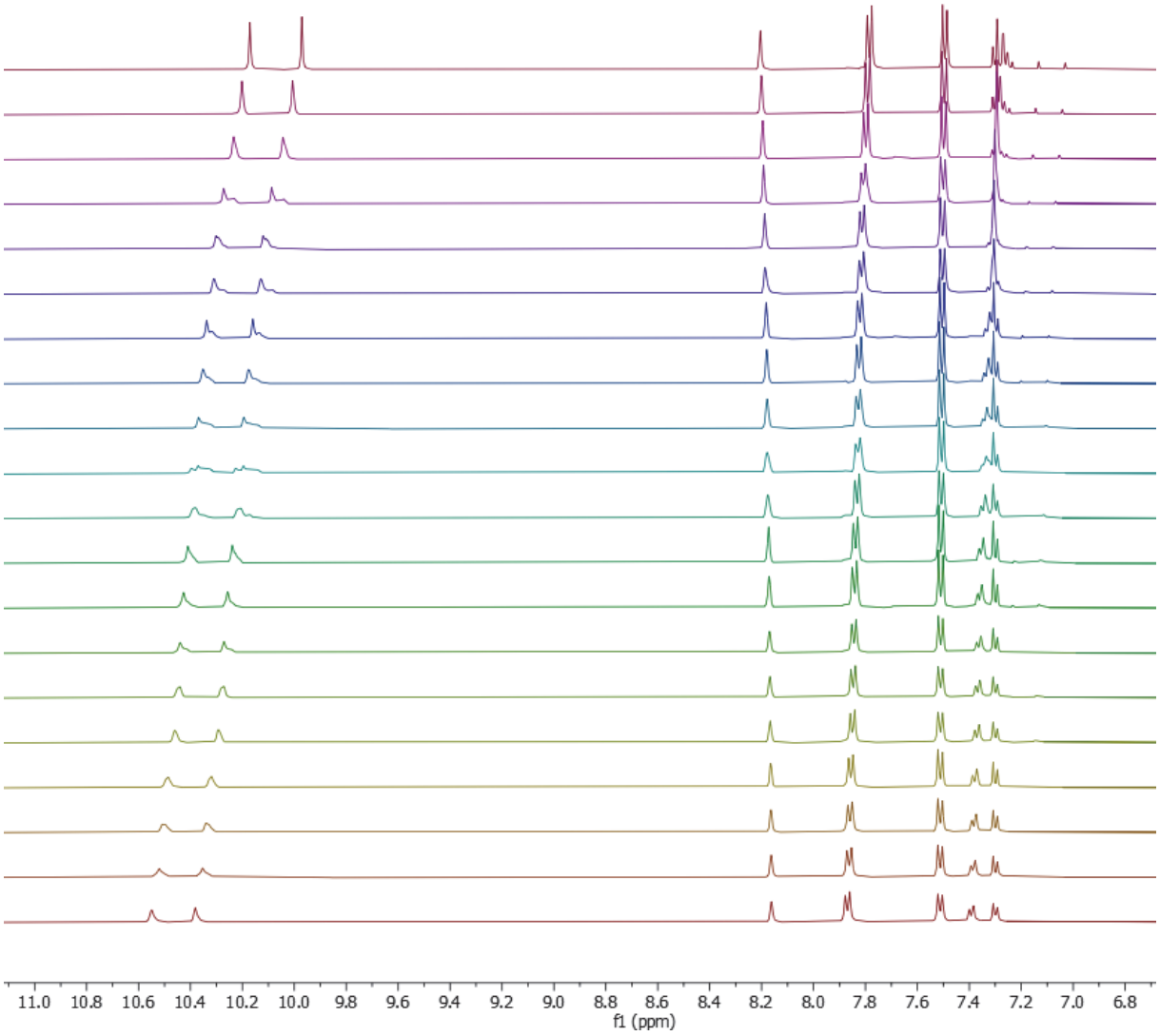

Figure S38. ^{1}H NMR spectral changes (500 MHz, 293 K) in the aromatic region of (*Z*)-**2b** in DMSO-d_6/0.5%H_2O (4.9×10^{-3} M) upon the stepwise addition of $[Bu_4N]^+[Cl]^-$ (from top to bottom: 0.00, 0.20, 0.39, 0.58, 0.76, 0.93, 1.10, 1.26, 1.42, 1.57, 1.71, 1.99, 2.25, 2.49, 2.72, 2.93, 3.42, 3.85, 4.56, 5.06 equivalents).

Addition of $[Bu_4N]^+[Cl]^-$ to (*Z*)-2c:

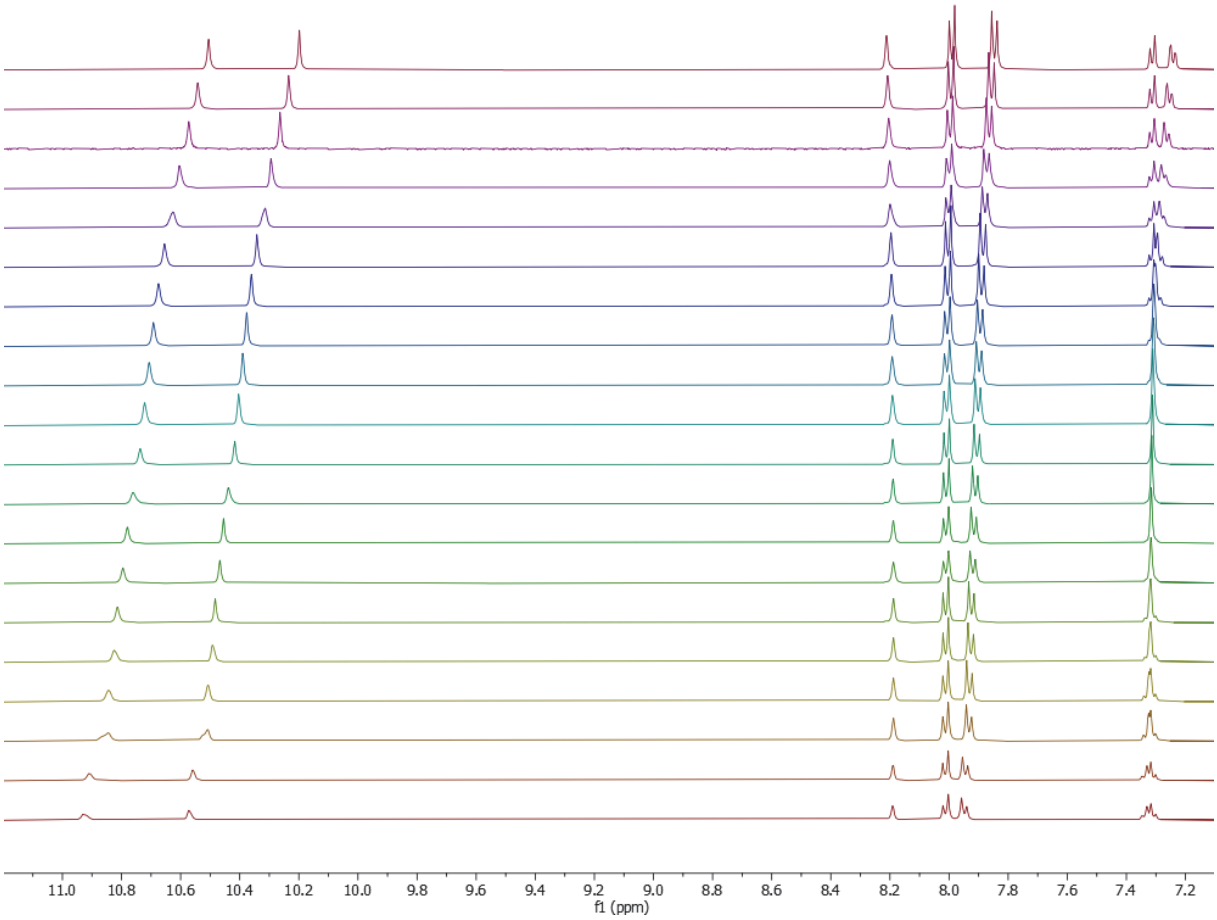

Figure S39. ^{1}H NMR spectral changes (500 MHz, 293 K) in the aromatic region of (*Z*)-**2c** in DMSO-d_6/0.5%H_2O (5.0×10^{-3} M) upon the stepwise addition of $[Bu_4N]^+[Cl]^-$ (from top to bottom: 0.00, 0.20, 0.39, 0.58, 0.75, 0.92, 1.09, 1.25, 1.40, 1.55, 1.69, 1.79, 2.22, 2.46, 2.69, 2.91, 3.39, 3.81, 4.52, 5.03 equivalents).

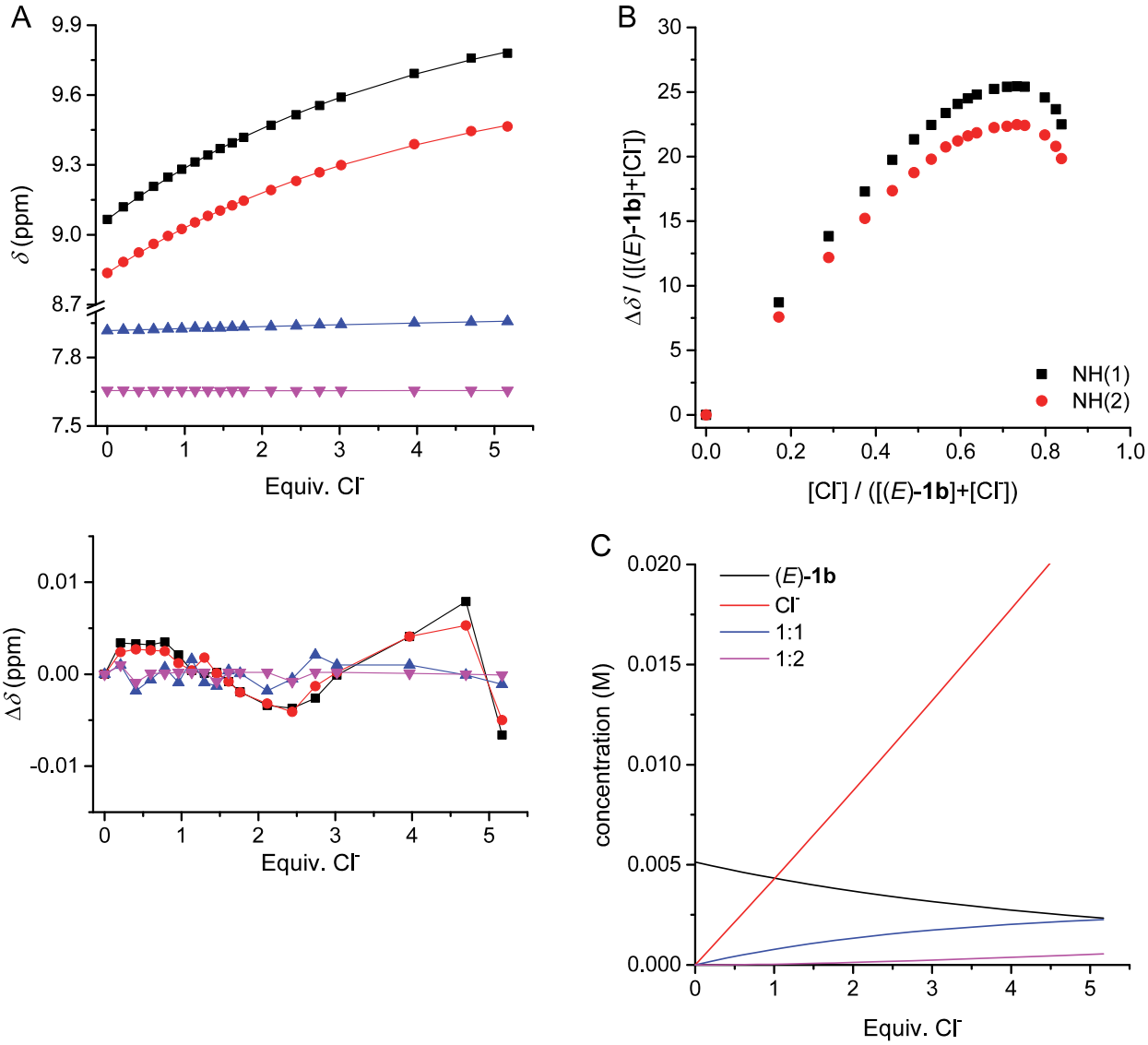

Figure S40. (A) Titration curve, data fit obtained by simultaneous analysis of multiple ^{1}H NMR signals, and below the residual plot for the addition of $[Bu_4N]^+[Cl]^-$ to (*E*)-**1b** using a 1:2 binding model; (B) Job plot analysis indicating a 1:2 binding stoichiometry and (C) speciation curves for the 1:2 binding model. $K_{11} = 4.17 \times 10^1$ M^{-1}; $K_{12} = 4.34 \times 10^2$ M^{-2}.

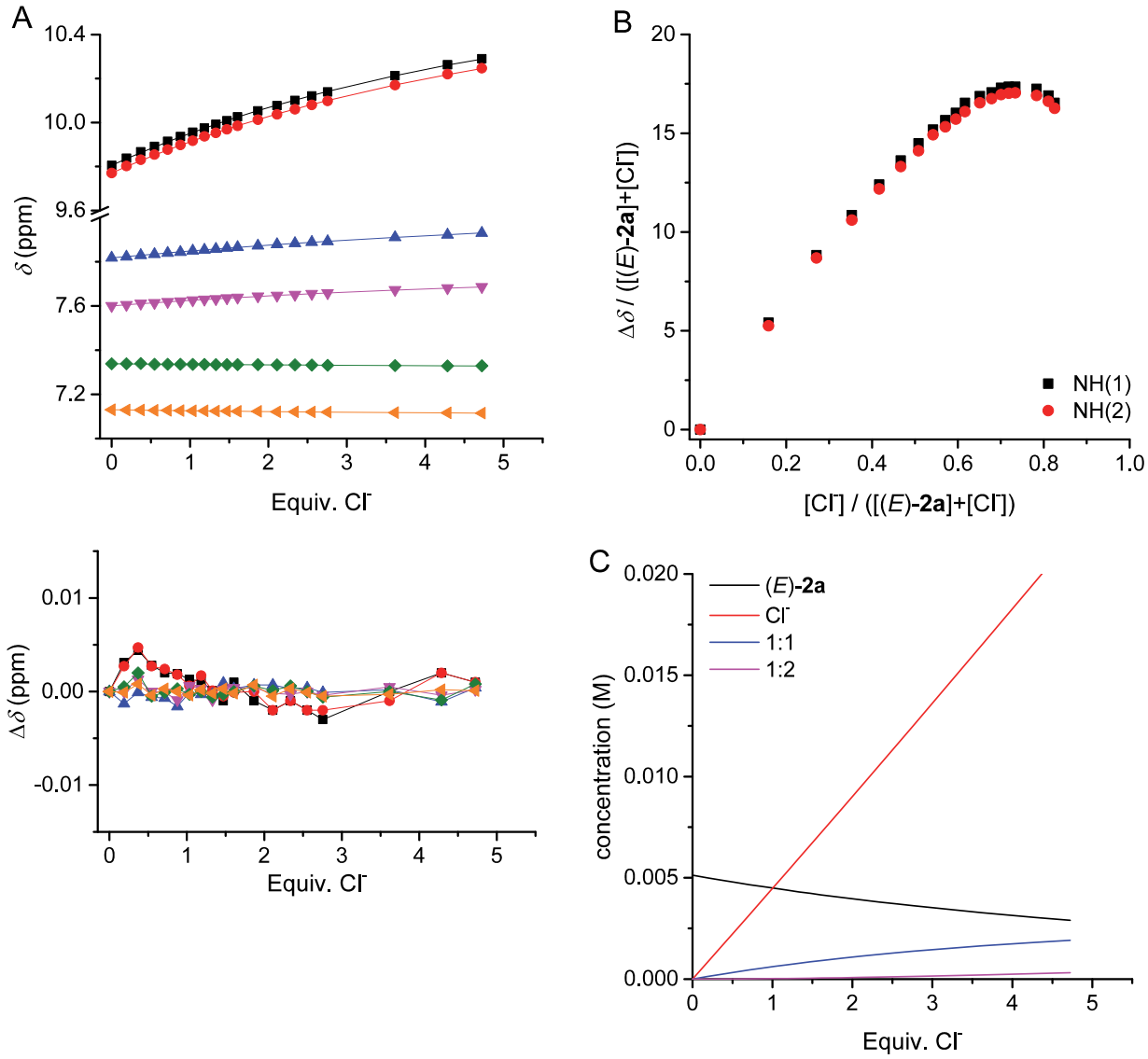

Figure S41. (A) Titration curve, data fit obtained by simultaneous analysis of multiple ^{1}H NMR signals, and below the residual plot for the addition of $[Bu_4N]^+[Cl]^-$ to (*E*)-**2a** using a 1:2 binding model; (B) Job plot analysis indicating a 1:2 binding stoichiometry and (C) speciation curves for the 1:2 binding model. $K_{11} = 3.04 \times 10^1$ M^{-1}; $K_{12} = 2.31 \times 10^2$ M^{-2}.

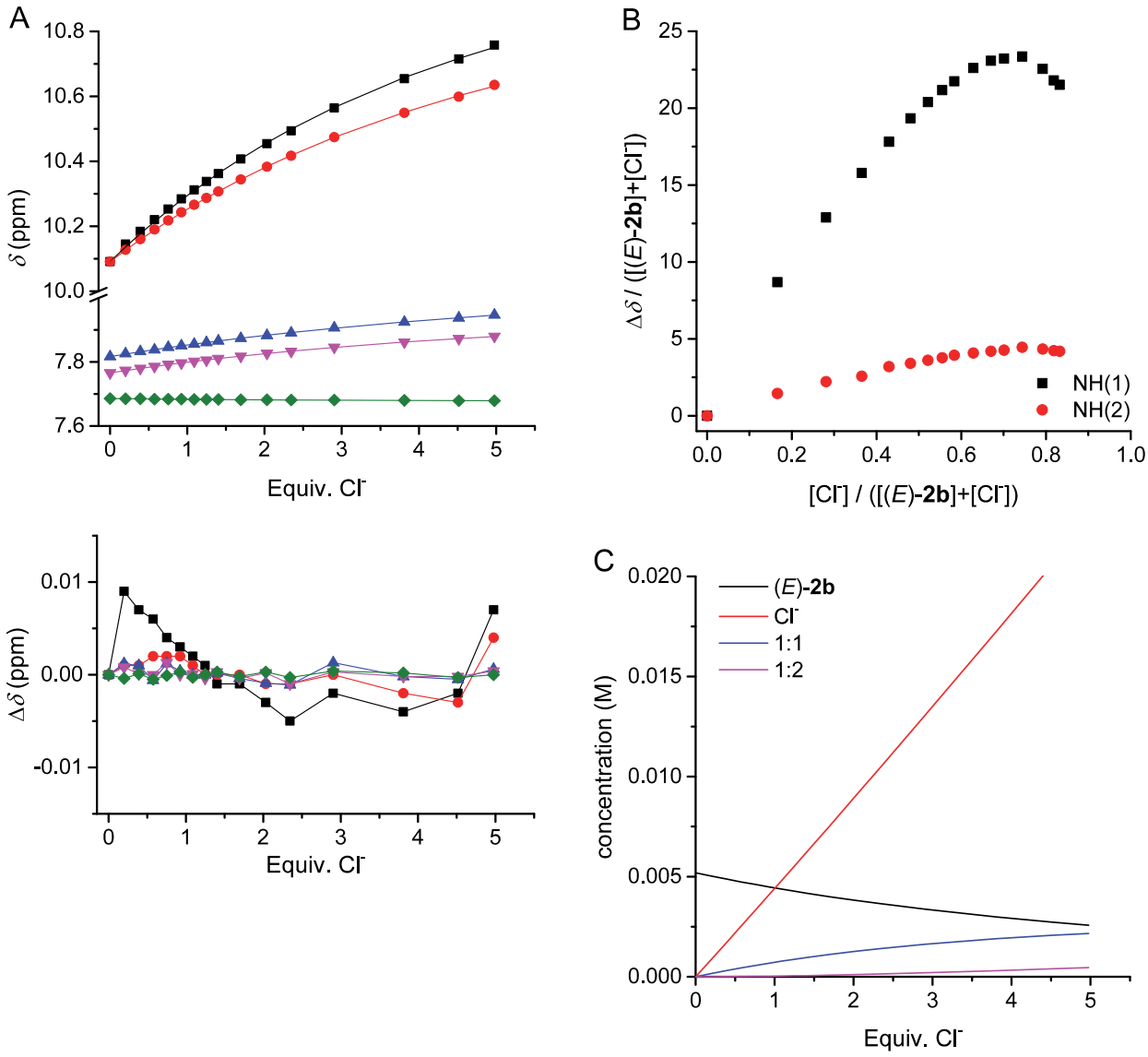

Figure S42. (A) Titration curve, data fit obtained by simultaneous analysis of multiple ^{1}H NMR signals, and below the residual plot for the addition of $[Bu_4N]^+[Cl]^-$ to (*E*)-**2b** using a 1:2 binding model; (B) Job plot analysis indicating a 1:2 binding stoichiometry and (C) speciation curves for the 1:2 binding model. $K_{11} = 3.69 \times 10^1$ M^{-1}; $K_{12} = 3.40 \times 10^2$ M^{-2}.

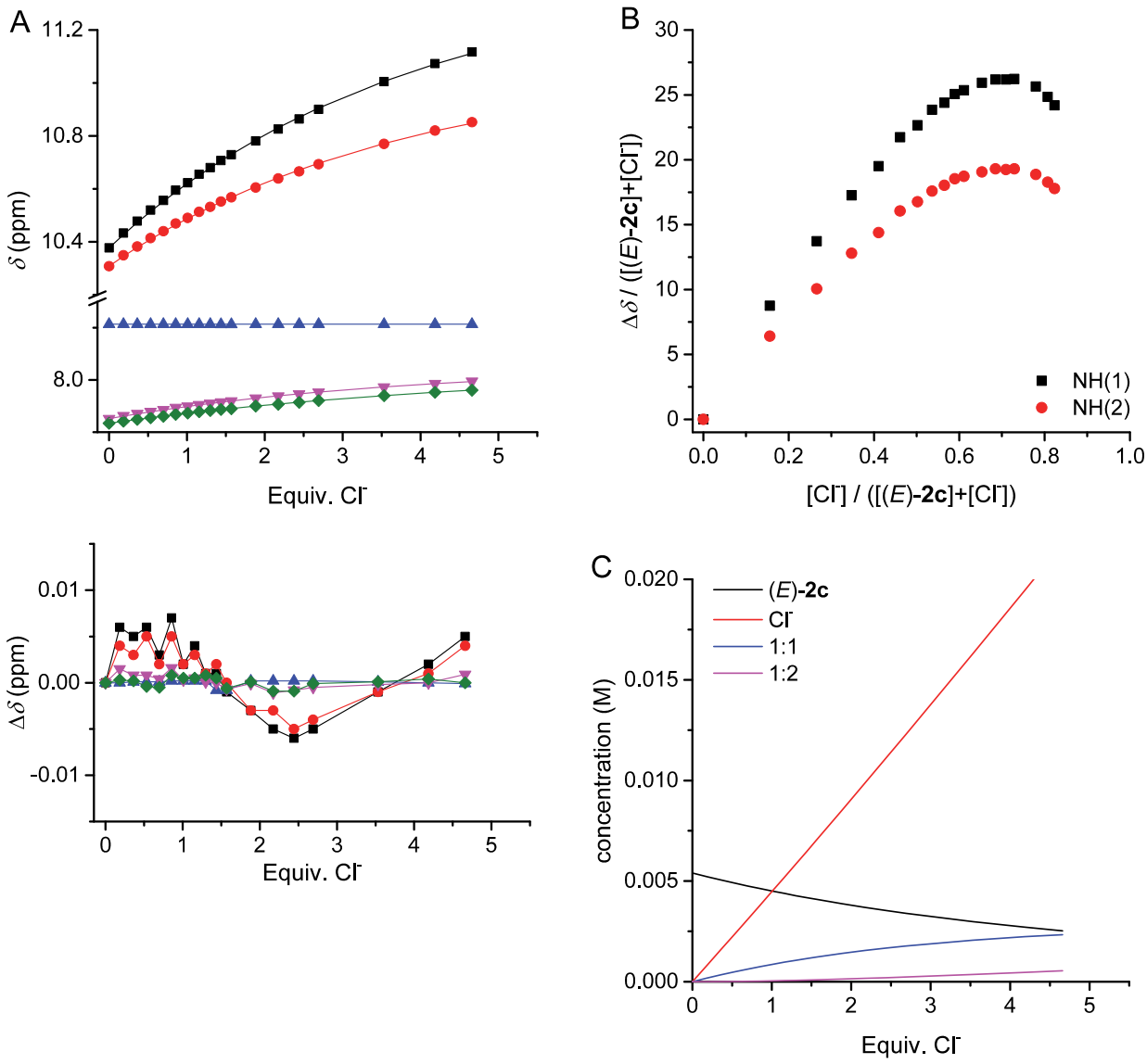

Figure S43. (A) Titration curve, data fit obtained by simultaneous analysis of multiple ^{1}H NMR signals, and below the residual plot for the addition of $[Bu_4N]^+[Cl]^-$ to (*E*)-**2c** using a 1:2 binding model; (B) Job plot analysis indicating a 1:2 binding stoichiometry and (C) speciation curves for the 1:2 binding model. $K_{11} = 4.25 \times 10^1$ M^{-1}; $K_{12} = 4.51 \times 10^2$ M^{-2}.

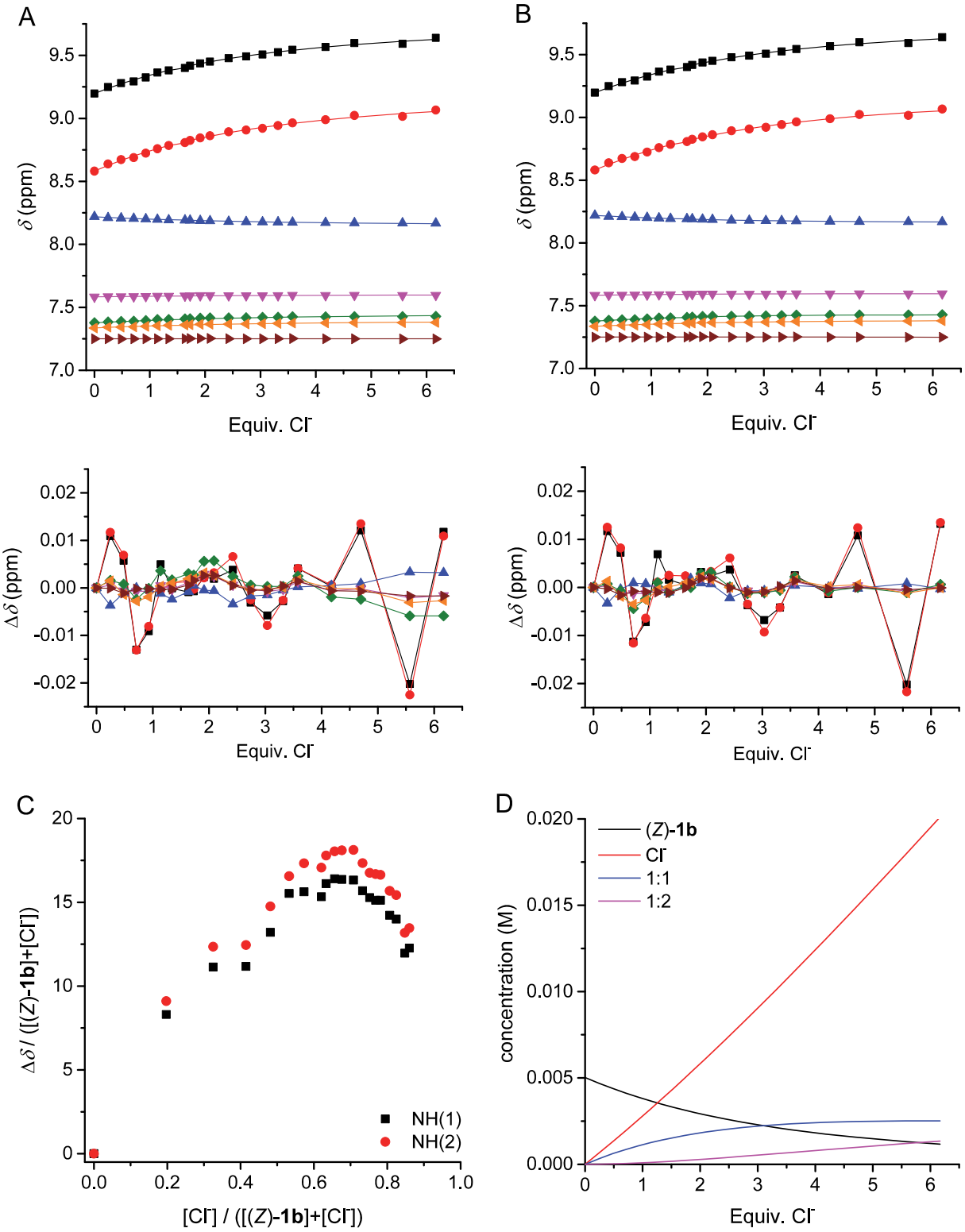

Figure S44. Titration curves, data fits obtained by simultaneous analysis of multiple ^{1}H NMR signals, and residual plots for the addition of $[Bu_4N]^+[Cl]^-$ to (*Z*)-**1b** using 1:1 (A) and 1:2 (B) binding models; Job plot analysis (C) indicating a 1:2 binding stoichiometry and speciation curves (D) for the 1:2 binding model. For 1:1 binding: $K_{11} = 1.07 \times 10^2$ M^{-1}. For 1:2 binding $K_{11} = 1.07 \times 10^2$ M^{-1}; $K_{12} = 2.85 \times 10^3$ M^{-2}.

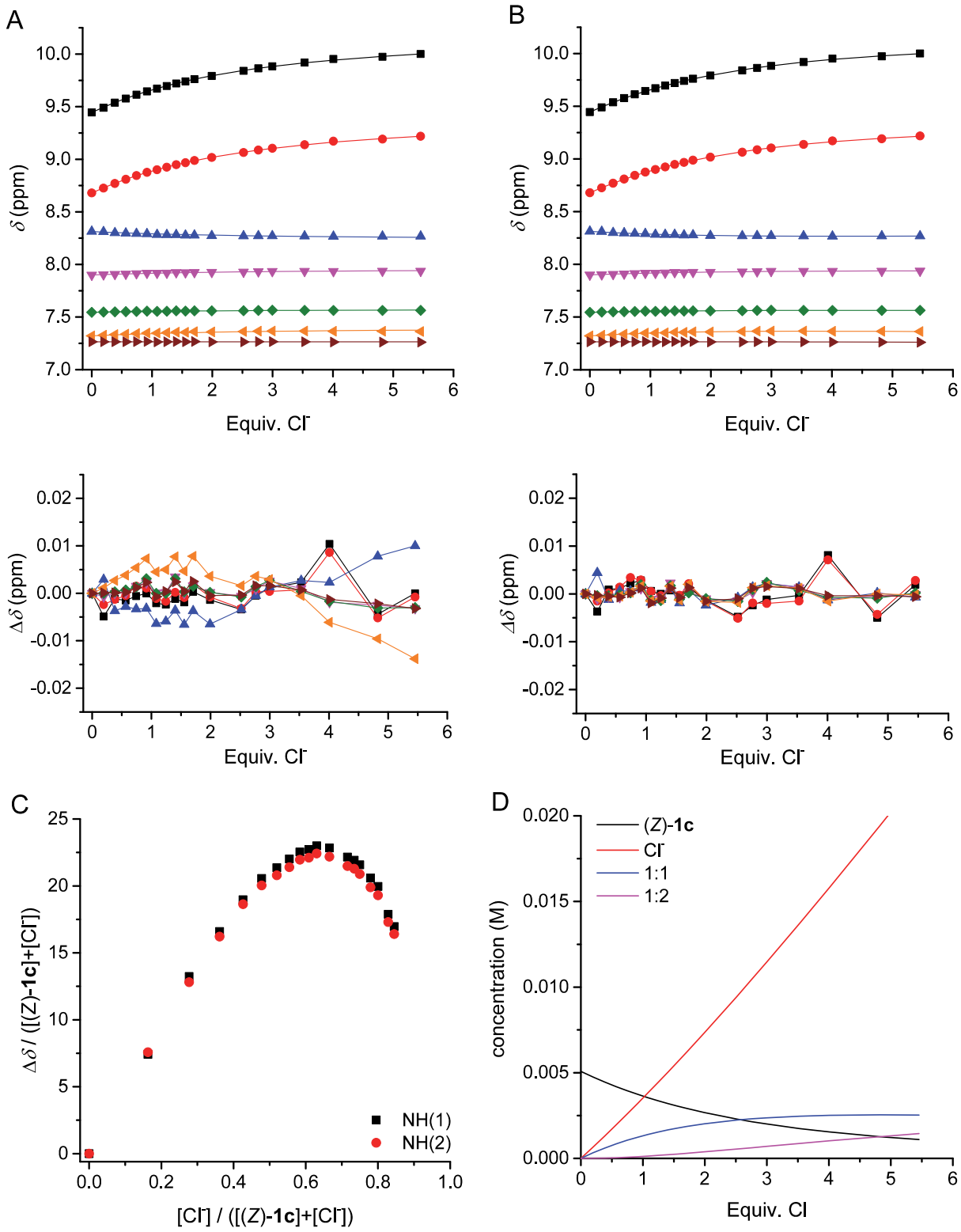

Figure S45. Titration curves, data fits obtained by simultaneous analysis of multiple ^{1}H NMR signals, and residual plots for the addition of $[Bu_4N]^+[Cl]^-$ to (*Z*)-**1c** using 1:1 (A) and 1:2 (B) binding models; Job plot analysis (C) indicating a 1:2 binding stoichiometry and speciation curves (D) for the 1:2 binding model. For 1:1 binding: $K_{11} = 1.03 \times 10^2$ M^{-1}. For 1:2 binding: $K_{11} = 1.03 \times 10^2$ M^{-1}; $K_{12} = 2.66 \times 10^3$ M^{-2}.

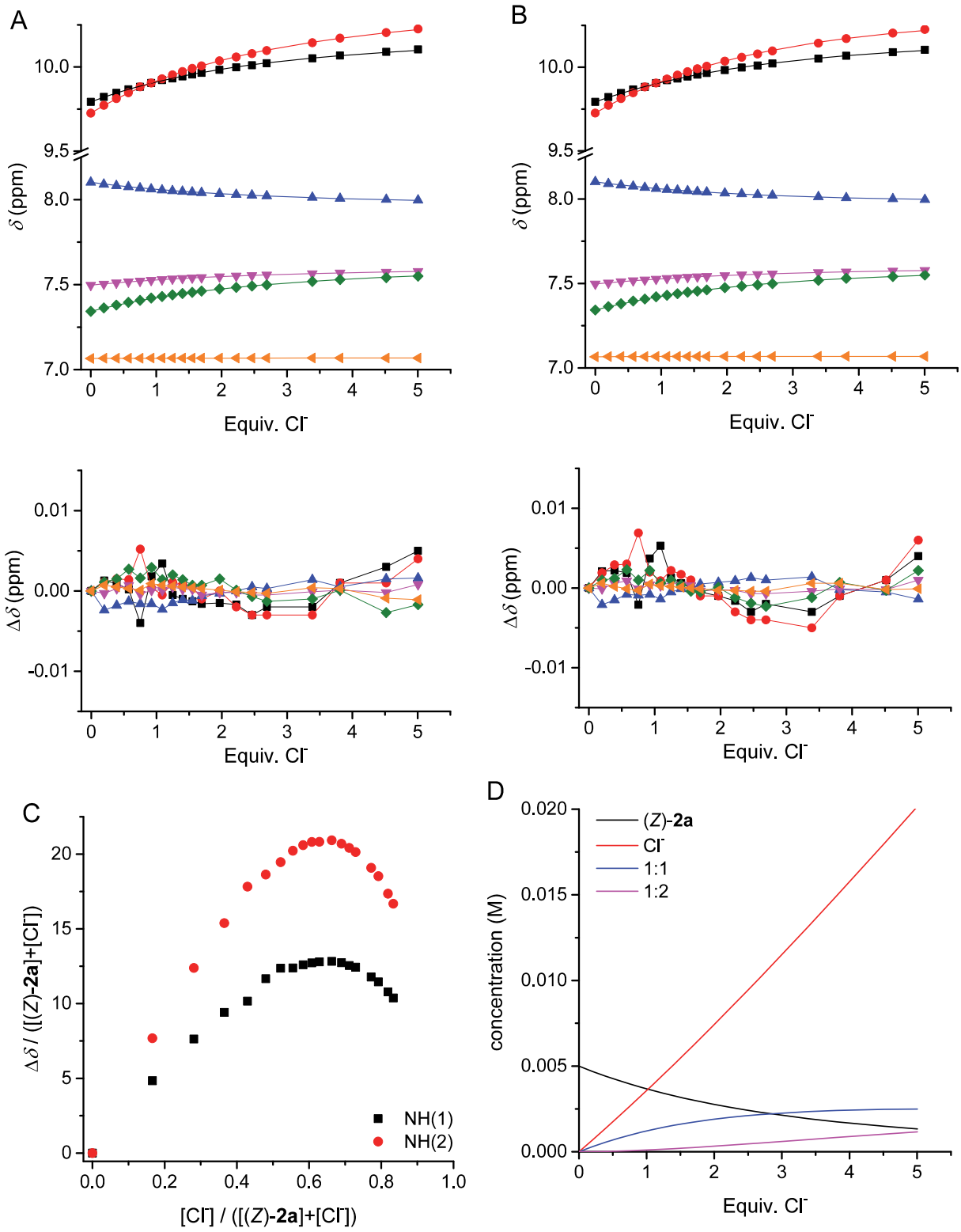

Figure S46. Titration curves, data fits obtained by simultaneous analysis of multiple ^{1}H NMR signals, and residual plots for the addition of $[Bu_4N]^+[Cl]^-$ to (*Z*)-**2a** using 1:1 (A) and 1:2 (B) binding models; Job plot analysis (C) indicating a 1:2 binding stoichiometry and speciation curves (D) for the 1:2 binding model. For 1:1 binding: $K_{11} = 9.27 \times 10^1$ M^{-1}; For 1:2 binding: $K_{11} = 9.27 \times 10^1$ M^{-1}; $K_{12} = 2.15 \times 10^3$ M^{-2}.

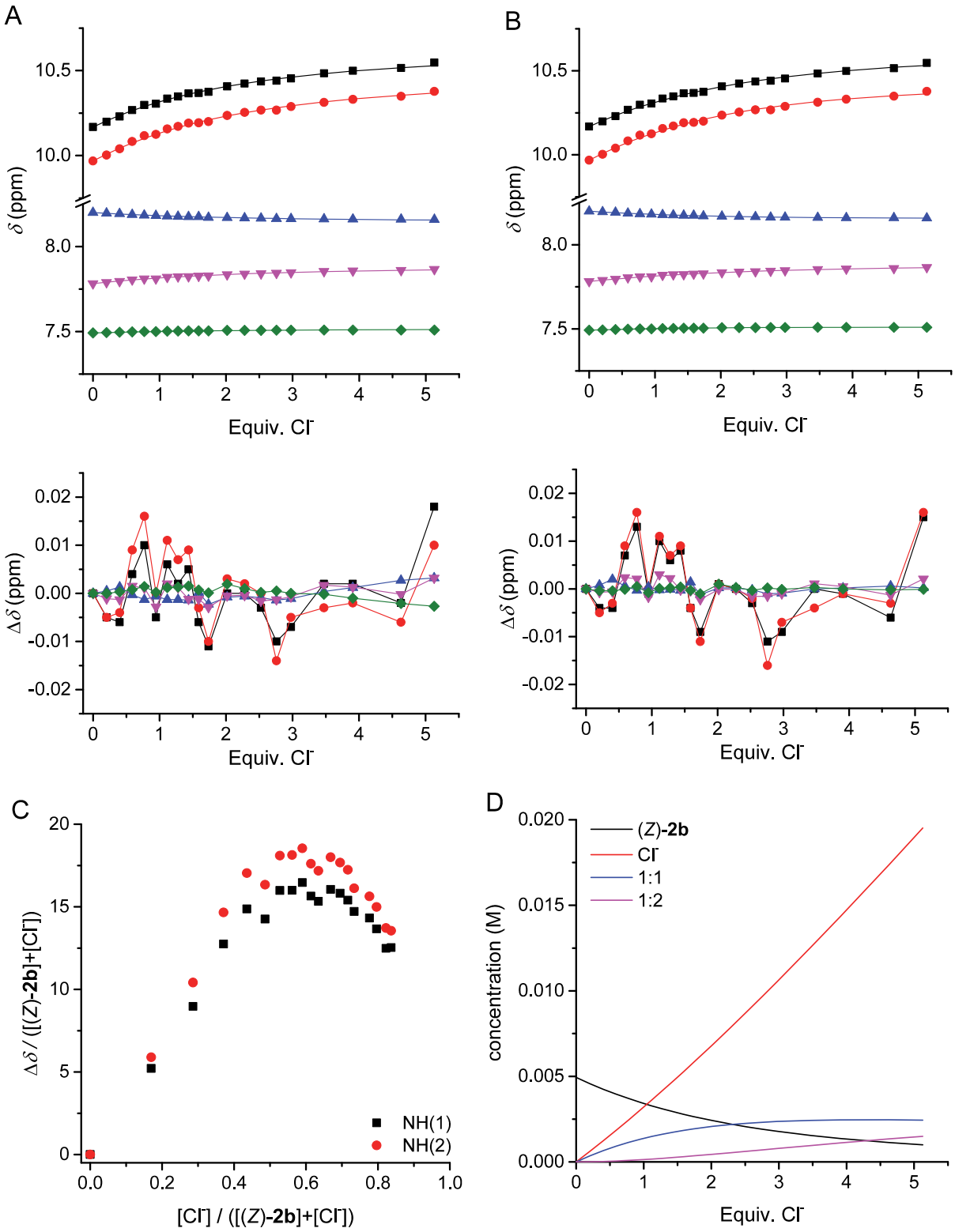

Figure S47. Titration curves, data fits obtained by simultaneous analysis of multiple ^{1}H NMR signals, and residual plots for the addition of $[Bu_4N]^+[Cl]^-$ to (*Z*)-**2b** using 1:1 (A) and 1:2 (B) binding models; Job plot analysis (C) indicating a 1:2 binding stoichiometry and speciation curves (D) for the 1:2 binding model. For 1:1 binding: $K_{11} = 1.25 \times 10^2$ M^{-1}. For 1:2 binding: $K_{11} = 1.25 \times 10^2$ M^{-1}; $K_{12} = 3.94 \times 10^3$ M^{-2}.

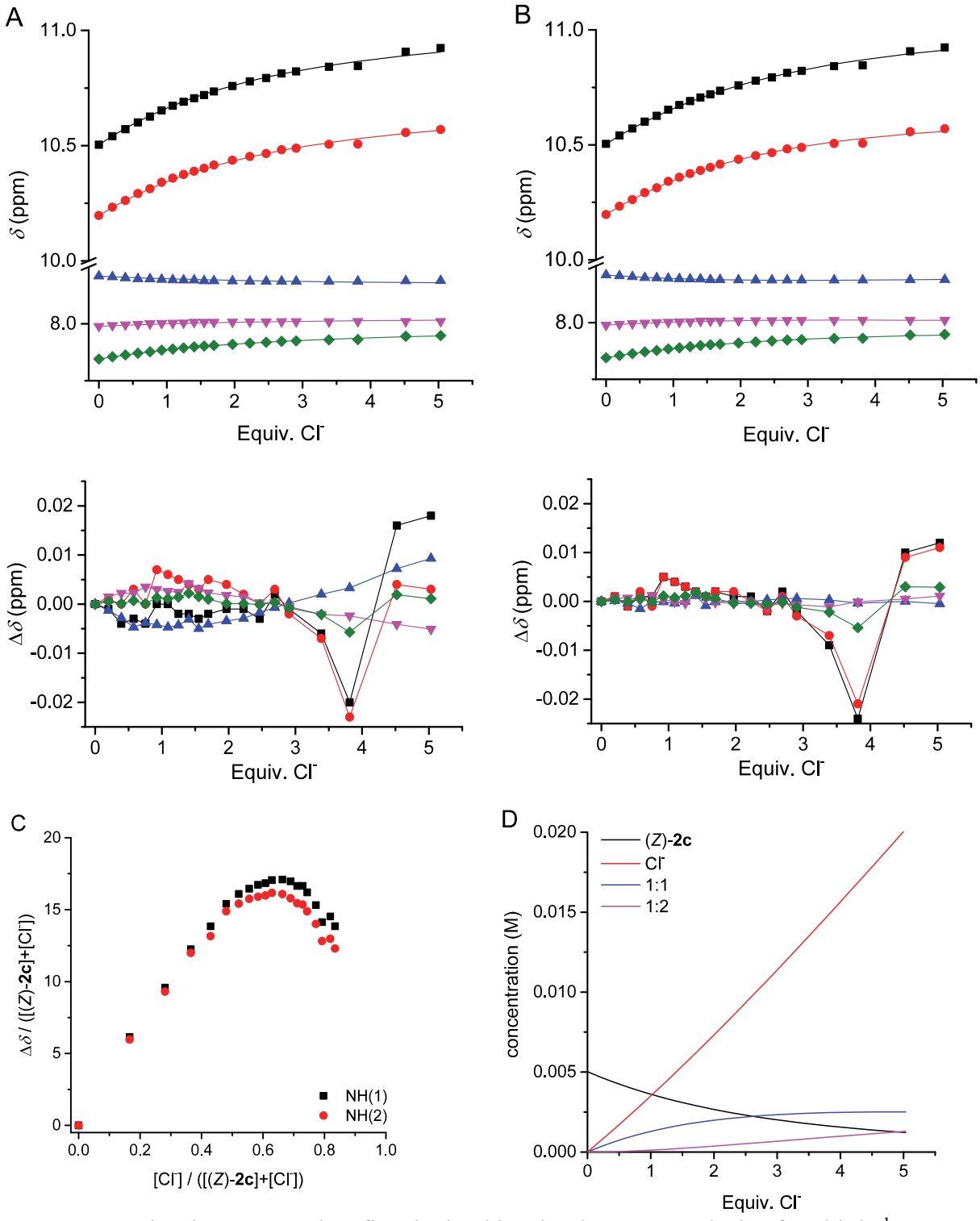

Figure S48. Titration curves, data fits obtained by simultaneous analysis of multiple ^{1}H NMR signals, and residual plots for the addition of $[Bu_4N]^+[Cl]^-$ to (*Z*)-**2c** using 1:1 (A) and 1:2 (B) binding models; Job plot analysis (C) indicating a 1:2 binding stoichiometry and speciation curves (D) for the 1:2 binding model. For 1:1 binding: $K_{11} = 1.02 \times 10^2$ M^{-1}. For 1:2 binding: $K_{11} = 1.02 \times 10^2$ M^{-1}; $K_{12} = 2.61 \times 10^3$ M^{-2}.

Transmembrane transport experiments

HPTS Assay: HPTS assays were conducted using POPC vesicles (mean diameter 200 nm) loaded with the pH-sensitive fluorescence dye HPTS (1 mM). The HPTS-loaded POPC LUVs were prepared as follows. A chloroform solution of POPC (contains ~1 mol% of free fatty acids) was evaporated in a round-bottom flask and the lipid film formed was dried under vacuum for at least 6 h. Then, the lipid film was hydrated by vortexing with an internal solution containing HPTS (1 mM) and NaCl (100 mM) buffered at pH 7.0 with 10 mM HEPES. The HEPES buffer of pH = 7.0 was prepared by dissolving an appropriate amount of solid HEPES (10 mM) and salt in deionized water. The lipid suspension was subjected to nine freeze/thaw cycles, where the suspension was alternatingly allowed to freeze in a liquid nitrogen bath, followed by thawing in a water bath. The lipid suspension was allowed to age for 30 min at room temperature and was subsequently extruded 25 times through a 200 nm polycarbonate membrane (NucleoporeTM) using an extruder set (Avanti Polar Lipids, Inc). The unentrapped HPTS was removed by size exclusion chromatography on a Sephadex® G-25 column using an external solution eluent that does not contain HPTS. The lipid solution obtained after Sephadex® was diluted to a standard volume (usually 5 mL) with the NaCl (100 mM) buffered to pH 7 with HEPES, external solution to obtain a lipid stock of known concentration.

For each test, the lipid stock was diluted with the external buffer solution to a standard volume (2.5 mL), to afford a solution with a lipid concentration of 0.1 mM. The compounds were added as a DMSO solution (prepared using HPLC grade DMSO, 5 μL) The sample was stirred at 298 K and the fluorescence ratio of HPTS (λ_{ex} = 460 nm, λ_{em} = 510 nm, base form divided by λ_{ex} = 403 nm, λ_{em} = 510 nm, acid form) was recorded over time. A pulse of NaOH (25 μL of 0.5 M solution, final concentration 5 mM) was added to the vesicle suspension to generate a pH gradient of pH 7 inside and pH 8 outside, before the addition of a DMSO solution of an anion transporter or DMSO (5 μL) at time 0 s. After 610 s, detergent (25 μL of Triton X-100 (11 w%) in H_2O: DMSO (7:1 *v/v*)) was added to lyse the vesicles and after 700 s a final reading was taken. This value represented 100 % and was used for calibration. The fractional fluorescence intensity (I_f) was calculated using:

$$I_f = \frac{R_t - R_0}{R_d - R_0}$$

where R_t is the fluorescence ratio at time t, R_0 is the fluorescence ratio at time 0 s and R_d is the fluorescence ratio at the end of the experiment, after the addition of detergent. The k_{ini} values were calculated by fitting the obtained chloride efflux with the asymptotic function $y = a - b \cdot c^x$ using Origin 8, where y is the chloride efflux (%), x is time (s) and k_{ini} is then given by $k_{ini} = -b \cdot ln(c)$ (obtained in % s^{-1}), or by fitting the initial linear range of the obtained chloride efflux to $y = a + b \cdot x$, where y is the chloride efflux (%), x is time (s) and k_{ini} is given by the slope b. In case of a sigmoidal time dependence, the first two or three data points were omitted from the fit. In order to obtain standard deviations on the initial rate of transport, the fits were performed for each individual repeat and subsequently averaged.

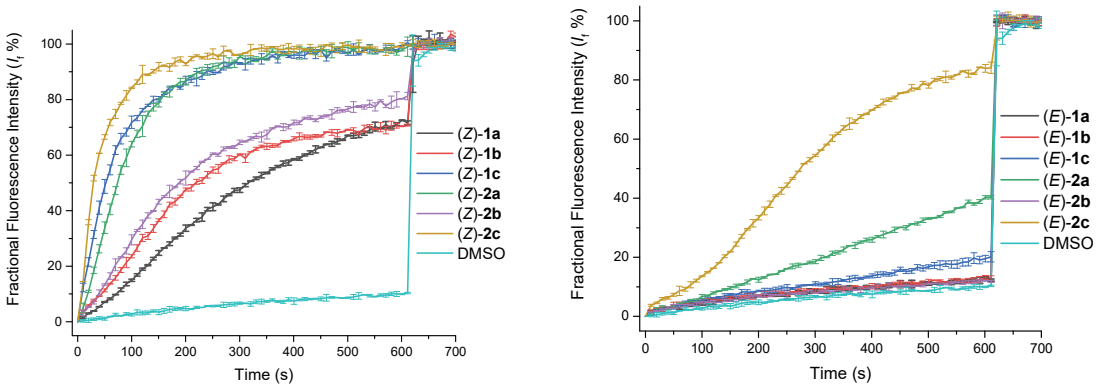

Figure S49. Plots of H^+/Cl^- symport (or Cl^-/OH^- antiport) against time (s) across a POPC membrane facilitated by (*Z*)-isomers (left, 1 mol% to lipid) and (*E*)-isomers (right, 1 mol% to lipid).

Hill plot analyses

Hill plot analyses were performed with samples loaded at different concentrations to quantify their transport activity. From these results the fluorescence ratio at 600 s was plotted as a function of the transporter concentration (mol%, with respect to lipid). The concentration profile data were evaluated at t = 600 s to get effective concentration, EC_{50} (*i.e.* the concentration of transporter needed to achieve 50% chloride efflux) using Hill equation:

$$y = y_0 + (y_{max} - y_0)\frac{x^n}{k^n + x^n} = V_{max}\frac{x^n}{k^n + x^n} = 100\%\ \frac{x^n}{(EC_{50})^n + x^n}$$

where y is the I_f at 600 s and x is the transporter concentration (mol %, with respect to lipid). y_0 is the I_f obtained for the blank DMSO run, y_{max} is the maximum I_f value and k and n are the parameters to be fitted. n is the Hill coefficient and k is the EC_{50}. The rate of pH dissipation through H^+/Cl^-symport (or Cl^-/OH^- antiport) by receptors is shown by the change in fluorescence intensity over time. The results of Hill analysis for each receptor are shown and receptor concentration is included in the legend for each assay.

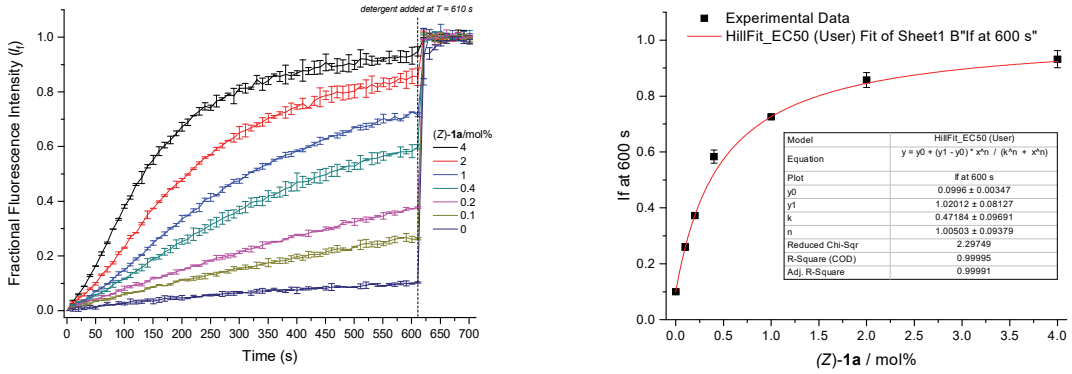

Figure S50. Hill analysis of H^+/Cl^- symport (or Cl^-/OH^- antiport) facilitated by (*Z*)-**1a** in the HPTS assay.

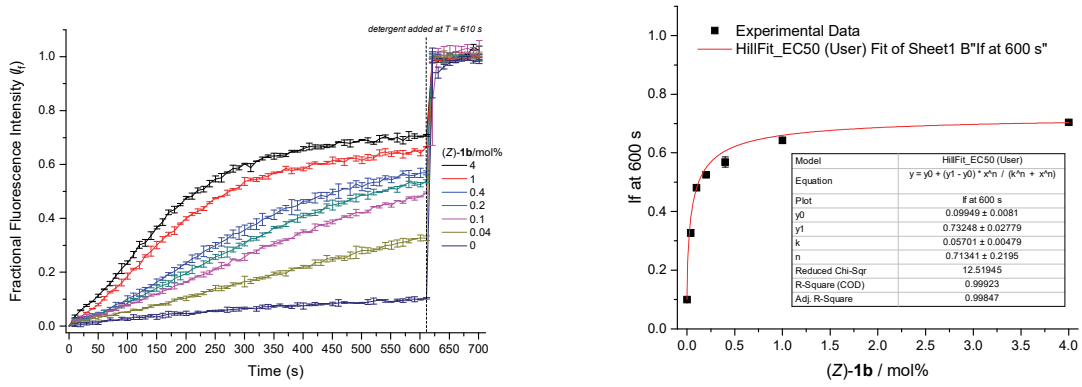

Figure S51. Hill analysis of H^+/Cl^- symport (or Cl^-/OH^- antiport) facilitated by (*Z*)-**1b** in the HPTS assay.

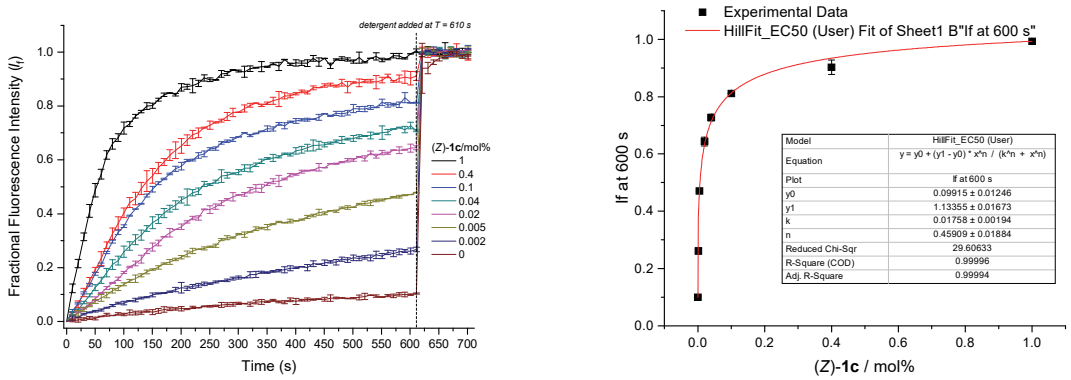

Figure S52. Hill analysis of H^+/Cl^- symport (or Cl^-/OH^- antiport) facilitated by (*Z*)-**1c** in the HPTS assay.

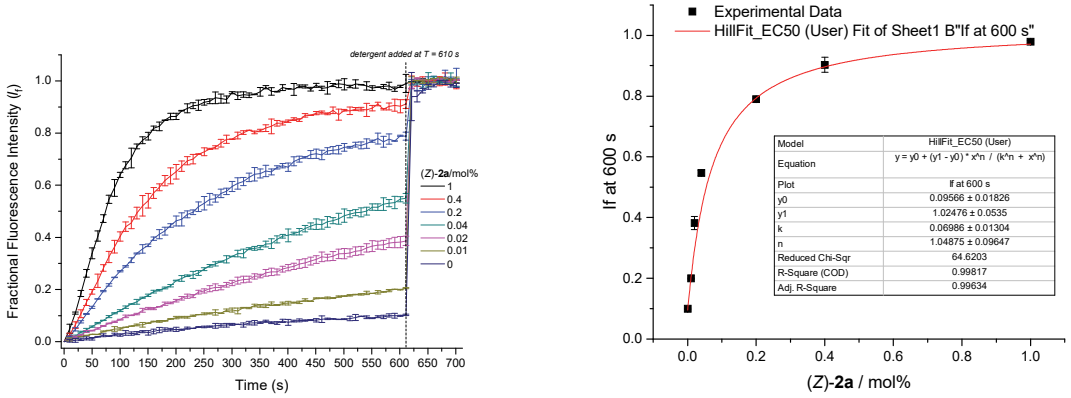

Figure S53. Hill analysis of H^+/Cl^- symport (or Cl^-/OH^- antiport) facilitated by (*Z*)-**2a** in the HPTS assay.

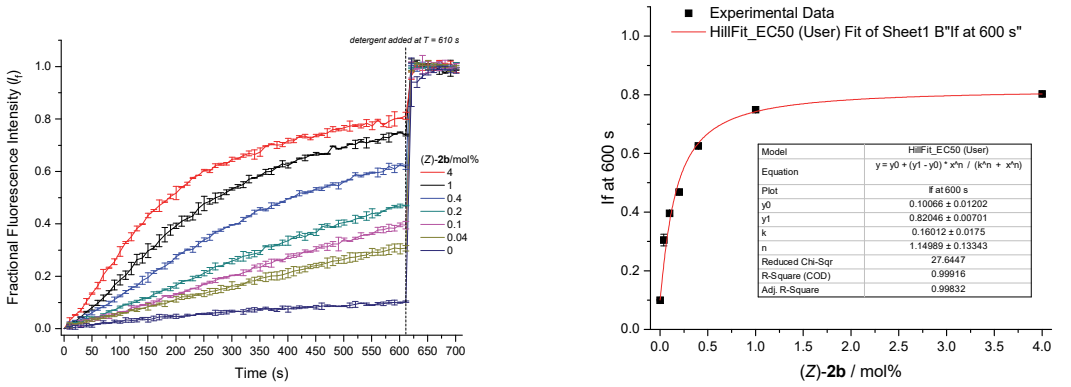

Figure S54. Hill analysis of H^+/Cl^- symport (or Cl^-/OH^- antiport) facilitated by (*Z*)-**2b** in the HPTS assay.

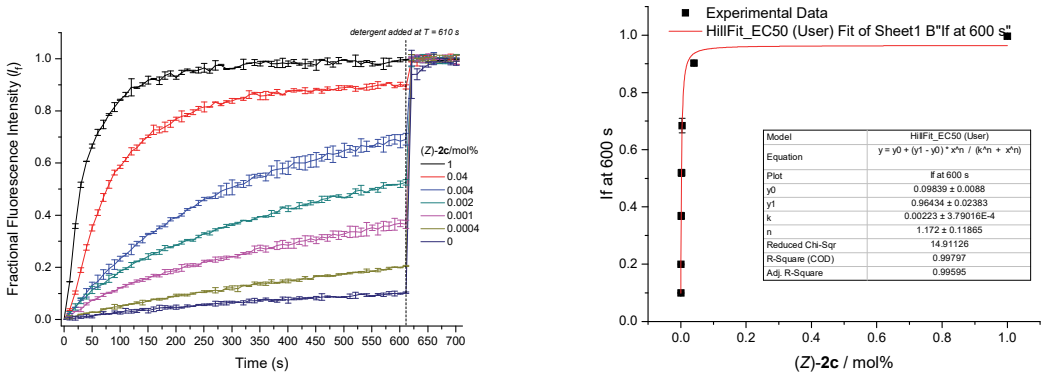

Figure S55. Hill analysis of H^+/Cl^- symport (or Cl^-/OH^- antiport) facilitated by (*Z*)-**2c** in the HPTS assay.

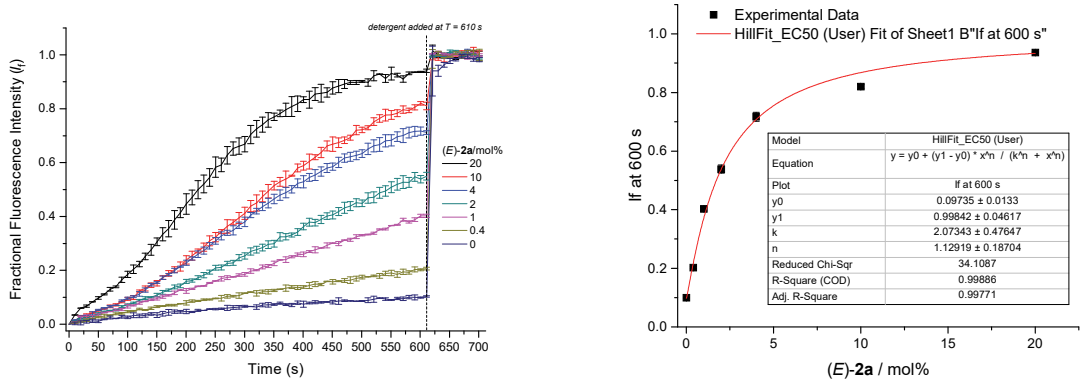

Figure S56. Hill analysis of H^+/Cl^- symport (or Cl^-/OH^- antiport) facilitated by (*E*)-**2a** in the HPTS assay.

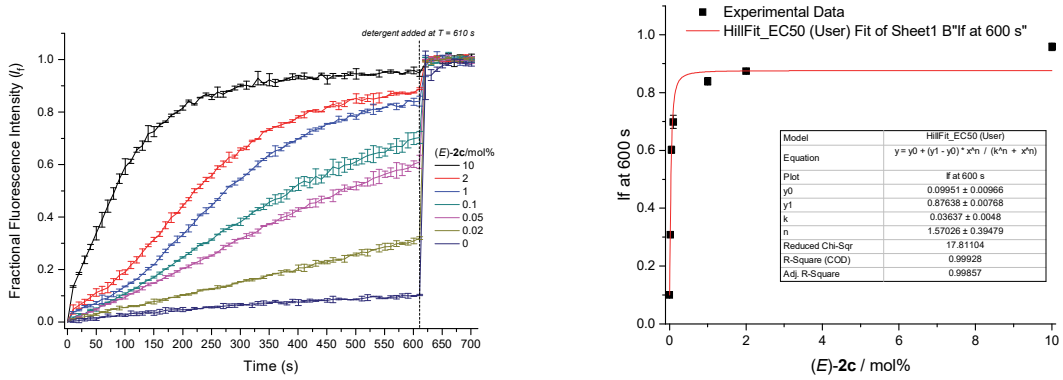

Figure S57. Hill analysis of H^+/Cl^- symport (or Cl^-/OH^- antiport) facilitated by (*E*)-**2c** in the HPTS assay.

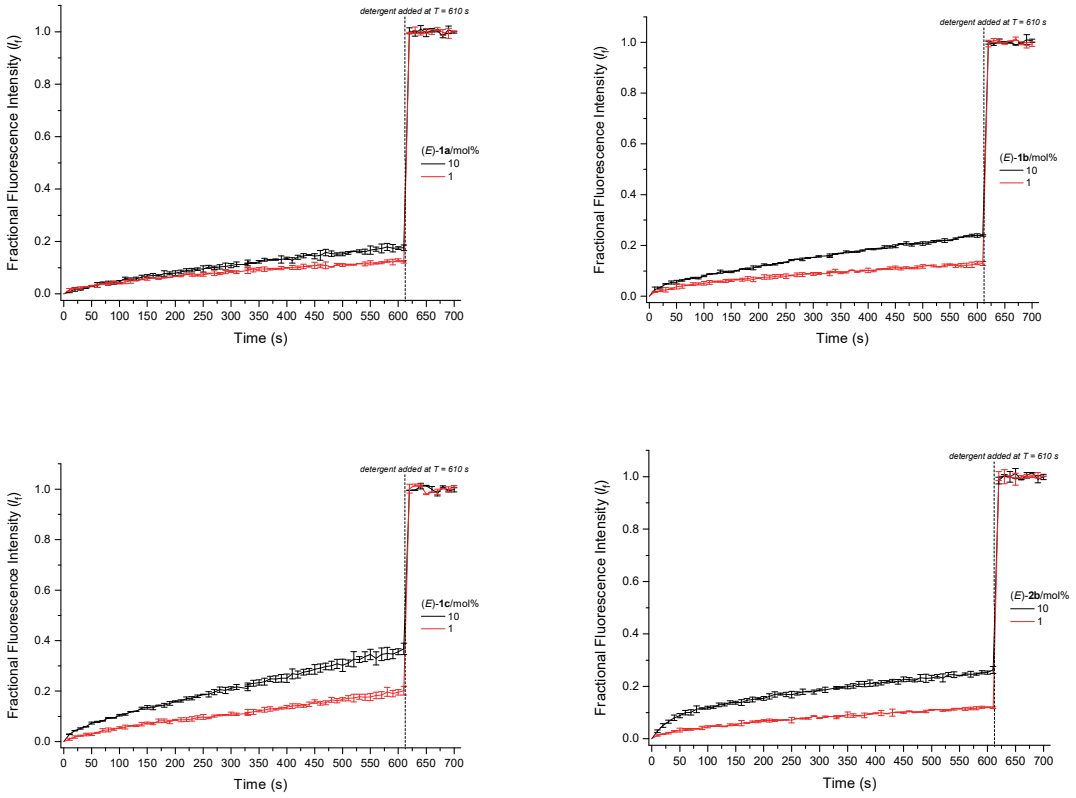

Figure S58. H^+/Cl^- symport (or Cl^-/OH^- antiport) facilitated by (*E*)-**1a**, (*E*)-**1b**, (*E*)-**1c**, and (*E*)-**2b** in the HPTS assay.

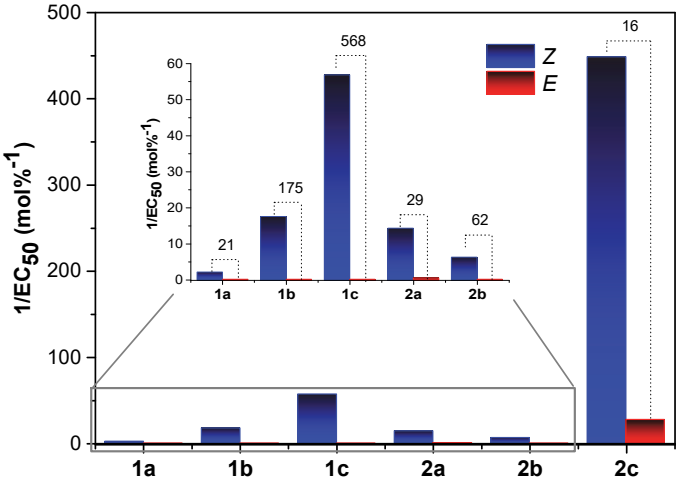

Figure S59. Bar chart comparison of transport activity calculated by EC_{50} values of (*Z*)-isomers and (*E*)-isomers. The numbers in the center of the plot are the factors of enhancement ($F'_{(Z/E)}$) for Cl^- transport activity between (*Z*)-isomer and (*E*)-isomer calculated by dividing the $EC_{50(E)}$ by the $EC_{50(Z)}$.

Effect of BSA and oleic acid

Our previous work has revealed the ability of most anion transporters to facilitate H^+ transport indirectly by catalysing the transmembrane translocation of deprotonated fatty acids.[6] To examine possible H^+ transport *via* the fatty acid shuttling mechanism for transporters, an HPTS base-pulse assay was conducted using vesicles treated with Bovine serum albumin (BSA, 1 mol%, to remove free fatty acids). The BSA treatment was performed by stirring a mixture of vesicles and BSA for 20 min. The mixture was then diluted with the external solution to a POPC concentration of 0.1 mM and used for the HPTS base-pulse study. The results demonstrate an enhancement of H^+/Cl^- symport (or Cl^-/OH^- antiport) rate by oleic acid, confirming the existence of a H^+ transport pathway *via* fatty acid shuttling for transporters. However, significant H^+ transport was observed for BSA-treated vesicles indicating that the transporter can also facilitate H^+ transport without fatty acids, presumably *via* a deprotonation mechanism. Note that here monensin (0.1 μM, 0.1 mol%) instead of detergent was used to calibrate the fluorescence response to 100% transport because of the interaction between BSA and HPTS after the vesicles are lysed with detergent. The results of Hill analysis for each receptor are shown and receptor concentration is included in the legend for each assay.

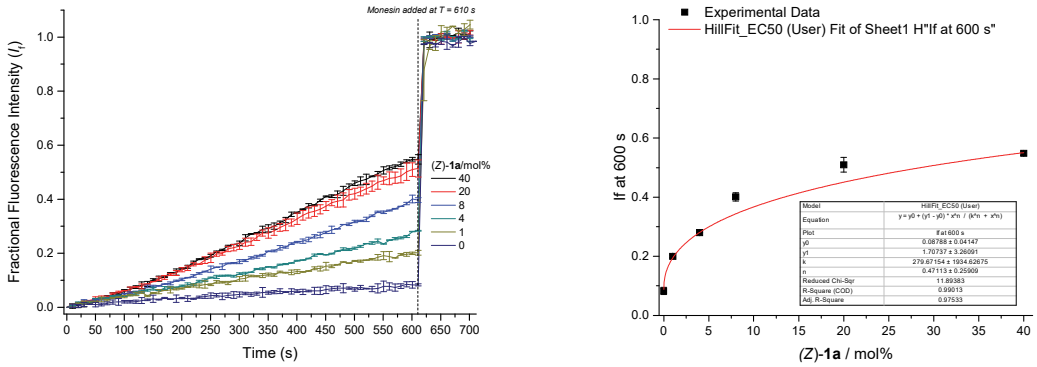

Figure S60. Hill analysis of H^+/Cl^- symport (or Cl^-/OH^- antiport) facilitated by (*Z*)-**1a** in the HPTS assay with 'fatty acid free conditions' in BSA treated vesicles.

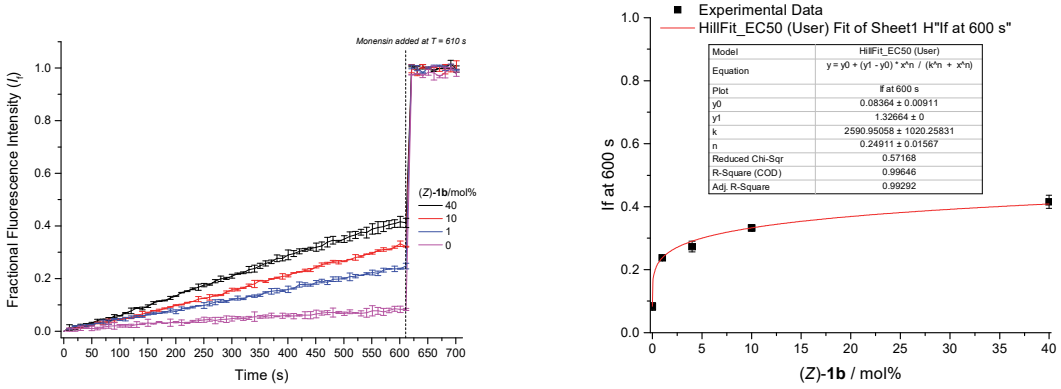

Figure S61. Hill analysis of H^+/Cl^- symport (or Cl^-/OH^- antiport) facilitated by (*Z*)-**1b** in the HPTS assay with 'fatty acid free conditions' in BSA treated vesicles.

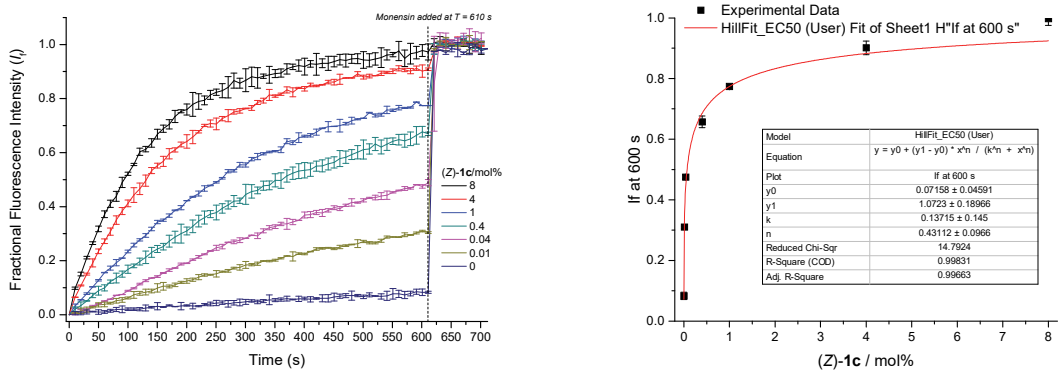

Figure S62. Hill analysis of H^+/Cl^- symport (or Cl^-/OH^- antiport) facilitated by (*Z*)-**1c** in the HPTS assay with 'fatty acid free conditions' in BSA treated vesicles.

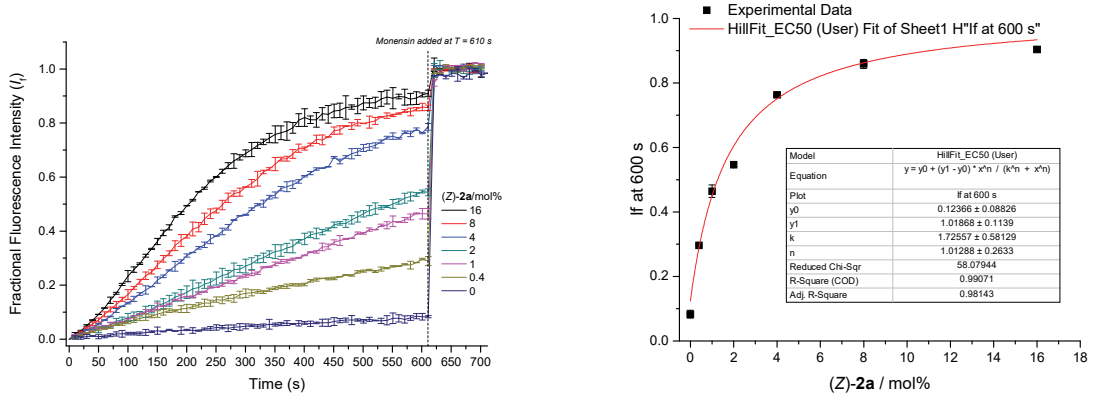

Figure S63. Hill analysis of H^+/Cl^- symport (or Cl^-/OH^- antiport) facilitated by (*Z*)-**2a** in the HPTS assay with 'fatty acid free conditions' in BSA treated vesicles.

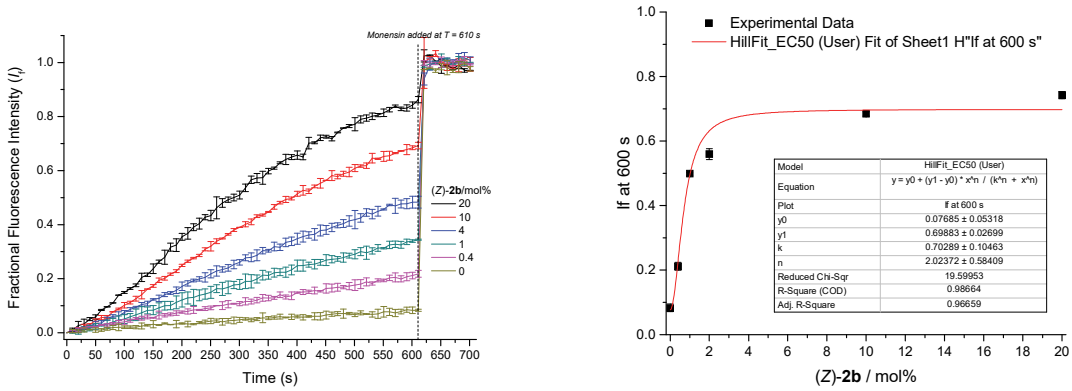

Figure S64. Hill analysis of H^+/Cl^- symport (or Cl^-/OH^- antiport) facilitated by (*Z*)-**2b** in the HPTS assay with 'fatty acid free conditions' in BSA treated vesicles.

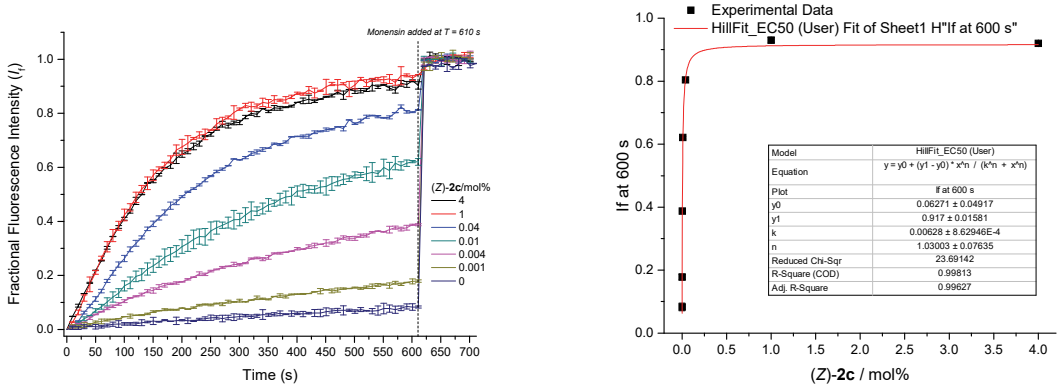

Figure S65. Hill analysis of H^+/Cl^- symport (or Cl^-/OH^- antiport) facilitated by (*Z*)-**2c** in the HPTS assay with 'fatty acid free conditions' in BSA treated vesicles.

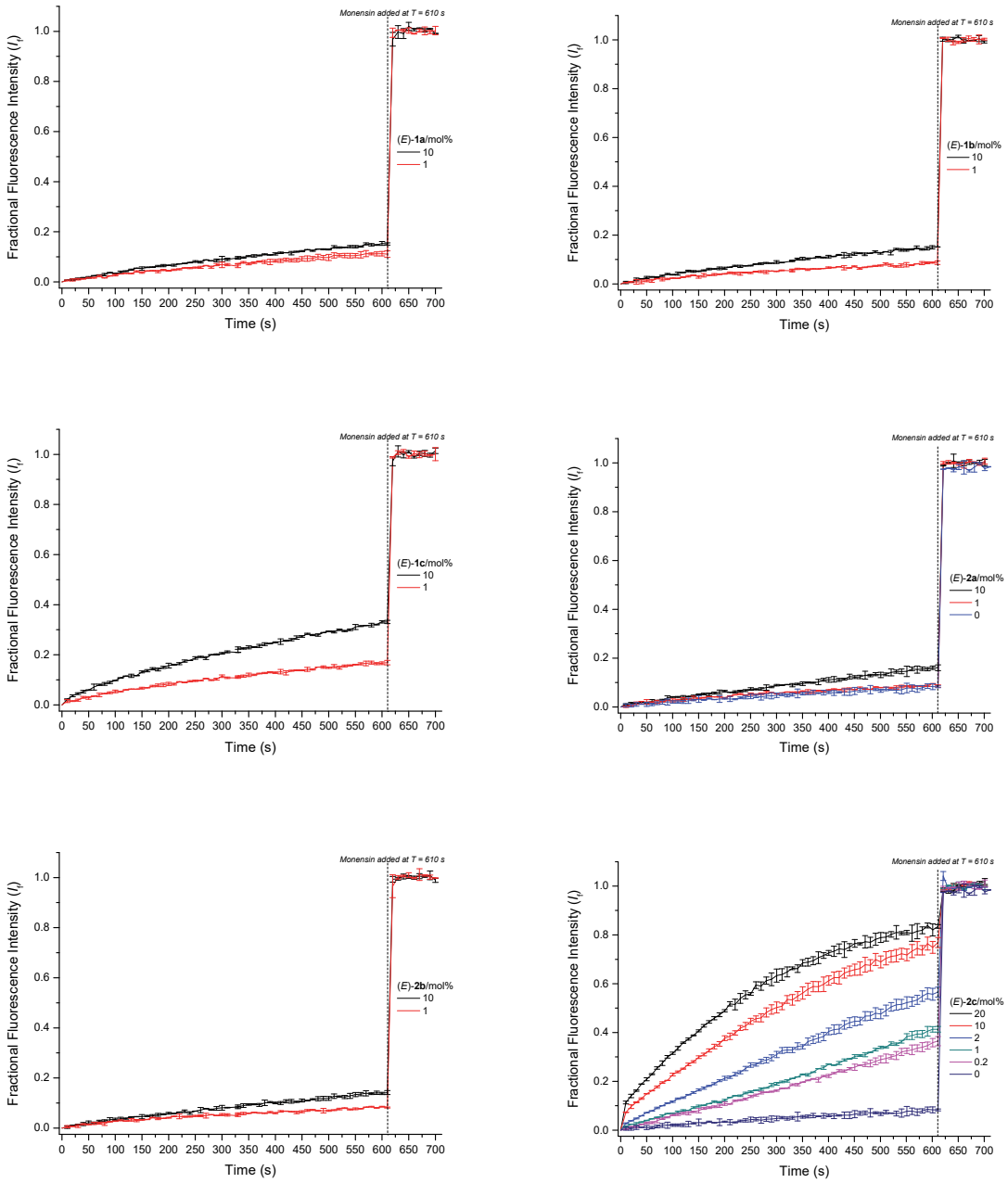

Figure S66. H^+/Cl^- symport (or Cl^-/OH^- antiport) facilitated by (*E*)-**1a**, (*E*)-**1b**, (*E*)-**1c**, (*E*)-**2a**, (*E*)-**2b**, and (*E*)-**2c** in the HPTS assay with 'fatty acid free conditions' in BSA treated vesicles.

Ion transport activity in the presence of FCCP

Following the same procedure as stated above vesicles were prepared. HPTS base-pulse assay was conducted using both untreated vesicles (contains ~1 mol% of free fatty acids) and BSA (1 mol%, to remove free fatty acids) treated vesicles. The fluorescence intensity of transporter was measured in the presence of trifluoromethoxy carbonylcyanide phenylhydrazone (FCCP) to monitor the Cl^- uniport with or without the presence of fatty acid. A DMSO solution of FCCP (0.1 μM, 0.1 mol%) was added to the vesicle suspension prior to the addition of the NaOH pulse. Note that for the HPTS assay with 'fatty acid free conditions', monensin (0.1 μM, 0.1 mol%) instead of detergent (25 μL of Triton X-100 (11 w%) in H_2O: DMSO (7:1 *v*/*v*)) was used to calibrate the fluorescence response to 100% transport. The results demonstrate an enhancement of H^+/Cl^- symport (or Cl^-/OH^- antiport) rate by FCCP, confirming the existence of a Cl^- uniport mechanism for transporters. The results of Hill Analysis for each receptor are shown and receptor concentration is included in the legend for each assay.

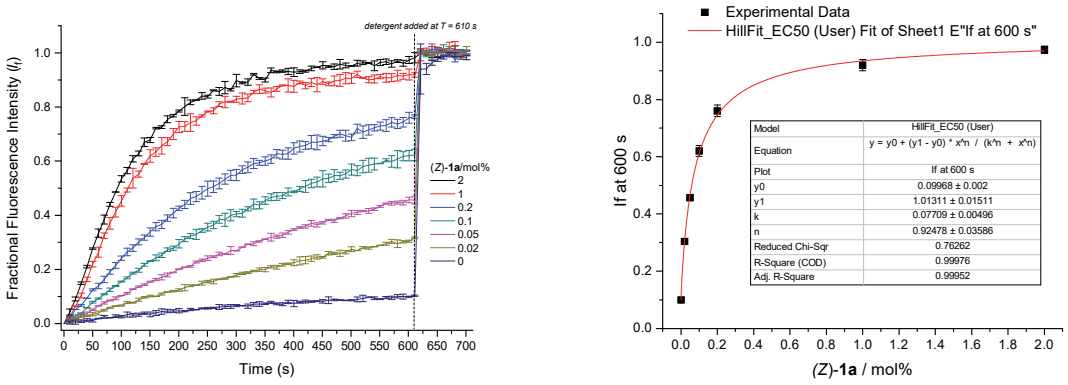

Figure S67. Hill analysis of H^+/Cl^- symport (or Cl^-/OH^- antiport) facilitated by a combination of FCCP and (*Z*)-**1a** in the HPTS assay.

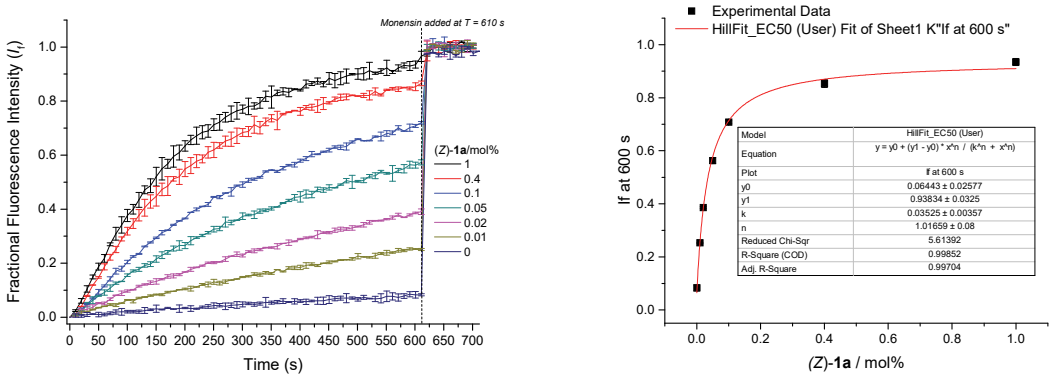

Figure S68. Hill analysis of H^+/Cl^- symport (or Cl^-/OH^- antiport) facilitated by a combination of FCCP and (*Z*)-**1a** in the HPTS assay with 'fatty acid free conditions' in BSA treated vesicles.

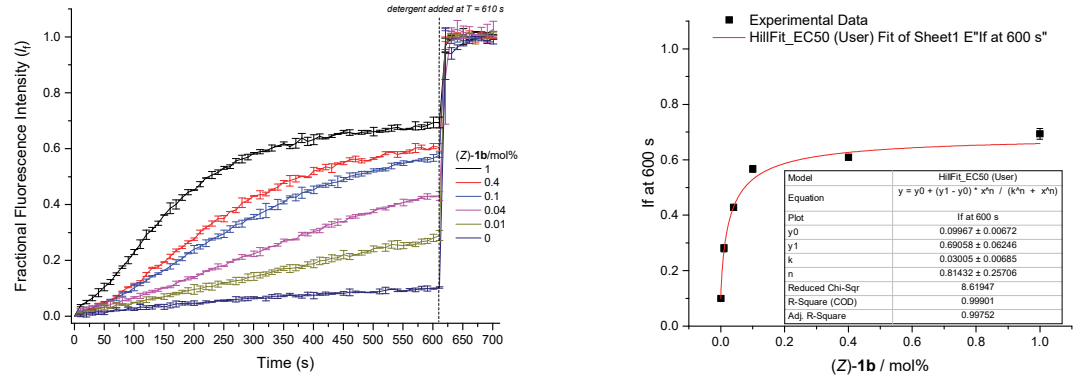

Figure S69. Hill analysis of H^+/Cl^- symport (or Cl^-/OH^- antiport) facilitated by a combination of FCCP and (*Z*)-**1b** in the HPTS assay.

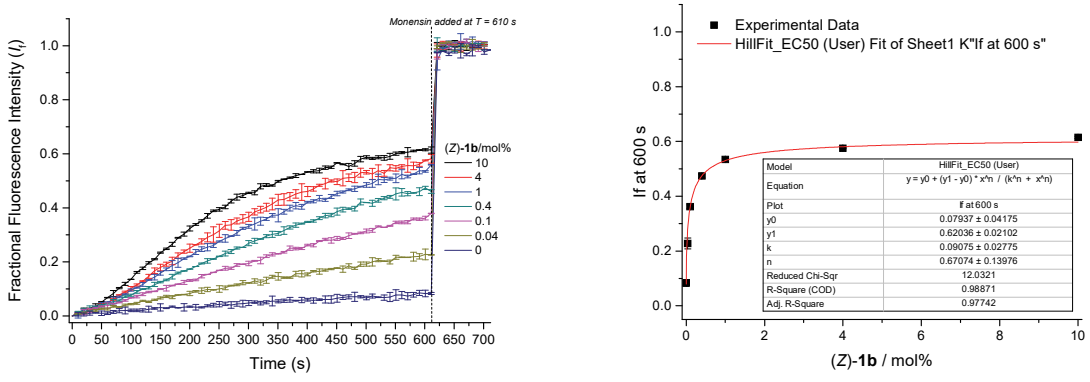

Figure S70. Hill analysis of H^+/Cl^- symport (or Cl^-/OH^- antiport) facilitated by a combination of FCCP and (*Z*)-**1b** in the HPTS assay with 'fatty acid free conditions' in BSA treated vesicles.

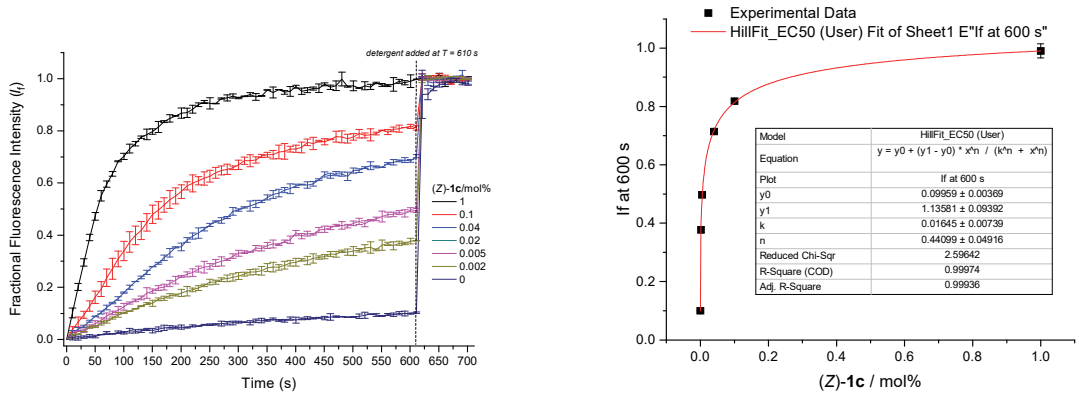

Figure S71. Hill analysis of H^+/Cl^- symport (or Cl^-/OH^- antiport) facilitated by a combination of FCCP and (*Z*)-**1c** in the HPTS assay.

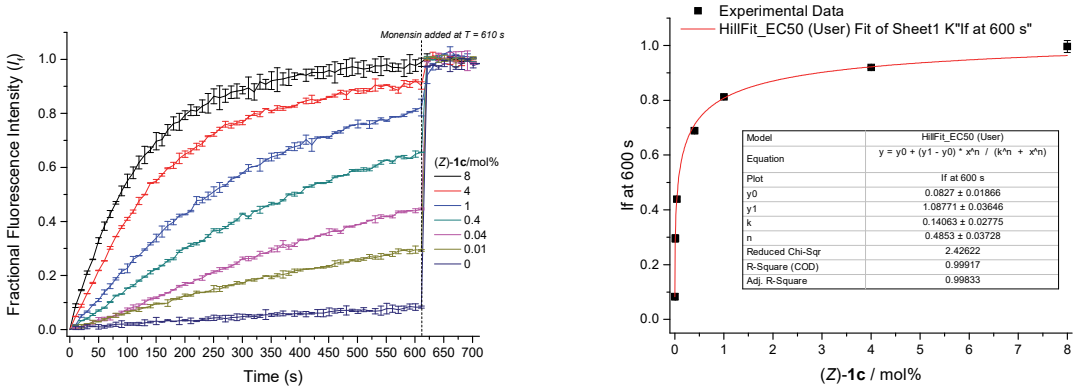

Figure S72. Hill analysis of H^+/Cl^- symport (or Cl^-/OH^- antiport) facilitated by a combination of FCCP and (*Z*)-**1c** in the HPTS assay with 'fatty acid free conditions' in BSA treated vesicles.

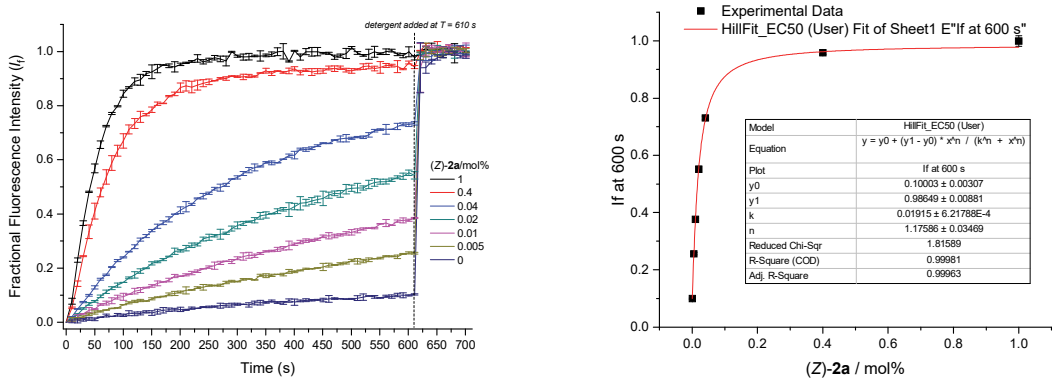

Figure S73. Hill analysis of H^+/Cl^- symport (or Cl^-/OH^- antiport) facilitated by a combination of FCCP and (*Z*)-**2a** in the HPTS assay.

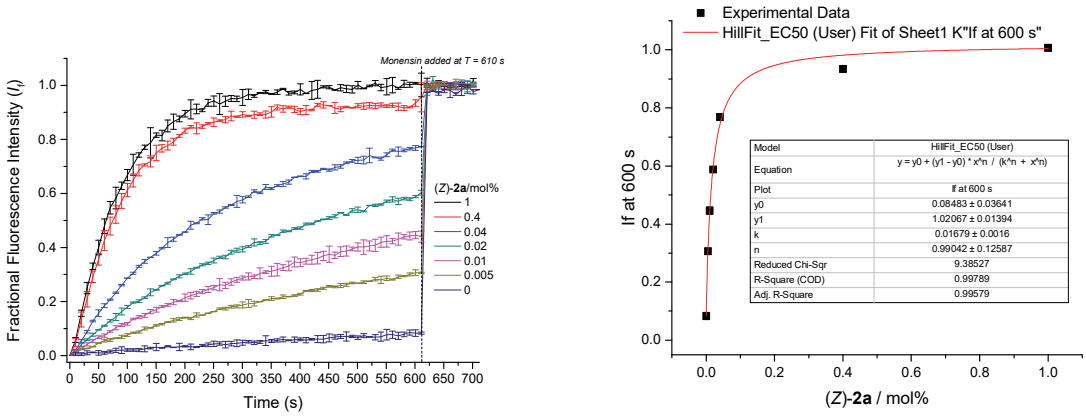

Figure S74. Hill analysis of H^+/Cl^- symport (or Cl^-/OH^- antiport) facilitated by a combination of FCCP and (*Z*)-**2a** in the HPTS assay with 'fatty acid free conditions' in BSA treated vesicles.

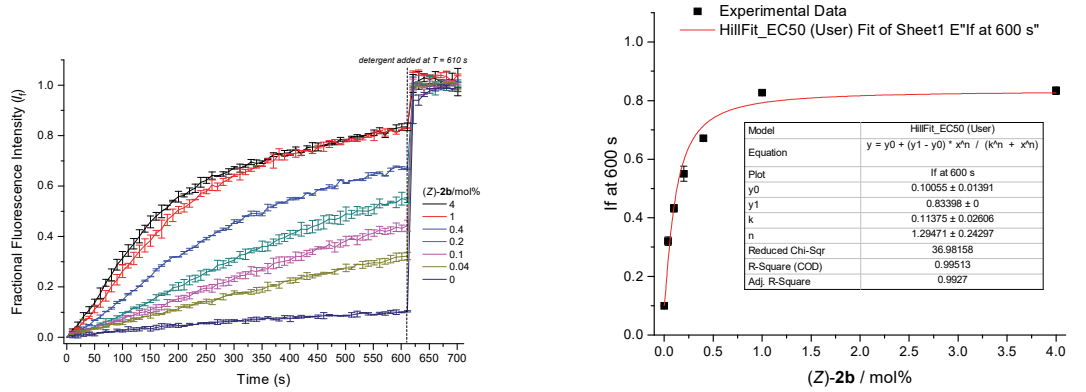

Figure S75. Hill analysis of H^+/Cl^- symport (or Cl^-/OH^- antiport) facilitated by a combination of FCCP and (*Z*)-**2b** in the HPTS assay.

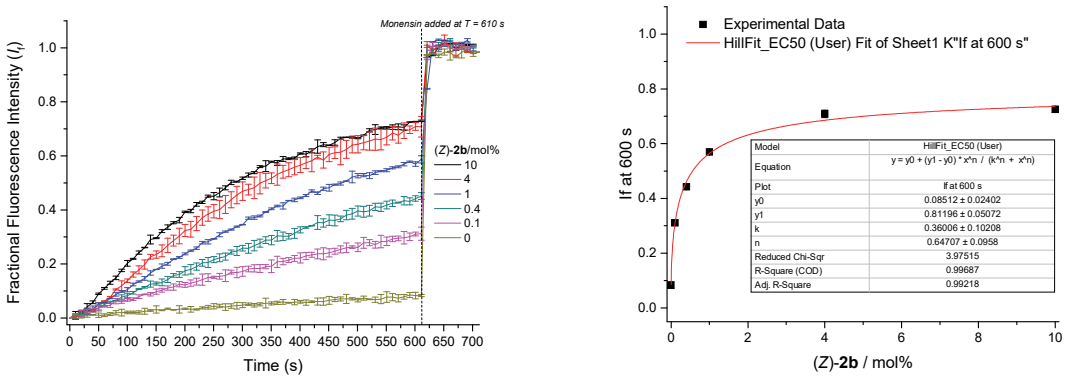

Figure S76. Hill analysis of H^+/Cl^- symport (or Cl^-/OH^- antiport) facilitated by a combination of FCCP and (*Z*)-**2b** in the HPTS assay with 'fatty acid free conditions' in BSA treated vesicles.

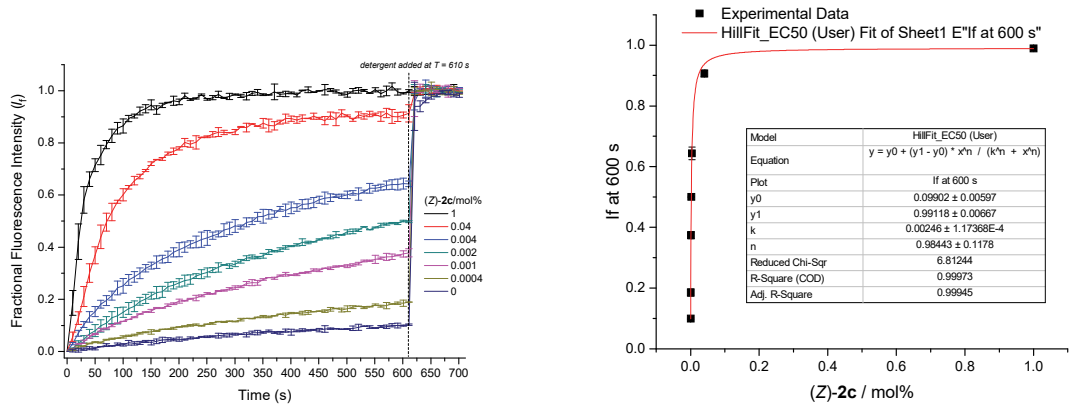

Figure S77. Hill analysis of H^+/Cl^- symport (or Cl^-/OH^- antiport) facilitated by a combination of FCCP and (*Z*)-**2c** in the HPTS assay.

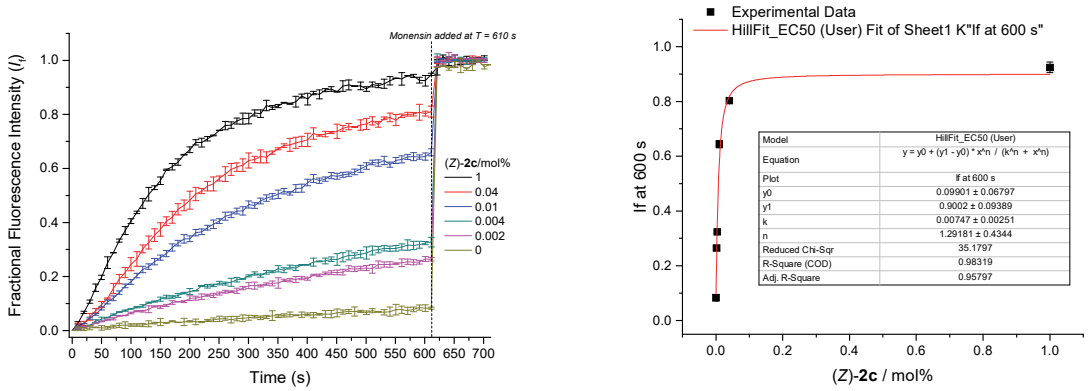

Figure S78. Hill analysis of H^+/Cl^- symport (or Cl^-/OH^- antiport) facilitated by a combination of FCCP and (*Z*)-**2c** in the HPTS assay with 'fatty acid free conditions' in BSA treated vesicles.

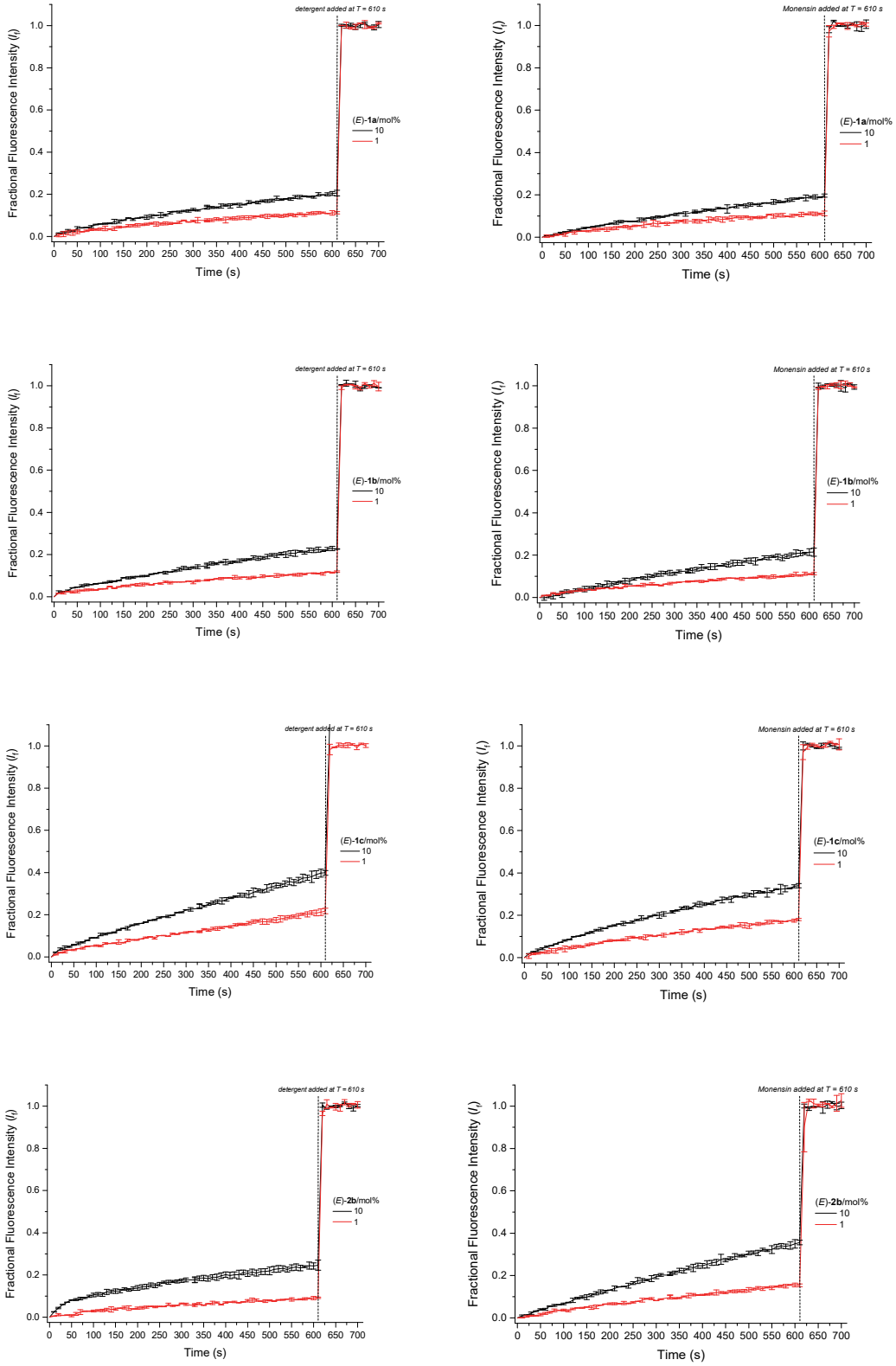

Figure S79. H^+/Cl^- symport (or Cl^-/OH^- antiport) facilitated by a combination of FCCP with (*E*)-**1a**, (*E*)-**1b**, (*E*)-**1c**, and (*E*)-**2b** in the HPTS assay (left) and with 'fatty acid free conditions' in BSA treated vesicles (right).

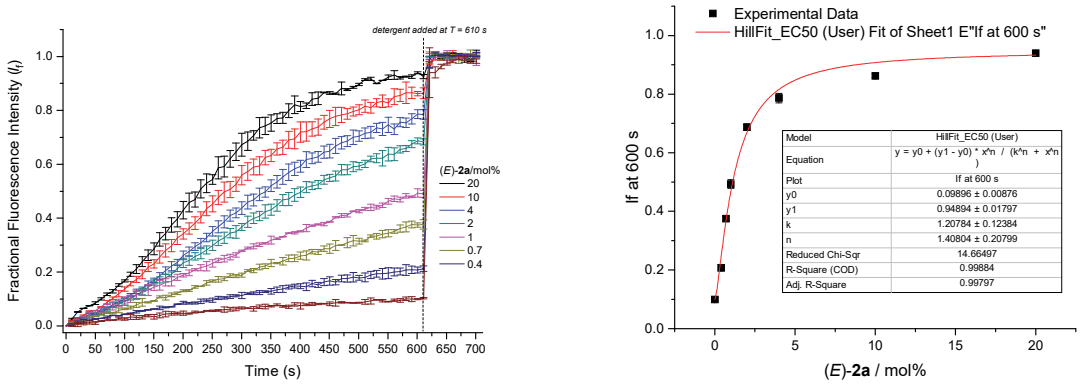

Figure S80. Hill analysis of H^+/Cl^- symport (or Cl^-/OH^- antiport) facilitated by a combination of FCCP and (*E*)-**2a** in the HPTS assay.

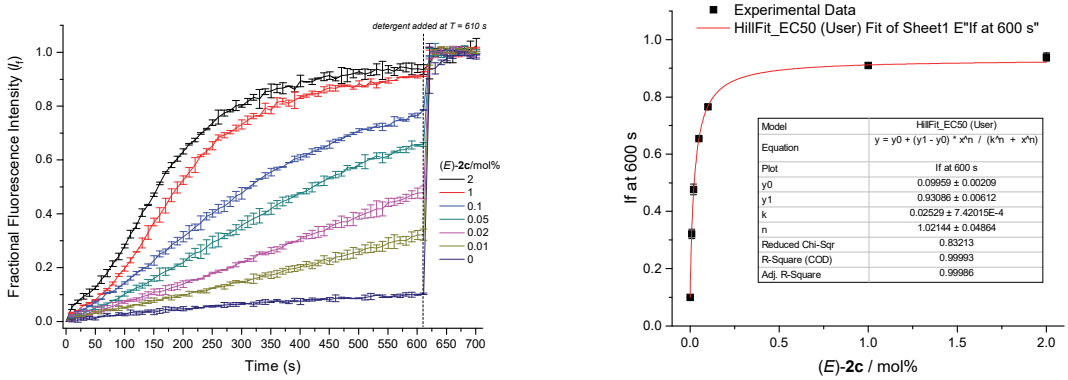

Figure S81. Hill analysis of H^+/Cl^- symport (or Cl^-/OH^- antiport) facilitated by a combination of FCCP and (*Z*)-**2c** in the HPTS assay.

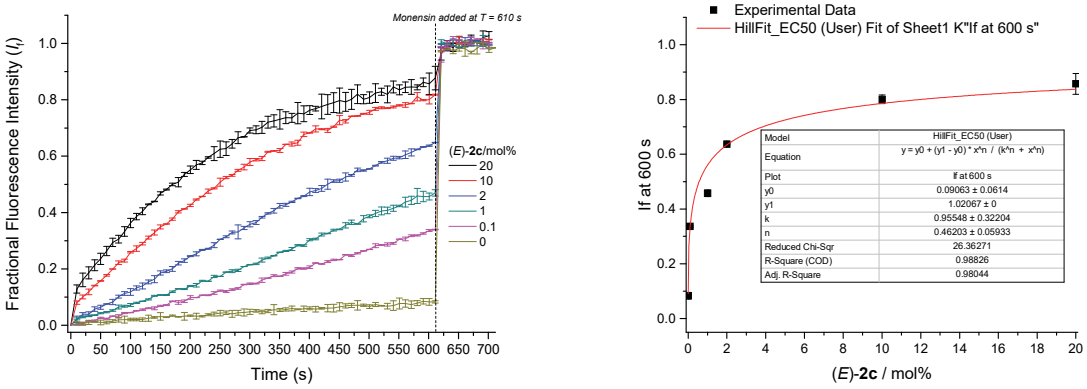

Figure S82. Hill analysis of H^+/Cl^- symport (or Cl^-/OH^- antiport) facilitated by a combination of FCCP and (*Z*)-**2c** in the HPTS assay with 'fatty acid free conditions' in BSA treated vesicles.

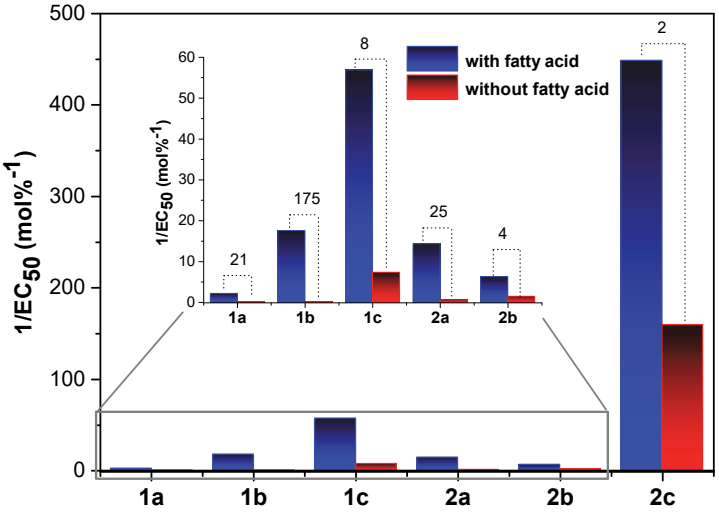

Figure S83. Bar chart comparison of transport activity calculated by EC_{50} values obtained in the absence and presence of fatty acid. The numbers on the top of the plot are the factors of enhancement (F_{FA}) of the overall rate of Cl^-/H^+ cotransport in the presence of fatty acid, calculated by dividing the $EC_{50(BSA)}$ by the EC_{50}. $F_{FA} > 1$ indicates the receptor can assist the flip-flop of fatty acid, increasing pH dissipation.

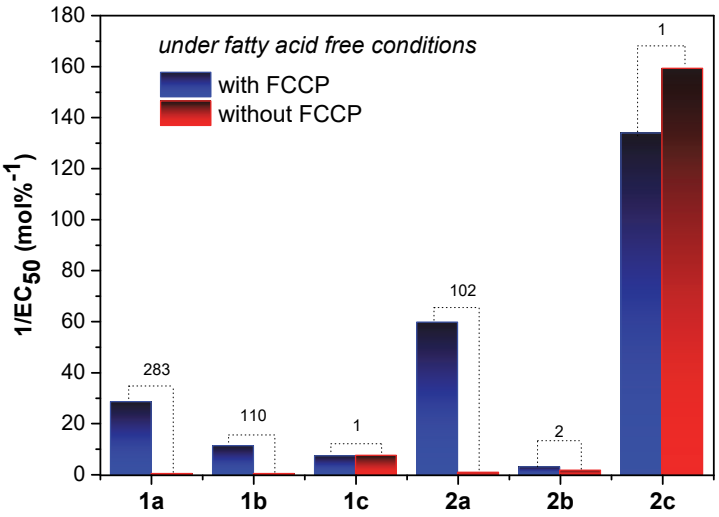

Figure S84. Bar chart comparison of transport activity calculated by EC_{50} values obtained in condition with and without the presence of FCCP with 'fatty acid free conditions' in BSA treated vesicles. The numbers in the middle of the plot are the factors of enhancement (F_s) of $Cl^- > H^+/OH^-$ selectivity, F_s is the ratio of $EC_{50(BSA)}$ divided by $EC_{50(BSA\_FCCP)}$, $F_s > 1$ indicates Cl^- transport is faster than H^+/OH^- transport, i.e., Cl^- selective transport.

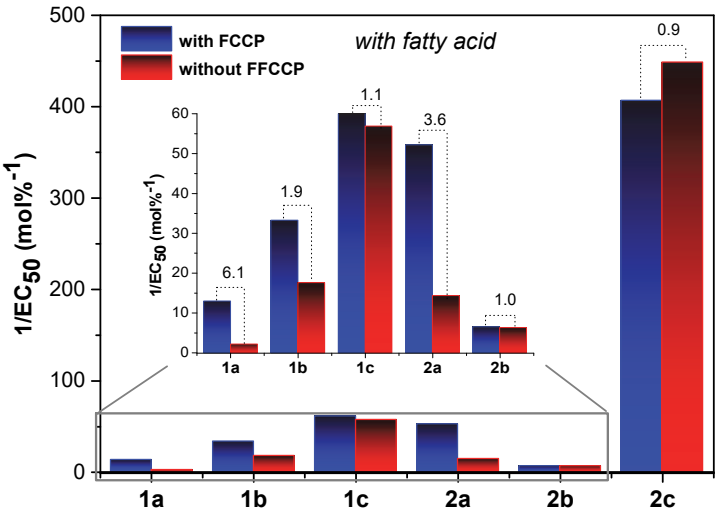

Figure S85. Bar chart comparison of transport activity calculated by EC_{50} values obtained in condition with and without the presence of FCCP. The numbers on the bars are the factors of enhancement (*F'*s) of Cl^-> H^+/OH^- selectivity retention in the presence of fatty acid, *F'*s is the ratio of EC_{50} divided by $EC_{50(FCCP)}$, *F'*s > 1 indicates Cl^- selectivity retention in the presence of fatty acid.

Cationophore Coupled Assay: Unilamellar vesicles were prepared using previously reported literature procedures. A lipid film of mixture of POPC and compound (*Z*)-**2a** (1 mol% with respect to POPC) was prepared from a chloroform solution under reduced pressure and then dried under vacuum for 6 hours. The lipid film was rehydrated by vortexing with an internal solution of HEPES buffered potassium chloride (KCl) at pH 7.2. The lipid suspension was then subjected to 9 freeze-thaw cycles and left to rest at room temperature for 30 minutes. After this the suspension was extruded 25 times through a 200 nm polycarbonate membrane resulting in unilamellar vesicles of an average diameter of 200 nm. The vesicles were then passed through a Sephadex® column saturated with HEPES buffered external potassium gluconate (KGlu) at pH 7.2, which allowed the exchange of any unencapsulated KCl for KGlu. The lipid solution obtained after Sephadex® was diluted to a standard volume (usually 10 mL) with the external KGlu solution to obtain a lipid stock of known concentration.

Chloride concentrations during the cationophore-coupled assay were determined using an Accumet chloride-selective electrode. The electrode was calibrated against sodium chloride solutions of known concentrations prior to each experiment according to the supplier's manual. For each measurement, the lipid stock solution was diluted with the external buffered solution to a standard volume (5.0 mL) with a lipid concentration of 1.0 mM. Where a

cationophore (valinomycin or monensin) was used, the addition of the cationophore as a DMSO solution (1 μM, 0.1 mol%) was added to start the experiment and the chloride efflux was monitored using a chloride selective electrode. After 5 minutes detergent (50 μL of Triton X-100 (11 w%) in H_2O: DMSO (7:1 *v/v*)) was added to lyse the vesicles and the 100% chloride efflux reading was taken at 7 minutes.

The screening was performed with the transporter alone, the transporter plus valinomycin or the transporter plus monensin, to assess the transport mechanism under different conditions. The electrode readings were converted to chloride concentrations using a standard calibration and subsequently converted to percentages. The results are given in Figure S85, including the initial rate of Cl^- transport (k_{ini}) observed under each condition. These k_{ini} values were calculated by fitting the obtained chloride efflux with the asymptotic function $y = a - b \cdot c^x$ using Origin 8, where y is the chloride efflux (%), x is time (s) and k_{ini} is then given by $k_{ini} = -b \cdot ln(c)$ (obtained in % s^{-1}), or by fitting the initial linear range of the obtained chloride efflux to $y = a + b \cdot x$, where y is the chloride efflux (%), x is time (s) and k_{ini} is given by the slope b. In case of a sigmoidal time dependence, the first two or three data points were omitted from the fit. In order to obtain standard deviations on the initial rate of transport, the fits were performed for each individual repeat and subsequently averaged.

The large and relatively polar gluconate anion should be hard to transport across a lipid bilayer. It is thus assumed that no transport will occur in the presence of the transporter under these conditions, because a membrane potential will build up in the case of an electrogenic Cl^- carrier or a pH gradient in the case of a H^+/Cl^- symporter or a Cl^-/OH^- antiporter. However, the addition of valinomycin can dissipate the membrane potential created by electrogenic Cl^- transport through electrogenic K^+ transport, while the addition of monensin can dissipate the pH gradient accumulated by Cl^-/OH^- antiport (or H^+/Cl^- symport) through K^+/H^+ antiport. Figure S85 show that compound (*Z*)-**2a** is capable of both electrogenic Cl^- transport (Cl^- efflux observed in the presence of valinomycin) and electroneutral H^+/Cl^- transport (Cl^- efflux observed in the presence of monensin). Faster Cl^- efflux observed when coupling with valinomycin than the one coupling with monensin, indicating compound (*Z*)-**2a** is a strong electrogenic Cl^- transporter but weak electroneutral H^+/Cl^- transporter.

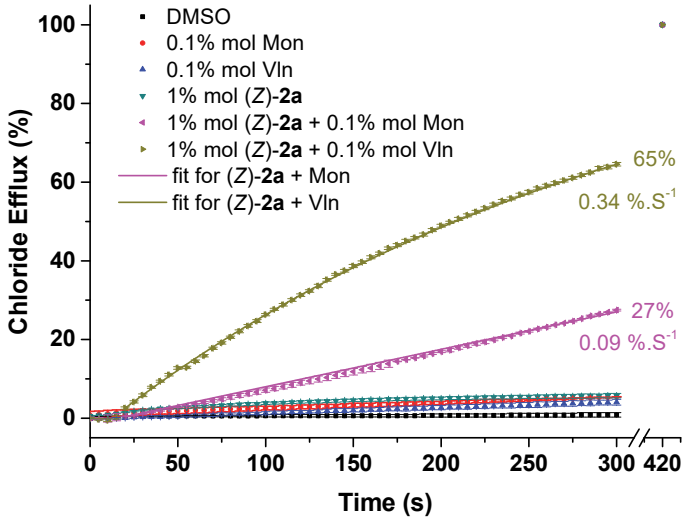

Figure S86. Electrogenic or electroneutral transport mediated by (*Z*)-**2a** (1 mol% with respect to lipid) in the presence of monensin or valinomycin (0.1 mol% with respect to lipid). Unilamellar POPC vesicles were loaded with 300 mM KCl buffered to pH 7.2 with 10 mM HEPES and dispersed in 300 mM KGlu buffered to pH 7.2 with 10 mM HEPES. Valinomycin or monensin were added to start the experiment. At the end of the experiment, detergent was added to lyse the vesicles and calibrate the ISE to 100% chloride efflux. Each point represents the average of a minimum of 3 repeats. DMSO was used as a control.

Osmotic Response Assay: The osmotic response assay was performed to support the findings that the transport mechanism is predominantly electrogenic and (*Z*)-**2a** has a selectivity for Cl^- > OH^- and H^+. Valinomycin or monensin and (*Z*)-**2a** facilitated Cl^- efflux was monitored using light scattering intensity. Vesicles containing KCl (300 mM) were suspended in KGlc (300 mM), with all solutions buffered to pH 7.2. Cl^- efflux occurs and is followed by efflux of water to dissipate the osmotic gradient. This leads to vesicle dehydration and shrinkage, and this increases the 90° light scattering, which was measured using a fluorimeter.

The osmotic response assay was prepared as follows. A thin lipid film was acquired from the evaporation of a chloroform solution of the mixture of POPC and compound (*Z*)-**2a** (1 mol% with respect to POPC) from a round bottom flask, this film was dried under vacuum for at least 6 h. The lipid film was hydrated by vortexing with the chosen internal solution and the lipid suspension was then subjected to nine freeze/thaw cycles and was then extruded through a 400 nm polycarbonate membrane 25 times to obtain the vesicle stock solution. Vesicles containing KCl (300 mM buffered to pH 7.2 using HEPES 10 mM) were suspended in KGlu

(300 mM buffered to pH 7.2 using HEPES 10 mM) to make a test solution of 0.4 mM lipid in 2.2 mL external solution. A DMSO solution of valinomycin (0.4 μM, 0.1 mol%) or monensin (0.4 μM, 0.1 mol%) was added to commence the experiment, the light scattering intensity at 600 nm was monitored. At 1 h, prodigiosin (0.04 μM, 0.01 mol%) and FCCP (4 μM, 1.0 mol%) were added to calibrate 100% Cl^- efflux. Only prodigiosin was required to be added when the assay was run with monensin. The fractional light scattering intensity (I_f) was calculated using the following equation:

$$I_f = \frac{I_t - I_0}{I_c - I_0}$$

Where I_t is light scattering intensity at a given time, I_0 is the light scatting intensity at 0 s and I_c is the light scattering intensity after the addition of Prod (and FCCP).

Consistent with the ISE results, the transport process of chloride by the active (*Z*)-**2a** is more electrogenic, since faster Cl^- efflux was observed when coupling with valinomycin than when coupling with monensin.

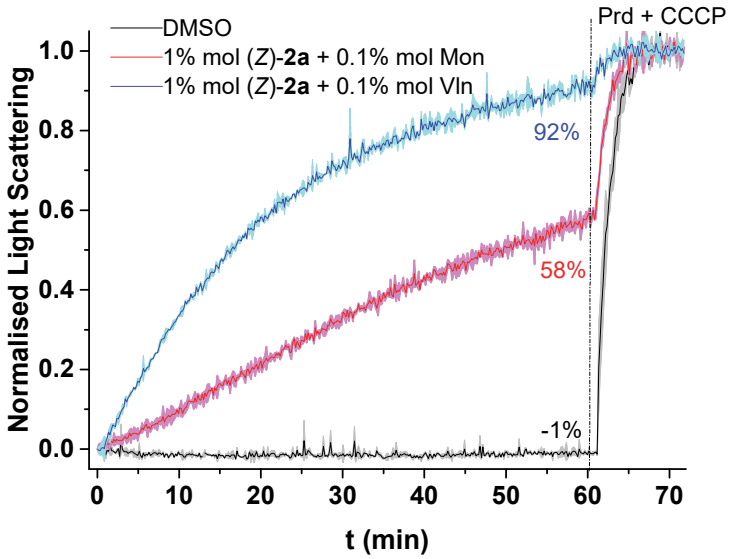

Figure S87. Electrogenic or electroneutral transport mediated by (*Z*)-**2a** (1 mol% with respect to lipid) in the presence of monensin or valinomycin (0.1 mol% with respect to lipid). Unilamellar POPC liposomes of mean diameter of 400 nm were loaded with 300 mM KCl buffered to pH 7.2 with 10 mM HEPES and dispersed in 300 mM KGlu buffered to pH 7.2 with 10 mM HEPES. Valinomycin or monensin were added to start the experiment. Each point represents the average of a minimum of 2 repeats. DMSO was used as a control.

Photocontrolled anion transport

HPTS Assay: The vesicles were prepared by following the protocol as stated above HPTS assay. Transporter (*E*)-**2a** was added in DMSO (5 μL, 1 μM, 1.0 mol% relative to lipid) at 0 s and fluorescence intensity was monitored over time. The sample (vesicles with (*E*)-**2a**) was *in situ* irradiated with 365 nm wavelength UV (using a Vilber Lourmat Bio-Link UV Lamps (VL-4.LC, 4W) placed at a distance about 2 cm) for time, t_R = 0, 20, 60 and 120 s during the test after adding transport to start the experiment (in a darkened room with the lid open and the lamp placed above the cuvette). Then the normalized fluorescence intensity (i.e., activity) value at t = 600 s were noted from plot. The data was further normalized to get *% transport efficiency* F_R by setting the HPTS fluorescence of the blank sample to 0 and that of (*Z*)-**2a** (1 mol%) to 100.

$$F_R = [(I_{S(t=600)} - I_{blank(t=600)}) / (I_{(Z)\text{-}\mathbf{2a}(t=600)} - I_{blank(t=600)})]$$

where, $I_{S(t=600)}$ is the normalized fluorescence intensity of a photoirradiated sample at 600 s, $(I_{(Z)\text{-}\mathbf{2a}(t=600)}$ is the normalized fluorescence intensity of sample (*Z*)-**2a** at 600 s, and $I_{blank(t=600)}$ is the normalized fluorescence intensity of the blank at 600 s.

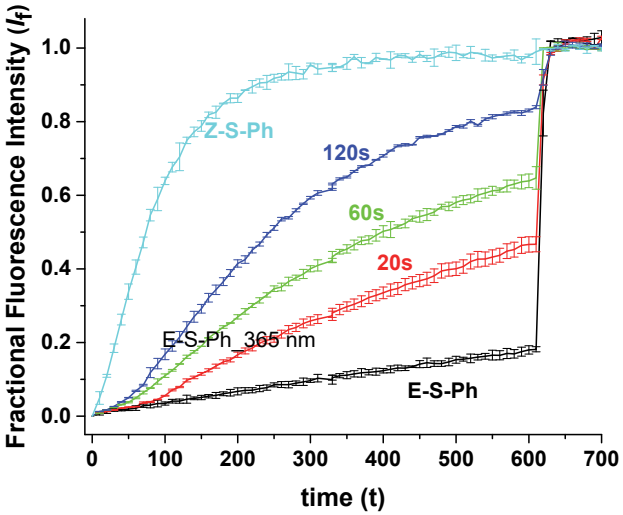

Figure S88. H^+/Cl^- symport (or Cl^-/OH^- antiport) facilitated by a photoirradiated sample of (*E*)-**2a** or (*Z*)-**2a** (1 mol% with respect to lipid) using a HPTS assay. Unilamellar POPC liposomes of mean diameter of 200 nm were loaded with 100 mM NaCl buffered to pH 7.0 with 10 mM HEPES and dispersed in 100 mM NaCl buffered to pH 7.0 with 10 mM HEPES. A pulse of NaOH (25 μL of 0.5 M solution, final concentration 5 mM) was added to the vesicle suspension to generate a pH gradient of pH 7 inside and pH 8 outside, before the addition of a DMSO solution of an anion transporter to start the experiment. Each point represents the average of a minimum of 2 repeats.

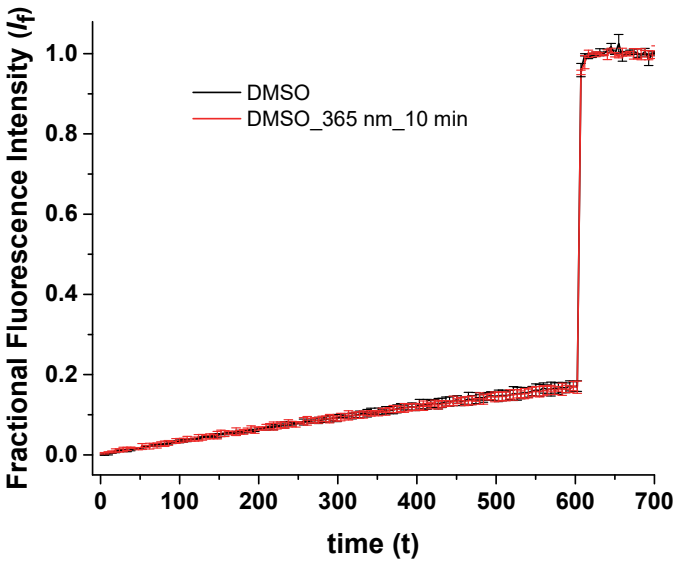

Figure S89. Ion transport of blank DMSO upon photoirradiation from a HPTS assay. Unilamellar POPC liposomes of mean diameter of 200 nm were loaded with 100 mM NaCl buffered to pH 7.0 with 10 mM HEPES and dispersed in 100 mM NaCl buffered to pH 7.0 with 10 mM HEPES. A pulse of NaOH (25 μL of 0.5 M solution, final concentration 5 mM) was added to the vesicle suspension to generate a pH gradient of pH 7 inside and pH 8 outside, before the addition of a DMSO solution of an anion transporter to start the experiment. Sample illumination was achieved using high powered LEDs. Each point represents the average of a minimum of 2 repeats.

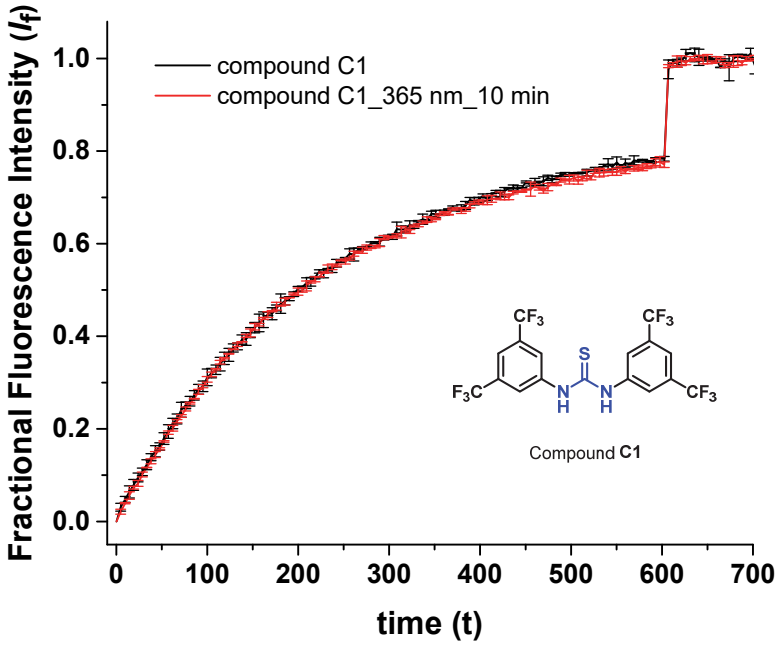

Figure S90. H^+/Cl^- symport (or Cl^-/OH^- antiport) facilitated by a control compound C1 (0.01 mol% relative to lipid) upon photoirradiation from a HPTS assay. Unilamellar POPC liposomes of mean diameter of 200 nm were loaded with 100 mM NaCl buffered to pH 7.0 with 10 mM HEPES and dispersed in 100 mM NaCl buffered to pH 7.0 with 10 mM HEPES. A pulse of NaOH (25 μL of 0.5 M solution, final concentration 5 mM) was added to the vesicle suspension to generate a pH gradient of pH 7 inside and pH 8 outside, before the addition of a DMSO solution of an anion transporter to start the experiment. Sample illumination was achieved using high powered LEDs. Each point represents the average of a minimum of 2 repeats.

Cationophore Coupled Assay: The vesicles were prepared by following the protocol as stated above in the cationophore coupled assay. This assay was performed to further support the light control turn-on effect on chloride transport of (*E*)-**2a**. Both (*E*)-**2a** and (*Z*)-**2a** are pre-incorporated within the lipid bilayer during the liposome preparation, at 1 mol% with respect to POPC. Monensin (1 μM, 0.1 mol%), and valinomycin (1 μM, 0.1 mol%) are added as solutions in DMSO. The (*E*)-**2a** sample was irradiated with 365 nm wavelength UV (a Thorlab model M365FP1 high-power LED (15.5 mW) positioned at a distance of 1 cm to the sample) for 20 s during the test. Then the chloride efflux percentage (i.e., activity) value at t = 300 s were noted from plot. The data was further normalized to get *% transport efficiency*

F_{R_CCA} by setting the chloride efflux percentage of the blank sample to 0 and that of (*Z*)-**2a** (1 mol%) with valinomycin to 100.

$$F_{R\_CCA} = [(I_{S(t = 300)} - I_{blank(t = 300)}) / (I_{(Z)\text{-}\mathbf{2a}(t = 300)} - I_{blank(t = 300)})]$$

where, $I_{S(t = 300)}$ is the chloride efflux percentage of a photoirradiated sample at 300 s, ($I_{(Z)\text{-}\mathbf{2a}(t = 300)}$ is the chloride efflux percentage of sample (*Z*)-**2a** at 300 s, and $I_{blank(t = 300)}$ is the chloride efflux percentage of the blank at 300 s.

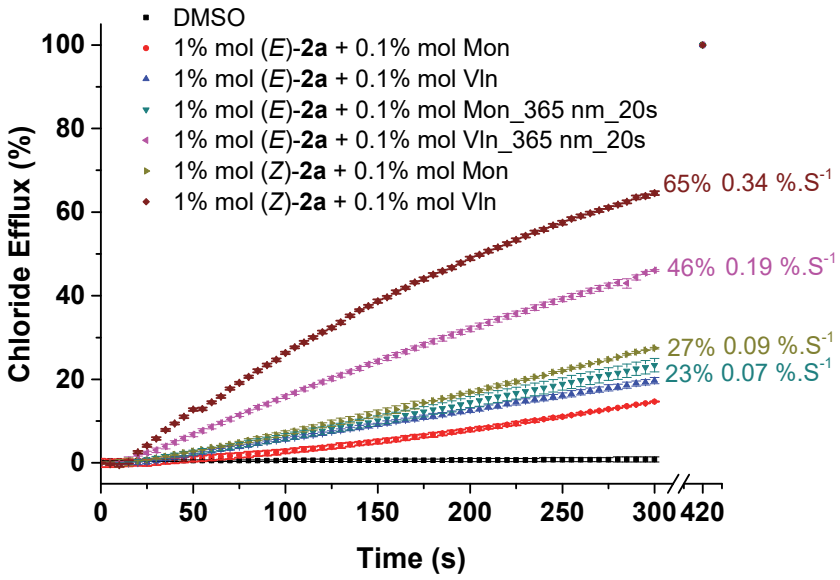

Figure S91. Electrogenic or electroneutral transport mediated by a photoirradiated sample of (*E*)-**2a** or (*Z*)-**2a** (1 mol% with respect to lipid). Unilamellar POPC liposomes of mean diameter of 200 nm were loaded with 300 mM KCl buffered to pH 7.2 with 10 mM HEPES and dispersed in 300 mM KGlu buffered to pH 7.2 with 10 mM HEPES. Valinomycin or monensin were added to start the experiment. Each point represents the average of a minimum of 2 repeats. DMSO was used as a control.

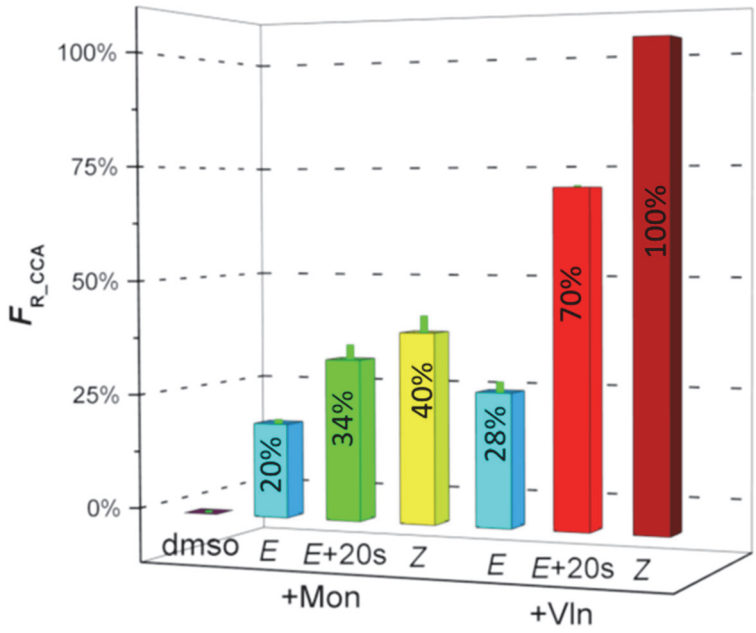

Figure S92. Percent electrogenic (with valinomycin) or electroneutral (with monensin) transport efficiencies of a photoirradiated sample of (*E*)-**2a** relative to the electrogenic transport activity of (*Z*)-**2a**.

Osmotic Response Assay: The osmotic response assay was performed to support the findings that transport can be switched on or off by light in situ. Vesicles were prepared by following the protocol as stated above for the osmotic response assay. Both (*E*)-**2a** and (*Z*)-**2a** are pre-incorporated within the lipid bilayer during the liposome preparation, at 1 mol% with respect to POPC. Monensin (0.4 μM, 0.1 mol%), and valinomycin (0.4 μM, 0.1 mol%) are added as solutions in DMSO. The liposomes with the sample (*E*)-**2a** was irradiated with 365 nm wavelength UV (using a Thorlab model M365FP1 high-power LED (15.5 mW) positioned at a distance of 1 cm from the sample) for 20 s during the test. The (*Z*)-**2a** sample was irradiated with 385 nm wavelength UV (using a Thorlab model M385FP1 high-power LED (23.2 mW) positioned at a distance of 1 cm from the sample) for 60 s during the test. Then the light scattering (chloride efflux percentage i.e., activity) value at t = 60 min was noted from plot. The data was further normalized to get *% transport efficiency* F_{R_ORA} by setting the chloride efflux percentage of blank sample to 0 and that of (*Z*)-**2a** (1 mol%) with valinomycin to 100.

$$F_{R\_ORA} = [(I_{S(t=60)} - I_{blank(t=60)}) / (I_{(Z)\text{-}\mathbf{2a}(t=60)} - I_{blank(t=60)})]$$

where, $I_{S(t=60)}$ is the chloride efflux percentage of a photoirradiated sample at 60 min, $(I_{(Z)\text{-}\mathbf{2a}(t=60)}$ is the chloride efflux percentage of sample (*Z*)-**2a** with valinomycin at 60 min, and $I_{blank(t=60)}$ is the chloride efflux percentage of the blank at 60 min.

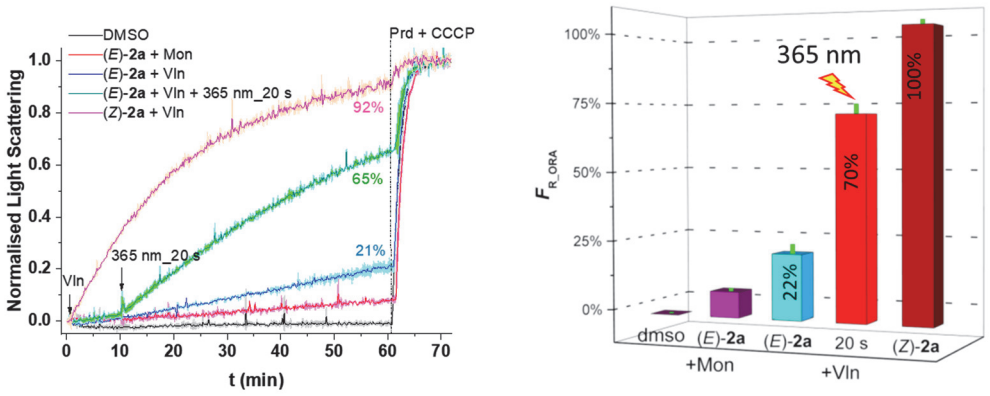

Figure S93. (a) Electrogenic or electroneutral transport mediated by a photoirradiated sample of (*E*)-**2a** measured relative to the electrogenic transport activity of (*Z*)-**2a** (1 mol% with respect to lipid) using an osmotic response assay. (b) Percent transport efficiencies of photoirradiated the sample (*E*)-**2a** measured relative to the electrogenic transport activity of (*Z*)-**2a** using osmotic response assay. Unilamellar POPC liposomes of mean diameter of 400 nm were loaded with 300 mM KCl buffered to pH 7.2 with 10 mM HEPES and dispersed in 300 mM KGlu buffered to pH 7.2 with 10 mM HEPES. Valinomycin or monensin were added to start the experiment. Each point represents the average of a minimum of 2 repeats. DMSO was used as a control.

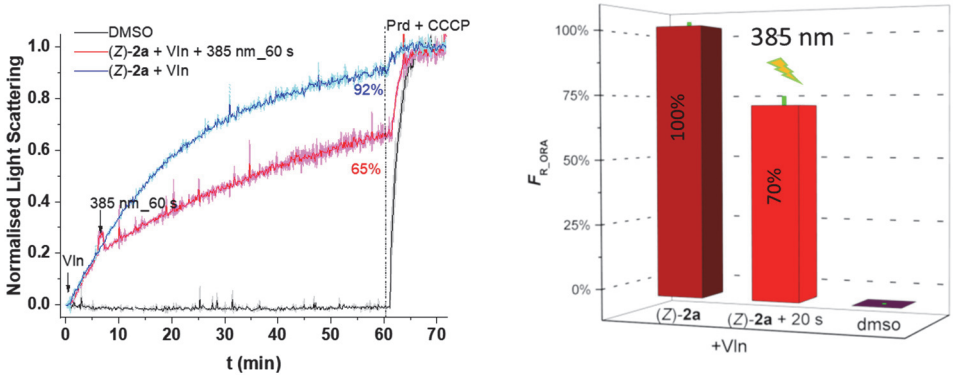

Figure S94. (a) Electrogenic transport mediated by a photoirradiated sample of (*Z*)-**2a** relative to the activity electrogenic transport of (*Z*)-**2a** (1 mol% with respect to lipid) using an osmotic response assay. (b) Percent transport efficiencies of photoirradiated the sample (*Z*)-**2a** measured relative to the electrogenic transport activity of nonirradiated (*Z*)-**2a** using an osmotic response assay. Unilamellar POPC liposomes of mean diameter of 400 nm were loaded with 300 mM KCl buffered to pH 7.2 with 10 mM HEPES and dispersed in 300 mM KGlu buffered to pH 7.2 with 10 mM HEPES. Valinomycin or monensin were added to start the experiment. Each point represents the average of a minimum of 2 repeats. DMSO was used as a control.

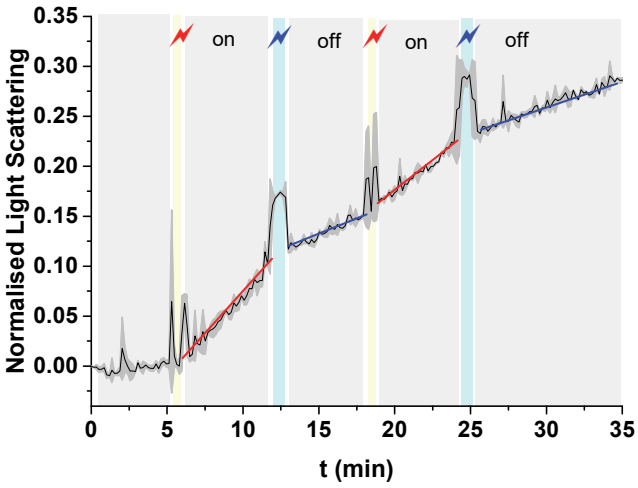

Figure S95. Photo-triggered ion transport by (*E*)-**2a** (1.0 mol% relative to lipid) form unilamellar POPC liposomes of mean diameter of 400 nm containing 300 mM KCl buffered to pH 7.2 with 10 mM HEPES, dispersed in 300 mM KGlu buffered to pH 7.2 with 10 mM HEPES. Valinomycin was added to start the experiment. Colors indicate commencement of sample irradiation using 365 nm (red, 20 s) or 385 nm (blue, 60 s) LEDs. Each point represents the average of a minimum of 2 repeats.

Measurement of membrane potential

Safranin O assays: Safranin O assays were conducted using POPC vesicles (mean diameter 200 nm) which were prepared as follows. A chloroform solution of POPC was evaporated in a round-bottom flask and the lipid film formed was dried under vacuum for at least 6 h. Then, the lipid film was hydrated by vortexing with an internal solution containing KCl (100 mM) buffered at pH 7.0 with 10 mM HEPES. The lipid suspension was subjected to nine freeze/thaw cycles and then extruded 25 times through a 200 nm polycarbonate membrane. The unentrapped salt was removed by size exclusion chromatography on a Sephadex® G-25 column using an external solution eluent. The lipid solution obtained after Sephadex® was diluted to a standard volume (usually 5 mL) with external solution to obtain a lipid stock of known concentration. To test the membrane potential depolarization activity of compounds **1a-c** and **2a-c** under conditions with and without a transmembrane Cl^- concentration gradient, we prepared two different types of extravesicular solutions. (a) Internal solution: KCl- 100 mM, HEPES- 10 mM, pH 7.0; External solution: NaCl (or NaCl-KCl) - 100 mM, HEPES- 10mM, pH 7.0; (b) Internal solution: KCl- 100 mM, HEPES- 10 mM, pH 7.0; External solution: Na_2SO_4 (or Na_2SO_4-K_2SO_4) - 50 mM, HEPES- 10 mM, safranin O- 60 nM, pH 7.0.

For each test, the lipid stock was diluted with the external buffer solution to a standard volume (2.5 mL), to afford a solution with a lipid concentration of 0.1 mM. The emission of safranin O at 580 nm was monitored with excitation wavelength of 520 nm. During the experiment with KCl-filled liposomes, K^+ ionophore valinomycin (0.1 μM, 0.1 mol%, added in 5 μL of DMSO) was added to produce polarized liposomes. Once stable emission was observed, 5 μL of a DMSO solution of tested compound was added. The stable emission value obtained after addition of valinomycin represented 100 % and was used for calibration. The fractional fluorescence intensity (I_f) was calculated using:

$$I_f = \frac{R_t - R_0}{R_v - R_0}$$

where R_t is the emission value at time t, R_0 is the emission value at the beginning of the experiment and R_v is the plateau emission value obtained after addition of valinomycin.

The membrane potential depolarization rates were measured as the initial rate of fluorescence fraction changes by fitting the obtained fraction with the asymptotic function $y = a - b \cdot c^x$ where y is the depolarization percentage (%), x is time (s) and k_{de} is then given by $k_{de} = -b \cdot ln(c)$ (obtained in % s^{-1}), or by fitting the obtained fraction with the two-phase exponential decay (ExpDec2) function $y = A_1 \cdot \exp(-x/t_1) + A_2 \cdot \exp(-x/t_2) + y0$, where y is the depolarization percentage (%), x is time (s) and k_{de} is given by $k_{de} = (dy/dx)_{x=0} = -A_1/t_1 - A_2/t_2$ (obtained in % s^{-1}).

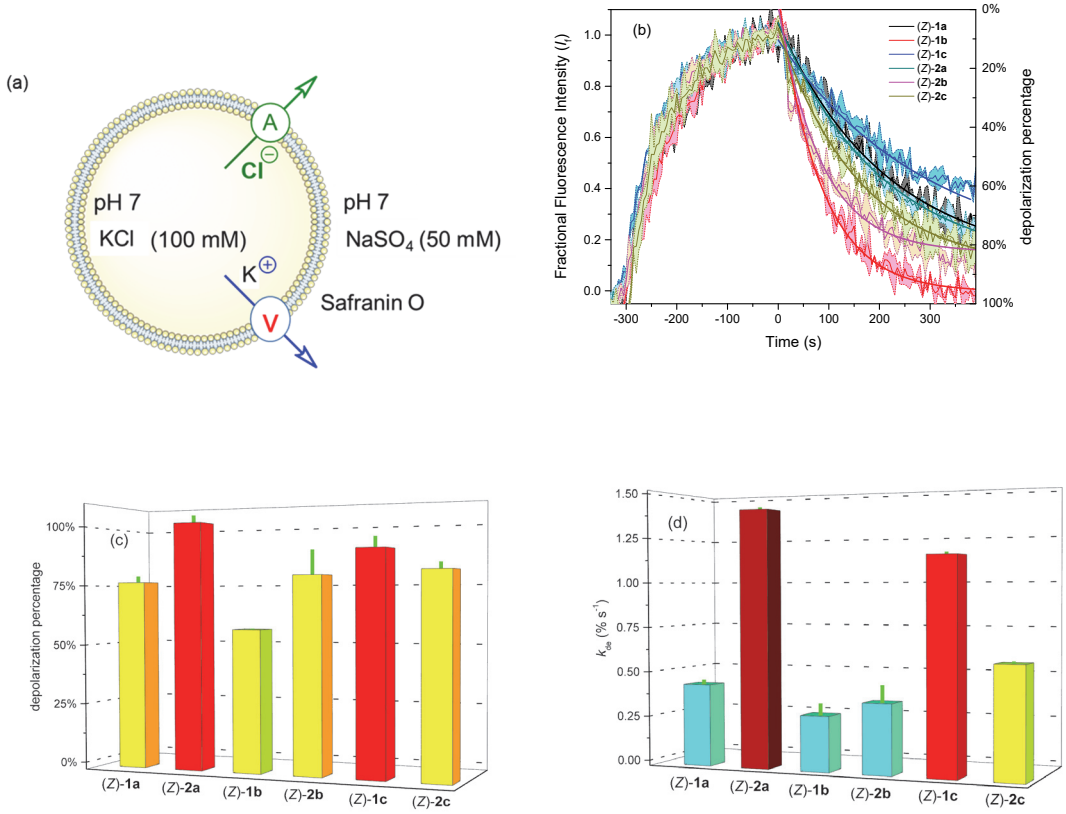

Figure S96. (*Z*) isomers **1a-c** and **2a-c** modulate membrane potential of liposomes experiencing a transmembrane Cl^- concentration gradient. (a) Schematic of the assays, monitored by Safranin O fluorescence. POPC vesicles were loaded with HEPES (10 mM) buffered KCl (100 mM) and suspended in HEPES (10 mM) buffered Na_2SO_4 (50 mM) with Safranin O and adjusted to pH 7.0. Valinomycin (0.1 μM, 0.1 mol%) were added to produce polarized liposomes. Once stable emission was observed, 5 μL of a DMSO solution of tested compound was added to start the experiment. (b) Fluorescence assay of the membrane potential of valinomycin polarized (E = -76 mV) POPC liposomes with *Z* isomers **1a-c** and **2a-c** (1 mol% with respect to lipid). Membrane potentials of liposomes were monitored by the changes in emission intensity of safranin O. The increase in fluorescence indicates polarization with increased negative charges inside liposomes. Bar chart comparisons of depolarization activity of all (*Z*) isomers **1a-c** and **2a-c** (1 mol% with respect to lipid) shown as depolarization percentage at t = 330 s (c) and membrane potential depolarization rates (d).

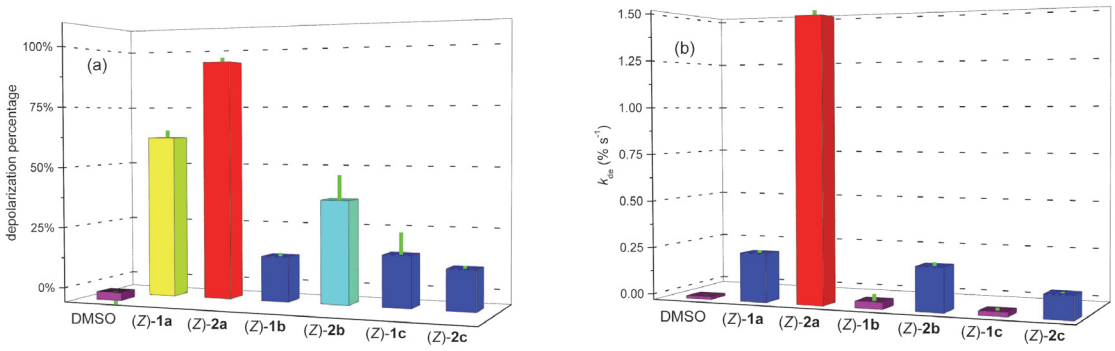

Figure S97. Comparison of depolarization activity of all (*Z*) isomers **1a-c** and **2a-c** (1 mol% with respect to lipid) shown as depolarization percentage at t = 800 s (a) and membrane potential depolarization rates (b). See related assay and graph with the fluorescent intensity in Figure 4a-b in the main manuscript. Unilamellar POPC liposomes were loaded with 100 mM KCl buffered to pH 7.0 with 10 mM HEPES and dispersed in 100 mM NaCl buffered to pH 7.0 with 10 mM HEPES. Valinomycin were added to produce polarized liposomes. Once stable emission was observed, 5 µL of a DMSO solution of tested compound was added to start the experiment. Each point represents the average of a minimum of 2 repeats. DMSO was used as a control.

Hill plot analyses

Hill plot analyses were performed with samples loaded at different concentrations to quantify their transport activity. From these results the depolarization percentage at 800 s was plotted as a function of the transporter concentration (mol%, with respect to lipid). The concentration profile data were evaluated at t = 800 s to get effective concentration, EC_{50} (*i.e.* the concentration of transporter needed to achieve 50% chloride efflux) using Hill equation:

$$y = y_0 + (y_{max} - y_0)\frac{x^n}{K^n + x^n} = V_{max}\frac{x^n}{K^n + x^n} = 100\%\ \frac{x^n}{(EC_{50})^n + x^n}$$

where y is the I_f at 800 s and x is the transporter concentration (mol %, with respect to lipid). y_0 is the I_f obtained for the blank DMSO run, y_{max} is the maximum I_f value and k and n are the parameters to be fitted. n is the Hill coefficient and k is the EC_{50}. The rate of depolarization through Cl^- transport by receptors is shown by the change in fluorescence intensity over time. The results of Hill analysis for each receptor are shown and receptor concentration is included in the legend for each assay.

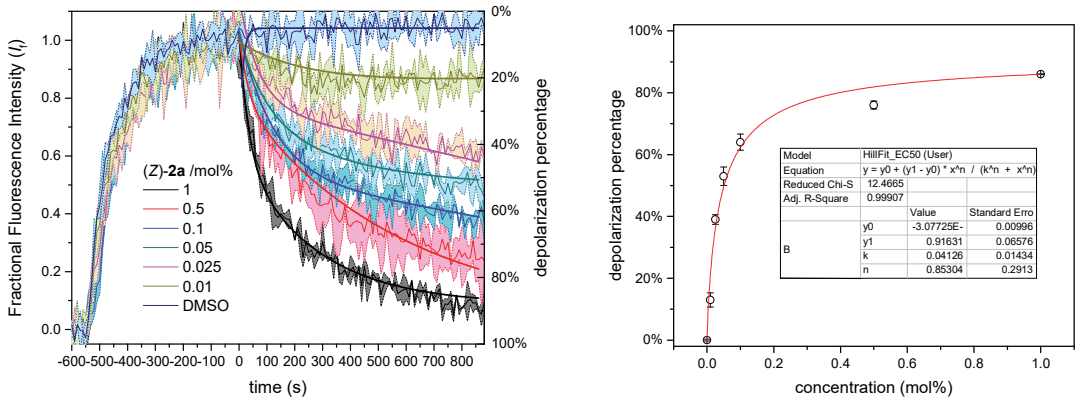

Figure S98. Hill analysis of depolarization activity facilitated by (*Z*)-**2a** in the polarized liposomes loaded with 100 mM KCl buffered to pH 7.0 with 10 mM HEPES and dispersed in 100 mM NaCl buffered to pH 7.0 with 10 mM HEPES.

Membrane Potential – Calibration. Polarized liposomes with different membrane potential were prepared using vesicles loaded with KCl (total concentration 100 mM) and suspended in an external solution containing NaCl and KCl (total concentration 100 mM) or Na_2SO_4 and K_2SO_4 (total concentration 75 mM), using K^+ ionophore valinomycin (0.1 mol%, added in 5 μL of DMSO) to set the membrane potential (Table S1). Theoretical membrane potentials were calculated based on the Nernst equation (at 25 °C):

$V(mV) = 59 \times \log([K^+_{out}]/ [K^+_{in}])$

where $[K^+_{out}]$ and $[K^+_{in}]$ are the extravesicular and intravesicular K^+ concentrations, respectively.

Table S1. Membrane potential generation using valinomycin based on K^+ concentration gradients.

$[K^+]$inside / mM	100	100	100	100	100	100	100
$[K^+]$outside / mM	0.04	0.1	1.0	5.1	10.0	15.1	20.0
Membrane potential / mV	-200	-177	-118	-76	-59	-48	-41

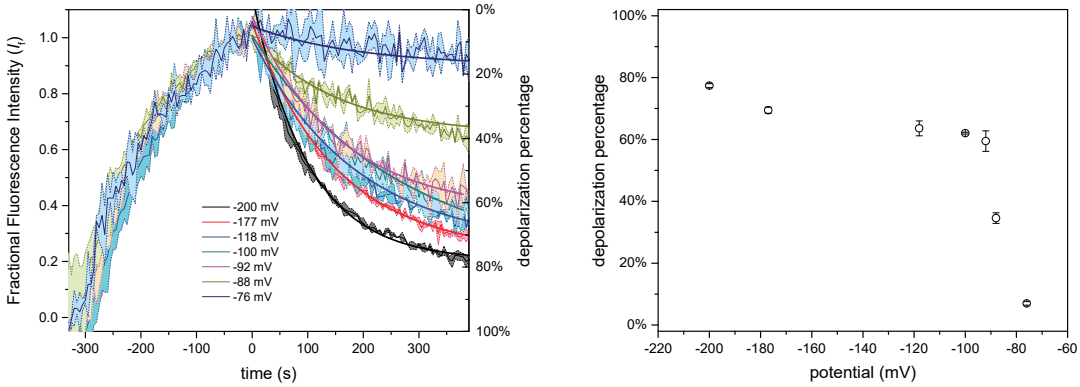

Figure S99. Dependence of membrane potential depolarization rate induced by (*Z*)-**2a** (1 mol% with respect to lipid) on the membrane potential. Liposomes loaded with 100 mM KCl buffered to pH 7.0 with 10 mM HEPES and dispersed in 100 mM NaCl-KCl mixture buffered to pH 7.0 with 10 mM HEPES.

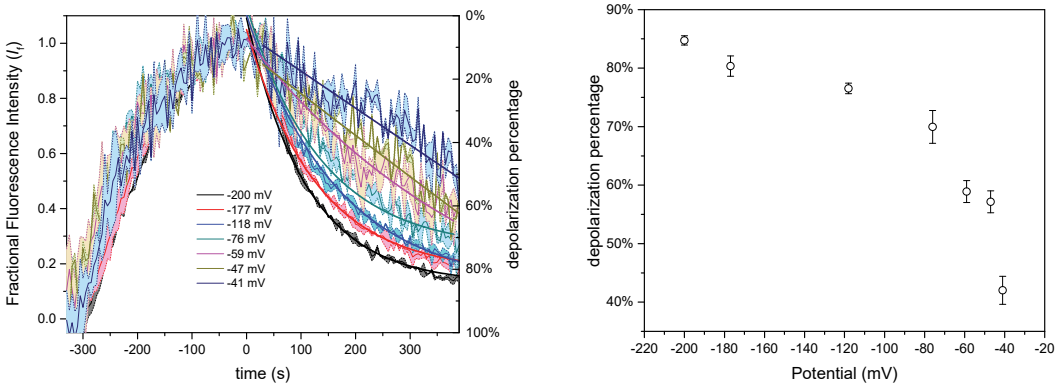

Figure S100. Dependence of membrane potential depolarization rate induced by (*Z*)-**2a** (1 mol% with respect to lipid) on the membrane potential. Liposomes loaded with 100 mM KCl buffered to pH 7.0 with 10 mM HEPES and dispersed in 50 mM Na_2SO_4-K_2SO_4 mixture buffered to pH 7.0 with 10 mM HEPES.

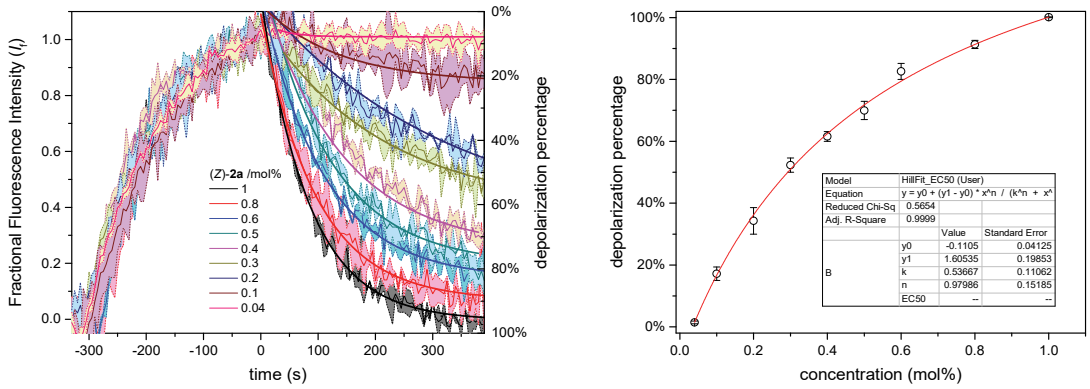

Figure S101. Hill analysis of depolarization activity facilitated by (*Z*)-**2a** in the polarized liposomes at E = -76 mV loaded with 100 mM KCl buffered to pH 7.0 with 10 mM HEPES and dispersed in 50 mM Na_2SO_4-K_2SO_4 mixture buffered to pH 7.0 with 10 mM HEPES.

Photoregulation of membrane potential

The vesicles were prepared by following protocol as stated above safranin O assays. Valinomycin were added to produce polarized liposomes. Once stable emission was observed, transporter (*E*)-**2a** was added in DMSO (10 μL, 1.0 mol% relative to lipid) at 0 s and fluorescence intensity was monitored over time. The sample was irradiated with 365 nm wavelength UV (using a Vilber Lourmat Bio-Link UV Lamps (VL-4.LC, 4W) placed at a distance about 2 cm) for time, t_R = 0, 10, 30 and 60 s during the test after adding transporter ((*E*)-**2a**) to start the experiment (in a darkened room with the lid open and the lamp placed above the cuvette). Then the normalized fluorescence intensity (i.e., activity) value at *t* = 800 s (or 360 s) were noted from plot. The data was further normalized to get *% depolarization efficiency* F_d by setting the safranin O fluorescence of blank sample to 0 and that of (*Z*)-**2a** (1 mol%) to 100.

$$F_d = [(I_{\mathbf{S}(t = 800 \text{ or } 360)} - I_{blank(t = 800 \text{ or } 360)}) / (I_{(Z)\text{-}\mathbf{2a}(t = 800 \text{ or } 360)} - I_{blank(t = 800 \text{ or } 360)})]$$

where, $I_{\mathbf{S}(t = 800 \text{ or } 360)}$ is the normalized fluorescence intensity of a photoirradiated sample at 800 s (or 360 s), ($I_{(Z)\text{-}\mathbf{2a}(t = 800 \text{ or } 360)}$ is the normalized fluorescence intensity of sample (*Z*)-**2a** at 800 s (or 360 s), and $I_{blank(t = 800 \text{ or } 360)}$ is the normalized fluorescence intensity of the blank at 800 s (or 360 s).

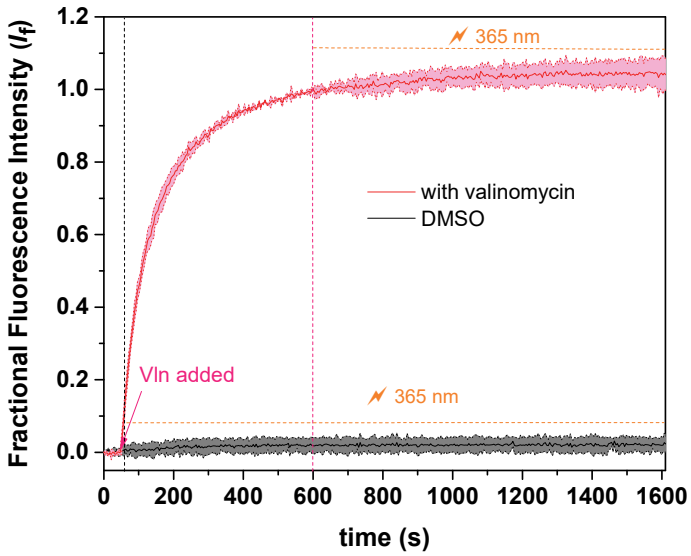

Figure S102. Photo-triggered membrane potential response upon UV irradiation monitored by the fluorescent probe Safranin O. POPC vesicles were loaded with HEPES (10 mM) buffered KCl (100 mM) and suspended in HEPES (10 mM) buffered NaCl (100 mM) with Safranin O and adjusted to pH 7.0. Valinomycin was added to produce polarized liposomes. Sample illumination was achieved using high powered LEDs. Each point represents the average of a minimum of 2 repeats.

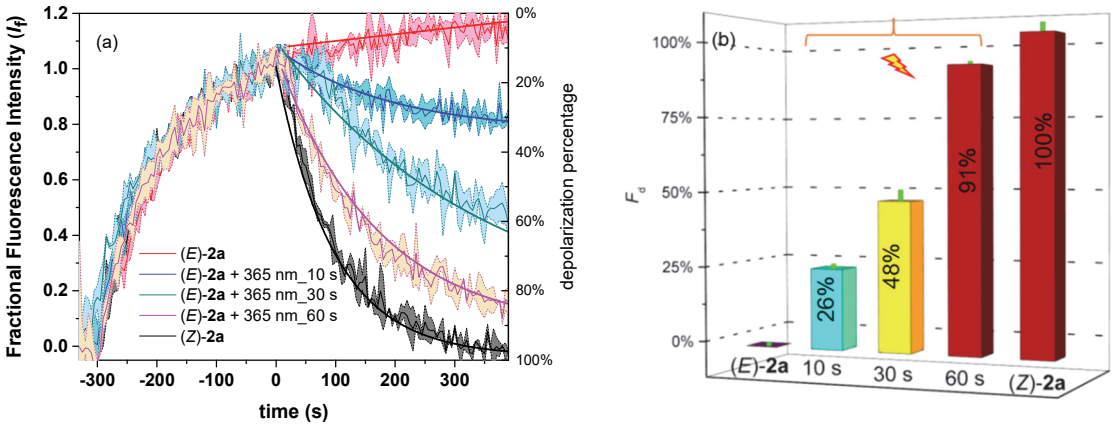

Figure S103. (a) Photo-triggered membrane potential depolarization by (*E*)-**2a** (1 mol% relative to lipid) from safranin O assay with the polarized liposomes at E = -76 mV loaded with 100 mM KCl buffered to pH 7.0 with 10 mM HEPES and dispersed in 75 mM Na_2SO_4-K_2SO_4 mixture buffered to pH 7.0 with 10 mM HEPES. (b) Depolarization efficiencies (%) of photoirradiated the sample (*E*)-**2a** measured relative to the activity of (*Z*)-**2a**.

Single crystal X-ray crystallography

All reflection intensities were measured at 110(2) K using a SuperNova diffractometer (equipped with Atlas detector) with Cu *K*α radiation (λ = 1.54178 Å) under the program CrysAlisPro (Version CrysAlisPro 1.171.39.29c, Rigaku OD, 2017). The same program was used to refine the cell dimensions and for data reduction. The structure was solved with the program SHELXS-2018/3 (Sheldrick, 2018) and was refined on F^2 with SHELXL-2018/3 (Sheldrick, 2018). Analytical numeric absorption correction using a multifaceted crystal model was applied using CrysAlisPro. The temperature of the data collection was controlled using the system Cryojet (manufactured by Oxford Instruments). The H atoms were placed at calculated positions (unless otherwise specified) using the instructions AFIX 23, AFIX 43 or AFIX 137 with isotropic displacement parameters having values 1.2 or 1.5 U_{eq} of the attached C atoms. The H atoms attached to N10, N13, N32 and N35 were found from difference Fourier maps, and their coordinates were refined pseudofreely using the DFIX instruction in order to keep the N–H bond distances within an acceptable range.

The structure is ordered.

Specified hydrogen bonds

D-H(Å)	H···A (Å)	D···A(Å)	<(DHA) °	
0.90(2)	2.37(2)	3.226(2)	159(2)	N10-H10N···Cl45
0.88(2)	2.35(2)	3.200(2)	162(3)	N13-H13N···Cl45
0.86(2)	2.74(3)	3.354(2)	130(2)	N32-H32N···Cl45
0.86(2)	2.64(3)	3.327(3)	138(2)	N32-H32N···O12_$2
0.88(2)	2.34(2)	3.181(2)	159(3)	N35-H35N···Cl45

* $2 = -x, -y, -z+1

Table S2. Crystallographic data for the structure of (*Z*)-1⊂Cl⁻.

	(*Z*)-**1c**⊂Cl^-
Crystal data	
Chemical formula	$C_{32}H_{26}N_6O_6 \cdot C_{16}H_{36}N \cdot Cl$
M_r	868.49
Crystal system, space group	Triclinic, *P*-1
Temperature (K)	110
a, *b*, *c* (Å)	10.7878 (7), 14.6227 (9), 15.0612 (4)
α, β, γ (°)	74.237 (4), 82.031 (4), 87.263 (5)
V (Å^3)	2264.3 (2)
Z	2
Radiation type	Cu *K*α
μ (mm^{-1})	1.20
Crystal size (mm)	0.19 × 0.08 × 0.02
Data collection	
Diffractometer	SuperNova, Dual, Cu at zero, Atlas
Absorption correction	Analytical *CrysAlis PRO* 1.171.41.93a (Rigaku Oxford Diffraction, 2020) Analytical numeric absorption correction using a multifaceted crystal model based on expressions derived by R.C. Clark & J.S. Reid. (Clark, R. C. & Reid, J. S. (1995). Acta Cryst. A51, 887-897) Empirical absorption correction using spherical harmonics, implemented in SCALE3 ABSPACK scaling algorithm.
T_{min}, T_{max}	0.869, 0.978
No. of measured, independent and observed [$I > 2\sigma(I)$] reflections	24810, 8081, 5814
R_{int}	0.068
$(\sin \theta/\lambda)_{max}$ (Å^{-1})	0.598
Refinement	
$R[F^2 > 2\sigma(F^2)]$, $wR(F^2)$, *S*	0.051, 0.133, 1.02
No. of reflections	8081
No. of parameters	575
No. of restraints	4
H-atom treatment	H atoms treated by a mixture of independent and constrained refinement
$\Delta\rho_{max}$, $\Delta\rho_{min}$ (e Å^{-3})	0.36, -0.33

Computer programs: *CrysAlis PRO* 1.171.39.29c (Rigaku OD, 2017), *SHELXS2018*/3 (Sheldrick, 2018), *SHELXL2018*/3 (Sheldrick, 2018), *SHELXTL* v6.10 (Sheldrick, 2008).[7]

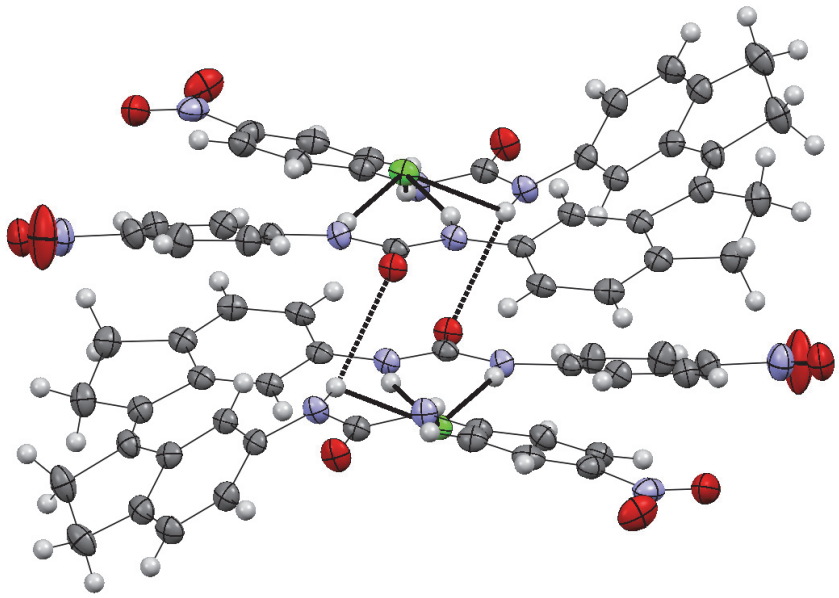

Figure S104. Displacement ellipsoid plot (50% probability level) of pair of (*M*)-(*Z*)-**1c**⊂Cl^- and (*P*)-(*Z*)-**1c**⊂Cl^- found in the solid state structure at 110(2) K showing intermolecular N-H•••O hydrogen bonding interactions. Tetrabutylammonium cations have been omitted for clarity.

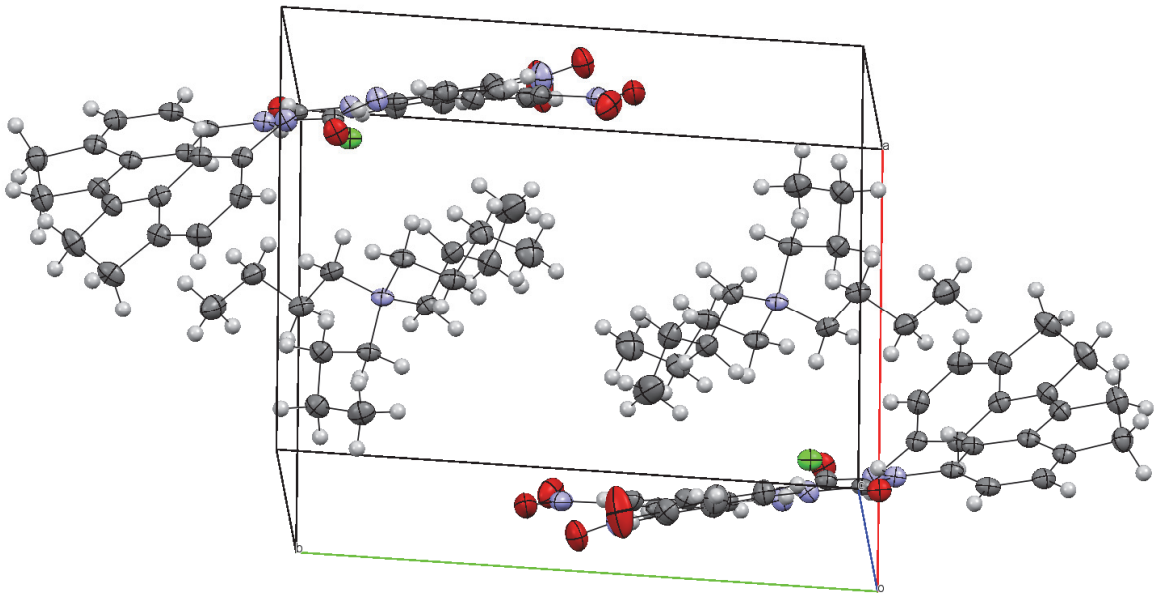

Figure S105. Crystal packing diagram of $[NBu_4]^+$[(*Z*)-**1c**⊂Cl]$^-$.

Geometry optimization by DFT

Input geometries were generated using ArgusLab.[8] The Gaussian 09 program[9] was used for geometry optimization: First, energy minimization was performed at the semi-empirical PM3 level of theory, and subsequently at the DFT B3LYP/6-31++G(d,p) level of theory using an IEFPCM DMSO solvation model. The DFT optimized geometries were found to have zero imaginary frequencies. For the single urea-bound chloride complexes, two possible geometries, with urea groups pointing in opposite directions, were optimized.

Table S3. Cartesian coordinates of (*Z*)-**1a**⊂Cl^- (simultaneously bound)

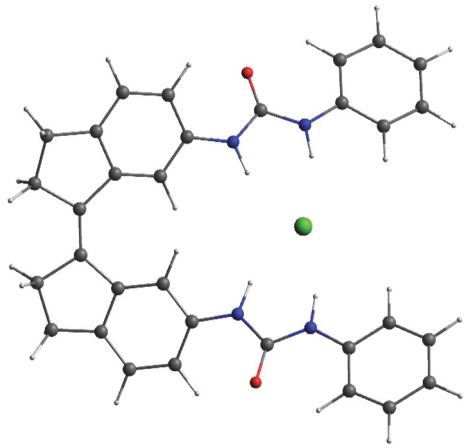

atom	X	Y	Z
C	4.6147130000	0.6205810000	-0.2682100000
C	4.6134680000	-0.6294290000	0.2677500000
C	3.5350340000	-1.5872240000	0.5985400000
C	4.0615790000	-2.6371170000	1.3837500000
C	5.5282000000	-2.4216430000	1.6667300000
C	5.9246550000	-1.3215850000	0.6540600000
C	3.5382370000	1.5806860000	-0.5986400000
C	4.0669220000	2.6298430000	-1.3833900000
C	5.5330910000	2.4115470000	-1.6665000000
C	5.9273460000	1.3100150000	-0.6545700000
C	2.1966730000	-1.6499690000	0.1842600000
C	1.3762790000	-2.7118950000	0.5995700000
C	1.9037850000	-3.7337180000	1.4088300000
C	3.2500250000	-3.6957030000	1.7833500000
C	2.1999670000	1.6459210000	-0.1844400000
C	1.3817120000	2.7096750000	-0.5992900000
C	1.9113560000	3.7308520000	-1.4080000000
C	3.2575160000	3.6902570000	-1.7824900000
C	-0.8203840000	3.7477640000	-0.0349200000

O	-0.4517590000	4.9270220000	-0.0966300000
C	-0.8275850000	-3.7460760000	0.0351400000
O	-0.4610100000	-4.9259770000	0.0969800000
N	0.0222120000	2.6702300000	-0.2159900000
N	0.0168790000	-2.6700000000	0.2161400000
N	-2.1189450000	3.3550400000	0.2287000000
N	-2.1254240000	-3.3511200000	-0.2286700000
C	-4.3812330000	6.2608690000	0.9010100000
C	-5.5846060000	5.5938140000	1.1438700000
C	-5.6077120000	4.1958040000	1.0766200000
C	-3.2100060000	5.5607340000	0.5938100000
C	-3.2351720000	4.1555640000	0.5273800000
C	-4.4494250000	3.4831190000	0.7729400000
C	-4.4560240000	-3.4751410000	-0.7733900000
C	-5.6155570000	-4.1858360000	-1.0769600000
C	-5.5950030000	-5.5839160000	-1.1435800000
C	-3.2430470000	-4.1497060000	-0.5273000000
C	-3.2204430000	-5.5549560000	-0.5930800000
C	-4.3928960000	-6.2530810000	-0.9001900000
Cl	-1.9894800000	0.0018990000	-0.0012900000
H	1.2686310000	-4.5503450000	1.7248700000
H	1.2778900000	4.5489450000	-1.7236700000
H	6.1192560000	-3.3365150000	1.5571700000
H	5.6752920000	-2.0673440000	2.6963200000
H	6.6586580000	-0.6229680000	1.0642400000
H	6.1260050000	3.3251450000	-1.5563200000
H	5.6794590000	2.0576760000	-2.6963400000
H	6.6595730000	0.6099320000	-1.0654000000
H	-0.3766820000	1.7425420000	-0.0696900000
H	-0.3803270000	-1.7416180000	0.0695700000
H	6.3815230000	-1.7800170000	-0.2348700000
H	6.3855980000	1.7668330000	0.2344600000
H	1.7817170000	-0.9053670000	-0.4835700000
H	3.6569110000	-4.4994850000	2.3918600000
H	1.7834340000	0.9018130000	0.4829700000
H	3.6660700000	4.4935150000	-2.3905900000
H	-2.2945100000	2.3497700000	0.2116400000
H	-2.2991600000	-2.3455300000	-0.2118600000
H	-4.3438080000	7.3458490000	0.9481700000
H	-6.4867530000	6.1495880000	1.3803100000
H	-6.5308540000	3.6538380000	1.2614800000
H	-2.2857840000	6.0876300000	0.4056500000
H	-4.4777890000	2.3977900000	0.7251400000
H	-4.4824000000	-2.3897300000	-0.7260800000
H	-6.5376750000	-3.6422620000	-1.2622300000
H	-6.4981260000	-6.1381320000	-1.3799400000
H	-2.2972150000	-6.0834400000	-0.4045100000
H	-4.3574610000	-7.3381410000	-0.9468600000

Sum of electronic and zero-point Energies = -2065.782137

Table S4. Cartesian coordinates of (*Z*)-**1a**⊂Cl^- (NH atoms towards each other)

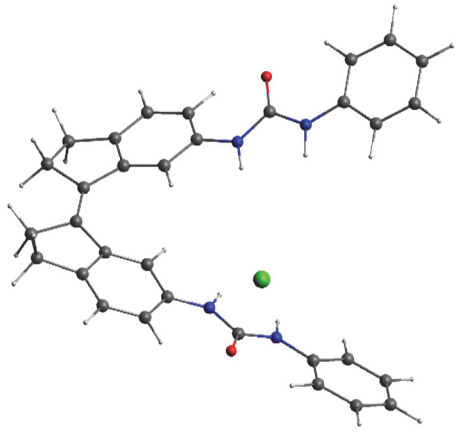

atom	X	Y	Z
C	4.2376660000	2.2876250000	1.2808430000
C	3.6394340000	1.2835140000	0.4888030000
C	5.6881430000	1.9662050000	1.5521610000
C	6.0056890000	0.8692750000	0.5058310000
C	4.6490810000	0.2607140000	0.1408250000
C	3.4984570000	3.3958190000	1.6845840000
C	2.1617260000	3.5359640000	1.2962080000
C	1.5722560000	2.5620120000	0.4709790000
C	2.3134100000	1.4401000000	0.0660460000
C	2.8486840000	-3.8496010000	-1.9540990000
C	1.5420640000	-3.8317310000	-1.4534120000
C	1.1558260000	-2.8307170000	-0.5407970000
C	2.0801680000	-1.8391020000	-0.1614990000
N	0.2253460000	2.6283870000	0.0428210000
C	-0.5648380000	3.7548480000	-0.0843740000
N	-1.8462280000	3.4609350000	-0.5135230000
C	-2.9041210000	4.3458730000	-0.8057300000
O	-0.1704650000	4.8977340000	0.1622890000
C	-4.1239900000	3.7647750000	-1.2020250000
C	-2.8057670000	5.7461690000	-0.7306520000
C	-3.9164260000	6.5340130000	-1.0500410000
C	-5.2214480000	4.5640650000	-1.5160290000
C	-5.1271620000	5.9584060000	-1.4427610000
C	-1.2524990000	-3.4839300000	-0.2634440000
N	-2.3114840000	-3.1757270000	0.5690970000
C	-3.6240740000	-3.6756730000	0.5391470000
O	-1.3179820000	-4.2978590000	-1.1938620000
C	-4.0973120000	-4.6194080000	-0.3915140000
C	-4.5106600000	-3.1821400000	1.5183670000
C	-5.8328260000	-3.6192600000	1.5660640000
C	-5.4276080000	-5.0471860000	-0.3300330000
C	-6.3052130000	-4.5573920000	0.6405580000

N	-0.1154400000	-2.7730290000	0.0643280000
C	3.3770600000	-1.8446560000	-0.6887500000
C	3.7666800000	-2.8774160000	-1.5696920000
C	5.2238270000	-2.7442500000	-1.9445480000
C	4.5425070000	-0.9797710000	-0.4014920000
C	5.7685820000	-1.7616730000	-0.8779330000
H	5.8134540000	1.5720830000	2.5700710000
H	6.3397720000	2.8413260000	1.4652920000
H	6.7105070000	0.1228490000	0.8815550000
H	6.4639790000	1.3267360000	-0.3829010000
H	3.9546920000	4.1660680000	2.3012640000
H	1.5872460000	4.3968270000	1.6079940000
H	1.8539390000	0.7183810000	-0.5998430000
H	0.8302850000	-4.5904830000	-1.7443620000
H	-1.8758470000	6.2030350000	-0.4251120000
H	-3.8248240000	7.6147950000	-0.9874150000
H	-4.2094070000	2.6827400000	-1.2634650000
H	-6.1518810000	4.0924900000	-1.8185750000
H	-0.1440120000	1.7581950000	-0.3162070000
H	-2.0814570000	2.4829530000	-0.6189940000
H	-3.4286400000	-5.0066650000	-1.1465470000
H	-4.1536250000	-2.4541240000	2.2418350000
H	-6.4949760000	-3.2234740000	2.3309820000
H	-5.7755720000	-5.7761500000	-1.0569860000
H	-2.1191960000	-2.4890960000	1.3038000000
H	-0.2098110000	-2.1029190000	0.8314660000
H	1.7798090000	-1.0964630000	0.5690360000
H	3.1426130000	-4.6441980000	-2.6355930000
H	6.2026110000	-2.3281420000	-0.0412190000
H	6.5554170000	-1.1115250000	-1.2690120000
H	5.3303360000	-2.3129310000	-2.9496260000
H	5.7501980000	-3.7039920000	-1.9500970000
H	-5.9815270000	6.5819580000	-1.6870990000
H	-7.3353510000	-4.8982130000	0.6771030000
Cl	-1.0841410000	-0.9269330000	2.6574500000

Sum of electronic and zero-point Energies = -2065.774776

Table S5. Cartesian coordinates of (*Z*)-**1a**⊂Cl^- (NH atoms away from each other)

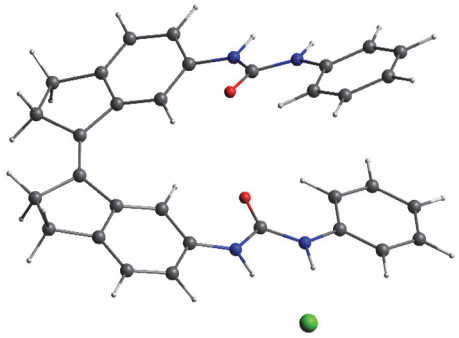

atom	X	Y	Z
C	-4.1534610000	-2.1805100000	1.7947900000
C	-3.5326300000	-1.3522000000	0.8360700000
C	-5.5856600000	-1.7596900000	2.0250300000
C	-5.8805900000	-0.8489800000	0.8070300000
C	-4.5080400000	-0.3553700000	0.3430500000
C	-3.4486410000	-3.2334000000	2.3735600000
C	-2.1357710000	-3.4893900000	1.9736700000
C	-1.5233110000	-2.6947110000	0.9858100000
C	-2.2201800000	-1.6190200000	0.4165500000
C	-2.5699100000	3.3734400000	-2.2793000000
C	-1.2739900000	3.3645390000	-1.7640400000
C	-0.9182600000	2.4787590000	-0.7241600000
C	-1.8699800000	1.5746590000	-0.2243900000
N	-0.1897210000	-3.0186810000	0.6395800000
C	0.4775790000	-2.7120010000	-0.5310700000
N	1.7821790000	-3.1718410000	-0.5382700000
C	2.7370390000	-3.0971610000	-1.5731600000
O	-0.0344910000	-2.0924510000	-1.4669100000
C	3.9578990000	-3.7650110000	-1.3584200000
C	2.5416990000	-2.3989510000	-2.7775000000
C	3.5579890000	-2.3820710000	-3.7381900000
C	4.9620590000	-3.7351110000	-2.3243100000
C	4.7699990000	-3.0434410000	-3.5255900000
C	0.9921900000	1.9115290000	0.8063900000
N	2.3236200000	2.2543390000	0.9541400000
C	3.2395900000	1.8119290000	1.9228400000
O	0.3995500000	1.1086790000	1.5384300000
C	2.9276800000	0.9198390000	2.9658600000
C	4.5542300000	2.3124790000	1.8261500000
C	5.5293300000	1.9331390000	2.7462600000
C	3.9183600000	0.5489790000	3.8809300000
C	5.2205400000	1.0461490000	3.7844400000
N	0.4057400000	2.5726890000	-0.2528000000
C	-3.1647600000	1.5673100000	-0.7688100000
C	-3.5212000000	2.4880500000	-1.7751200000

C	-4.9819200000	2.3584300000	-2.1363300000
C	-4.3596800000	0.7895100000	-0.3723800000
C	-5.5597300000	1.5394100000	-0.9549900000
H	-5.6773900000	-1.1894300000	2.9598500000
H	-6.2709110000	-2.6099800000	2.1001200000
H	-6.5605400000	-0.0288300000	1.0517700000
H	-6.3586100000	-1.4397300000	0.0121000000
H	-3.9164310000	-3.8708600000	3.1191900000
H	-1.5885410000	-4.3202910000	2.4112400000
H	-1.7473400000	-1.0332710000	-0.3554400000
H	-0.5321700000	4.0595990000	-2.1477400000
H	1.6098400000	-1.8813710000	-2.9521800000
H	3.3919600000	-1.8377310000	-4.6636400000
H	4.1177690000	-4.3092410000	-0.4309400000
H	5.8956590000	-4.2569810000	-2.1353100000
H	0.2687290000	-3.6491210000	1.2836500000
H	2.1073090000	-3.6469910000	0.2932800000
H	1.9241700000	0.5289690000	3.0510000000
H	4.8042900000	3.0011190000	1.0236200000
H	6.5346100000	2.3333390000	2.6490700000
H	3.6591500000	-0.1400810000	4.6802800000
H	2.6898200000	2.9304490000	0.2790000000
H	1.0033700000	3.2339890000	-0.7549900000
H	-1.5962300000	0.9228790000	0.5894500000
H	-2.8312300000	4.0826200000	-3.0605800000
H	-5.9798100000	2.2226500000	-0.2025500000
H	-6.3646500000	0.8670700000	-1.2636000000
H	-5.1035100000	1.8066300000	-3.0788600000
H	-5.4746800000	3.3272700000	-2.2666600000
H	5.5510990000	-3.0206010000	-4.2791100000
H	5.9799100000	0.7504490000	4.5018200000
Cl	2.8364900000	4.4985490000	-1.4452100000

Sum of electronic and zero-point Energies = -2065.774843

References

[1] Wezenberg, S. J.; Feringa, B. L. *Org. Lett.* **2017**, *19*, 324-327.

[2] Wezenberg, S. J.; Feringa, B. L. *Nat. Commun.* **2018**, *9*, 1984.

[3] Gottlieb, H. E.; Kotlyar, V.; Nudelman, A. *J. Org. Chem.* **1997**, *62*, 7512-7515.

[4] Thordarson, P. *Chem Soc. Rev.* **2011**, *40*, 1305-1323.

[5] Frassineti, C.; Ghelli, S.; Gans, P.; Sabatini, A.; Moruzzi, M. S.; Vacca, A. *Anal. Biochem.* **1995**, *231*, 374-382.

[6] Wu, X.; Gale, P. A. *J. Am. Chem. Soc.* **2016**, *138*, 16508-16514

[7] Sheldrick, G. M. *Acta Cryst.* **2015**, *C71*, 3-8.

[8] http://www.arguslab.com/arguslab.com/ArgusLab.html

[9] Gaussian 09, Revision D.01, Frisch, M. J.; Trucks, G. W.; Schlegel, H. B.; Scuseria, G. E.; Robb, M. A.; Cheeseman, J. R.; Scalmani, G.; Barone, V.; Mennucci, B.; Petersson, G. A.; Nakatsuji, H.; Caricato, M.; Li, X.; Hratchian, H. P.; Izmaylov, A. F.; Bloino, J.; Zheng, G.; Sonnenberg, J. L.; Hada, M.; Ehara, M.; Toyota, K.; Fukuda, R.; Hasegawa, J.; Ishida, M.; Nakajima, T.; Honda, Y.; Kitao, O.; Nakai, H.; Vreven, T.; Montgomery, Jr., J. A.; Peralta, J. E.; Ogliaro, F.; Bearpark, M.; Heyd, J. J.; Brothers, E.; Kudin, K. N.; Staroverov, V. N.; Keith, T.; Kobayashi, R.; Normand, J.; Raghavachari, K.; Rendell, A.; Burant, J. C.; Iyengar, S. S.; Tomasi, J.; Cossi, M.; Rega, N.; Millam, J. M.; Klene, M.; Knox, J. E.; Cross, J. B.; Bakken, V.; Adamo, C.; Jaramillo, J.; Gomperts, R.; Stratmann, R. E.; Yazyev, O.; Austin, A. J.; Cammi, R.; Pomelli, C.; Ochterski, J. W.; Martin, R. L.; Morokuma, K.; Zakrzewski, V. G.; Voth, G. A.; Salvador, P.; Dannenberg, J. J.; Dapprich, S.; Daniels, A. D.; Farkas, O.; Foresman, J. B.; Ortiz, J. V.; Cioslowski, J.; Fox, D. J.; Gaussian, Inc., Wallingford CT, **2013**.